

DSMS Telecommunications Link  
Design Handbook

---

207, Rev. A  
34-m and 70-m Telemetry Reception

June 13, 2003

---

Document Owner:

Signature on file at DSMS Library

\_\_\_\_\_  
L. Paal, Date  
Telemetry System Engineer

Approved by:

Signature on file at DSMS Library

\_\_\_\_\_  
J. B. Berner Date  
Telecommunications Services  
System Development Engineer

Author

Signature on file at DSMS Library

\_\_\_\_\_  
P. W. Kinman Date

Released by:

Signature on file at DSMS Library

\_\_\_\_\_  
DSMS Document Release Date

### *Change Log*

<b>Rev</b>	<b>Issue Date</b>	<b>Affected Paragraphs</b>	<b>Change Summary</b>
Initial	11/30/2000	All	All
A	6/13/2003	Many	Revised to include concatenated codes, QPSK/OQPSK modulation, and to improve description of turbo code performance.

### *Note to Readers*

There are two sets of document histories in the 810-005 document that are reflected in the header at the top of the page. First, the overall document is periodically released as a revision when major changes affect a majority of the modules. For example, the original release of this document was part of Revision E. Second, the individual modules also change, starting as an initial issue that has no revision letter. When a module is changed, a change letter is appended to the module number on the second line of the header and a summary of the changes is entered in the module's change log.

## *Contents*

<u>Paragraph</u>	<u>Page</u>
1 Introduction .....	7
1.1 Purpose .....	7
1.2 Scope .....	7
1.3 General Information .....	7
2 Telemetry Capability .....	8
2.1 Modulation .....	9
2.2 Symbol Rate .....	9
2.3 Carrier Loop Bandwidth.....	10
3 Definitions.....	11
4 Receiver Acquisition .....	13
4.1 FFT .....	14
4.2 Loop Locking .....	19
4.3 Acquisition Time.....	20
5 Telemetry Performance .....	26
5.1 Comparison of Residual Carrier and Suppressed Carrier.....	26
5.2 Decoding Threshold and System Loss .....	30
5.3 Carrier Synchronization.....	31
5.3.1 Residual Carrier .....	32
5.3.2 Suppressed-Carrier BPSK.....	48
5.3.3 QPSK and OQPSK .....	49
5.3.4 Two/Three-Way Coherent .....	50
5.3.5 Radio Loss .....	50
5.4 Subcarrier Synchronization .....	56
5.5 Symbol Synchronization .....	61
5.6 Waveform Distortion.....	65
5.7 Amplitude Scintillation at Small Sun-Earth-Probe (SEP) Angles .....	65
Appendix A, Baseline BER and FER Performance .....	69
A.1 Uncoded and Convolutionally Coded Telemetry .....	69
A.2 Concatenated and Turbo-Coded Telemetry.....	70
Appendix B, High-Rate Model (HRM) Radio Loss.....	72

<b><u>Paragraph</u></b>	<b><u>Page</u></b>
Appendix C, Static Phase Error.....	77
Appendix D, Transmitter Phase Noise.....	78
Appendix E, Solar Phase Noise.....	80
Appendix F, Subcarrier Demodulation Loss.....	81
Appendix G, Symbol Loop Squaring Loss.....	82
Appendix H, Symbol Synchronization Loss.....	83
Appendix I, Rician Fading at Small Sun-Earth-Probe (SEP) Angles.....	84
Appendix J, References.....	85

### *Illustrations*

<b><u>Figure</u></b>	<b><u>Page</u></b>
1. Receiver Architecture.....	8
2. Number of Data Points for FFT; Sample Rate = 2000 Hz.....	17
3. Number of Data Points for FFT; Sample Rate = 20 Hz.....	18
4. Loop Locking Time.....	21
5. Receiver Acquisition Time; Residual Carrier.....	23
6. Receiver Acquisition Time; Suppressed Carrier, $E_S/N_0 = -3$ dB.....	24
7. Receiver Acquisition Time; Suppressed Carrier, $E_S/N_0 = 0$ dB.....	25
8. Comparison of Residual Carrier and Suppressed Carrier.....	27
9. Comparison of Optimized and Non-optimized Modulation Index.....	29
10. Telemetry Performance; Uncoded, Residual Carrier.....	34
11. Telemetry Performance; ( $k=7, r=1/2$ ) Convolutional Code with Residual Carrier.....	35
12. Telemetry Performance; ( $k=15, r=1/4$ ) Convolutional Code with Residual Carrier.....	36
13. Telemetry Performance; ( $k=15, r=1/6$ ) Convolutional Code with Residual Carrier.....	37
14. Telemetry Performance; Concatenated RS and ( $k=7, r=1/2$ ), Convolutional Codes with Residual Carrier.....	38
15. Telemetry Performance; Concatenated RS and ( $k=15, r=1/6$ ) Convolutional Code with Residual Carrier.....	39
16. Telemetry Performance; (1784, 1/2) Turbo Code with Residual Carrier.....	40
17. Telemetry Performance; (1784, 1/3) Turbo Code with Residual Carrier.....	41

<b><u>Figure</u></b>	<b><u>Page</u></b>
18. Telemetry Performance; (8920, 1/4) Turbo Code with Residual Carrier.....	42
19. Telemetry Performance; (8920, 1/6) Turbo Code with Residual Carrier.....	43
20. Optimum Modulation Index; Uncoded .....	44
21. Optimum Modulation Index; ( $k=7, r=1/2$ ) Convolutional Code.....	45
22. Optimum Modulation Index; ( $k=15, r=1/6$ ) Convolutional Code.....	46
23. Optimum Modulation Index; Turbo Codes .....	47
24. Symbol Loop Squaring Loss .....	62
25. (1784, 1/3) Turbo Code Performance at S-Band With Amplitude Scintillation .....	66
26. (1784, 1/3) Turbo Code Performance at X-Band With Amplitude Scintillation .....	67
27. (1784, 1/3) Turbo Code Performance at Ka-Band With Amplitude Scintillation.....	68

### ***Tables***

<b><u>Table</u></b>	<b><u>Page</u></b>
1. Telemetry Capabilities.....	8
2. Symbol Rates.....	9
3. FFT Sample Frequencies .....	14
4. FFT Section Bandwidths .....	15
5. Coefficients $\alpha_1$ and $\alpha_2$ in the Calculation of $P_{CTP}/N_0$ .....	19
6. Baseline $E_b/N_0$ for Uncoded and Convolutionally Coded Data, dB .....	30
7. Effective Threshold $E_b/N_0$ for Concatenated Codes, dB.....	30
8. Effective Threshold $E_b/N_0$ for Turbo Codes, dB .....	31
9. Interpolation Factor Coefficients $c_1$ and $c_2$ for Concatenated Codes.....	52
10. Interpolation Factor Coefficients $c_1$ and $c_2$ for Turbo Codes.....	52
11. HRM Coefficients $c_{H0}$ and $c_{H1}$ for Uncoded Telemetry.....	53
12. HRM Coefficients $c_{H0}$ and $c_{H1}$ for ( $k=7, r=1/2$ ) Convolutional Code .....	53
13. HRM Coefficients $c_{H0}$ and $c_{H1}$ for $k=15$ Convolutional Codes .....	54
14. HRM Coefficients $c_{H0}$ and $c_{H1}$ for Concatenated Codes .....	54
15. HRM Coefficients $c_{H0}$ and $c_{H1}$ for Turbo Codes, Residual Carrier .....	55
16. HRM Coefficients $c_{H0}$ and $c_{H1}$ for Turbo Codes, Suppressed Carrier .....	55
17. LRM Coefficients $c_{L0}$ and $c_{L1}$ for All Codes.....	55
18. Interpolation Factor Coefficients $c_1$ and $c_2$ for Concatenated Codes.....	57

<b><u>Table</u></b>	<b><u>Page</u></b>
19. Subcarrier Demodulation HRM Loss Coefficients for Uncoded and Convolutionally Coded Data using Squarewave Subcarriers.....	58
20. Subcarrier Demodulation HRM Loss Coefficients for Uncoded and Convolutionally Coded Data using Sinewave Subcarriers.....	59
21. Subcarrier Demodulation HRM Loss Coefficients for Concatenated Codes Using Squarewave Subcarriers .....	59
22. Subcarrier Demodulation HRM Loss Coefficients for Concatenated Codes Using Sinewave Subcarriers .....	60
23. Subcarrier Demodulation HRM Loss Coefficients for Turbo Codes Using Squarewave Subcarriers.....	60
24. Subcarrier Demodulation HRM Loss Coefficients for Turbo Codes Using Sinewave Subcarriers.....	61
25. Symbol Synchronization HRM Loss Coefficients for Concatenated Codes .....	64
26. Symbol Synchronization HRM Loss Coefficients for Turbo Codes .....	64
A-1. Coefficients $a_0$ and $a_1$ for Equation (A-4) .....	69
A-2. Coefficients $a_0$ and $a_1$ for Equation (A-6), Concatenated Codes.....	70
A-3. Rate 1/2 Turbo Code Baseline Data .....	71
A-4. Rate 1/3 Turbo Code Baseline Data .....	72
A-5. Rate 1/4 Turbo Code Baseline Data .....	73
A-6. Rate 1/6 Turbo Code Baseline Data .....	74
C-1. Static Phase Error (rad) .....	77
D-1. Carrier Phase Error Variance, $\sigma_\phi^2$ (rad <sup>2</sup> ).....	79

## ***1 Introduction***

### ***1.1 Purpose***

This module provides the performance parameters for telemetry reception at the Deep Space Network (DSN) 34-m and 70-m stations.

### ***1.2 Scope***

The scope of this module is limited to those features of the Downlink Channel at the 34-m and 70-m stations that relate to telemetry reception and demodulation. Under the Network Simplification Plan (NSP), each Block-V Receiver has been renamed the Receiver and Ranging Processor (RRP) and has become part of a Downlink Channel. The Downlink Channel also performs the frame synchronization and data decoding that are discussed in Module 208, Telemetry Data Decoding.

### ***1.3 General Information***

Figure 1 shows the architecture used in the 34-m and 70-m stations to process an arriving telemetry signal through the point at which it becomes a stream of data symbols. The arriving signal is routed from the Antenna Feed/Low Noise Amplifier (LNA) to the Downlink Channel. Within the radio-frequency (RF) to Intermediate-frequency (IF) Downconverter (RID) at the antenna, a local oscillator is generated by frequency multiplication of a highly stable frequency reference from the Frequency and Timing Subsystem (FTS), and the incoming downlink signal is heterodyned with this local oscillator. The Intermediate-Frequency (IF) signal that results is sent to the Signal Processing Center (SPC). Here, the Intermediate-frequency to Digital Converter (IDC) alters the frequency of the IF signal by a combination of up-conversion and down-conversion to a final analog frequency of approximately 200 MHz and then performs analog-to-digital conversion. The final analog stage of down-conversion uses a local oscillator supplied by the Channel-Select Synthesizer (CSS), that is also part of the Downlink Channel. The CSS is adjusted before the beginning of a pass to a frequency appropriate for the channel of the incoming downlink signal; during the pass, the frequency of the CSS remains constant. The frequency of the CSS (and, indeed, of all local oscillators in the analog chain of down-conversion) are synthesized within the Downlink Channel from highly stable frequency references provided by the FTS. The RRP accepts the digital signal and performs carrier, subcarrier, and symbol synchronization, Doppler compensation, and data demodulation (Reference 1). For purposes of telemetry, the output of the RRP is a stream of soft-quantized symbols, suitable for input to a decoder.

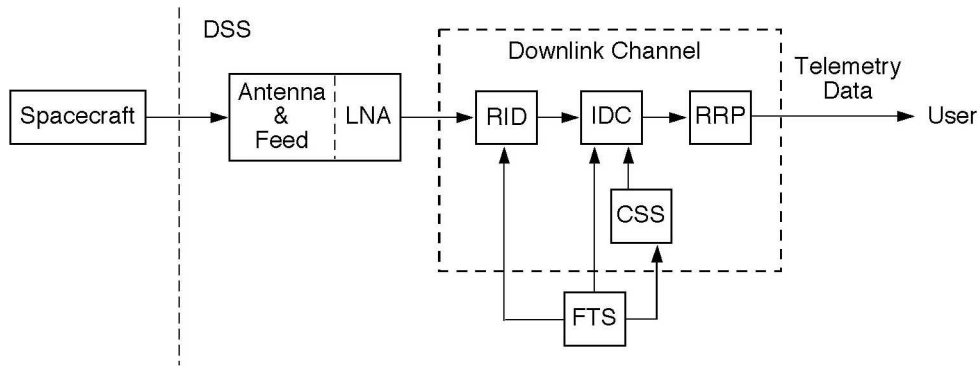


Figure 1. Receiver Architecture

## 2 Telemetry Capability

Table 1 shows the types of telemetry signals that can be tracked at the 34-m and 70-m stations. The new CCSDS bandwidth-efficient modulation schemes, which generally involve non-rectangular pulse shapes, are not shown. The Downlink Channel can, in fact, demodulate these new modulation schemes. However, there are large losses that result from using equipment that was designed for the optimum demodulation of rectangular pulse shapes to demodulate non-rectangular pulse shapes.

Table 1. Telemetry Capabilities

Parameter	Capabilities
Data Formats	NRZ (-L, -M, -N) Bi- $\phi$ (-L, -M, -N)
Modulation Types	Residual-carrier BPSK Suppressed-carrier BPSK QPSK, OQPSK
Subcarriers	Squarewave Sinewave
Symbol Rates	See Table 2
Carrier Loop Bandwidth	$B_L \leq 200$ Hz, residual carrier $B_L \leq \min(200 \text{ Hz}, R_{SYM}/20)$ , suppressed carrier
Loop Types	2, 3

## 2.1 Modulation

Both residual-carrier and suppressed-carrier binary phase-shift keying (BPSK) can be coherently demodulated. A suppressed carrier is tracked with a Costas loop (Reference 2). Both squarewave and sinewave subcarriers can be coherently demodulated. Non-Return to Zero (NRZ) and Bi- $\phi$  (i.e., bi-phase or Manchester) data formats are supported.

Table 2. Symbol Rates

Data Type	Symbol Rates
Residual-Carrier	
Subcarrier Present	$4 \text{ sps} \leq R_{SYM} \leq 0.67 f_{subcarrier}$
Direct Modulation	
NRZ	$4 \text{ sps} \leq R_{SYM} \leq 26 \text{ Msps}$
Bi- $\phi$	$4 \text{ sps} \leq R_{SYM} \leq 13 \text{ Msps}$
Suppressed-Carrier	
Subcarrier Present	$20B_L \leq R_{SYM} \leq 0.67 f_{subcarrier}$
Direct Modulation	
NRZ	$20B_L \leq R_{SYM} \leq 26 \text{ Msps}$
Bi- $\phi$	$20B_L \leq R_{SYM} \leq 13 \text{ Msps}$
QPSK or OQPSK	$40 \text{ ksps} \leq R_{QSYM} \leq 26 \text{ Msps}$

When the incoming carrier has a quadriphase shift keyed (QPSK) or Offset QPSK (OQPSK), with symbols on both the in-phase and quadrature components of the carrier, the Downlink Channel can synchronize to the carrier and coherently demodulate and detect the symbols on both of its components. The four-fold phase ambiguity that arises in QPSK needs to be resolved downstream in the telemetry decoding operation. In Table 2, the limits on symbol rate for QPSK and OQPSK are written in terms of the quaternary channel symbol rate,  $R_{QSYM}$ . For QPSK and OQPSK, the information bit rate is  $2rR_{QSYM}$ , where  $r$  is the code rate.

## 2.2 Symbol Rate

When tracking a residual carrier, the smallest symbol rate that can be used is 4 sps. When tracking a suppressed carrier, there is an additional constraint on the relationship between symbol rate  $R_{SYM}$  and carrier loop bandwidth  $B_L$  of the Costas loop.

$$\frac{R_{SYM}}{B_L} \geq 20, \quad \text{suppressed carrier} \quad (1)$$

The reason that suppressed-carrier BPSK has a different minimum symbol rate than does residual carrier has to do with the implementation of the Costas loop that tracks the suppressed carrier. The effective update rate of this loop is equal to the smaller of 2 kHz or the symbol rate. The update rate must be large relative to the loop bandwidth otherwise good tracking will not be obtained.

For QPSK and OQPSK, the minimum symbol rate given in Table 2 represents a recommended minimum. The Downlink Channel can demodulate symbol rates smaller than this minimum but with an additional performance degradation that increases as the symbol rate decreases. There is no good reason to use QPSK or OQPSK for these smaller symbol rates since other modulation schemes offer better performance at small symbol rates and there is no pressing need for bandwidth efficiency under these circumstances.

Paragraph 5.5 provides information on symbol synchronization. This includes an equation for the Signal-to-Noise Ratio (SNR) in the symbol loop and the required value of symbol loop SNR.

It is recommended that the symbol transition density be greater than or equal to 0.25. (It is 0.5 for truly random data.) When the symbol transition density is less than 0.25, more signal-to-noise ratio will be required for symbol synchronization.

The baseband telemetry bandwidth is 36 MHz (half-power, i.e., -3 dB). In the absence of a subcarrier, the maximum symbol rate that can be demodulated and detected is 26 Msps for NRZ data and 13 Msps for Bi- $\phi$  (Manchester) data. Other limitations on symbol rate arise in the telemetry processing stages that are downstream from the RRP. Module 206, Telemetry General Information, should be consulted for greater detail.

If the symbol rate is derived from the same frequency source as the subcarrier frequency (i.e., synchronous), it is recommended that there be at least three subcarrier cycles per data symbol. If the subcarrier and symbol rate are asynchronous, a subcarrier frequency to symbol rate ratio of greater than 1.5 is recommended. Furthermore, it is recommended that all proposed combinations of subcarrier frequency and symbol rate be tested to ensure efficient subcarrier demodulation. If the subcarrier and symbol rate are asynchronous, the frequency difference between the subcarrier and any of the first ten harmonics of the symbol rate should be greater than the bandwidth of the subcarrier loop.

### **2.3            *Carrier Loop Bandwidth***

In this module, carrier loop bandwidth means the one-sided, noise-equivalent carrier loop bandwidth of the receiver. It is denoted  $B_L$ . There are limits on the carrier loop bandwidth.  $B_L$  can be no larger than 200 Hz. The lower limit on  $B_L$  is determined by the phase noise on the downlink. In addition, when operating in the suppressed-carrier mode,  $B_L$  is subject to the constraint given in Equation (1).

In general, the value selected for  $B_L$  should be small in order to maximize the carrier loop signal-to-noise ratio. On the other hand,  $B_L$  must be large enough that neither of the following variables becomes too large:

- a) The static phase error due to Doppler dynamics,
- b) The contribution to carrier loop phase error variance due to phase noise on the downlink.

The best  $B_L$  to select will depend on circumstances. Often, it will be possible to select a  $B_L$  of less than 1 Hz. A larger value for  $B_L$  is necessary when there is significant uncertainty in the downlink Doppler dynamics, when the Sun-Earth-probe angle is small (so that solar coronal phase scintillations are present on the downlink), or when the spacecraft transmitter (such as an auxiliary oscillator) has relatively poor frequency stability.

When tracking a spinning spacecraft, it may be necessary to set the carrier loop bandwidth to a value that is somewhat larger than would otherwise be needed. The loop bandwidth must be large enough to track out the variation due to the spin. Also, the coherent AGC in the receiver must track out the amplitude variations (Coherent AGC bandwidth is one-tenth of the carrier loop bandwidth).

The user may select either a type 2 or type 3 carrier loop. Both loop types are perfect, meaning that the loop filter implements a true accumulation.

### **3**            *Definitions*

When a subcarrier is present, the modulation index of the data on the subcarrier is normally  $90^\circ$  so there is no residual subcarrier. There is no performance advantage to using a residual subcarrier since the Downlink Channel was designed to track the data and ignores the presence or absence of a residual subcarrier. Throughout this document, it is assumed that the modulation index of data onto the subcarrier is  $90^\circ$  and all subsequent references to modulation index refer to the modulation index of the carrier.

A residual carrier is present in each of the following cases:

- a) With no subcarrier, the modulation index is less than or equal to  $80^\circ$ ,
- b) With a squarewave subcarrier, the modulation index is less than  $80^\circ$ ,
- c) With a sinewave subcarrier, the peak modulation index is less than  $105^\circ$ .

The carrier is considered to be suppressed when the modulation is BPSK and there is either no subcarrier or a squarewave subcarrier and the modulation index is greater than  $80^\circ$ .

$P_T$  is the total received signal power at the input to the low-noise amplifier.  $N_0$  is the one-sided noise spectral density referenced to the input to the low-noise amplifier. It equals the system noise temperature (referenced to the input to the low-noise amplifier) times

Boltzmann's constant,  $1.380622 \times 10^{-23}$  W/(Hz·K). In decibel units, Boltzmann's constant is  $-198.6$  dBm/(Hz·K). The ratio  $P_T / N_0$  is a useful parameter.

When there is only a single telemetry channel present and no ranging modulation, the carrier power  $P_C$  and data power  $P_D$  are given by

$$P_C = \begin{cases} P_T \cos^2 \theta, & \text{no subcarrier or squarewave subcarrier} \\ P_T J_0^2(\theta), & \text{sinewave subcarrier} \end{cases} \quad (2)$$

$$P_D = \begin{cases} P_T \sin^2 \theta, & \text{no subcarrier or squarewave subcarrier} \\ P_T 2J_1^2(\theta), & \text{sinewave subcarrier} \end{cases} \quad (3)$$

where  $\theta$  is the peak modulation index and  $J_0$  and  $J_1$  are Bessel functions of the first kind of orders zero and one. In the case of a sinewave subcarrier, the Downlink Channel uses the power in the fundamental harmonics (upper and lower) of the subcarrier and does not use the power in the higher-order harmonics. In this case,  $P_D$  represents the power in just these harmonics.

When there is only a single suppressed carrier and there is no ranging modulation present, the total received signal power and the data power are the same.

$$P_D = P_T, \quad \text{suppressed carrier} \quad (4)$$

If two telemetry channels are present, or if one telemetry channel and a ranging code are present, more complicated expressions are needed. For example, with two telemetry channels, each of which has a squarewave subcarrier (or one with no subcarrier and one with a squarewave subcarrier), the carrier and data powers are given by

$$P_C = P_T \cos^2 \theta_1 \cos^2 \theta_2 \quad (5)$$

$$P_{D1} = P_T \sin^2 \theta_1 \cos^2 \theta_2 \quad (6)$$

$$P_{D2} = P_T \cos^2 \theta_1 \sin^2 \theta_2 \quad (7)$$

where  $P_{D1}$  and  $P_{D2}$  are the data powers for the first and second telemetry channels, and  $\theta_1$  and  $\theta_2$  are the corresponding modulation indices.

If ranging modulation is present on the downlink carrier, then the equations for residual-carrier power and data power need to be adjusted to reflect the fact that some of the downlink power is being allocated to ranging signal and noise that is present in the transponder ranging channel. The proper equations to use depend on the type of ranging signal. With sequential ranging, the equations are given in Reference 3.

The input energy per bit to noise spectral density ratio (bit SNR) is

$$\frac{E_b}{N_0} = \frac{P_D}{N_0 R_{BIT}} \quad (8)$$

where  $R_{BIT}$  is the bit rate (before encoding). The energy per symbol to noise spectral density ratio (symbol SNR) is

$$\frac{E_S}{N_0} = \frac{P_D}{N_0 R_{SYM}} \quad (9)$$

where  $R_{SYM}$  is the symbol rate (after encoding). For a convolutional code with code rate  $r$  ( $r=1/2, 1/4, \text{ or } 1/6$ ),

$$R_{SYM} = \frac{R_{BIT}}{r} \quad (10)$$

## 4 Receiver Acquisition

The following paragraphs describe normal receiver acquisition. There is also a Fast Acquisition algorithm, which is applicable to telemetry with low symbol rates. Fast Acquisition, which is similar in many respects to normal acquisition, has been described in Reference 4. Guidelines for estimating the receiver acquisition times are given in this section. These guidelines apply to residual carrier and suppressed-carrier BPSK. QPSK and OQPSK normally are used only for high data rates that have very short acquisition times.

The general procedure for normal acquisition is as follows. The carrier frequency is measured by searching the downlink signal spectrum in fixed bandwidth sections using a fast Fourier transform (FFT). This is true for both suppressed-carrier downlinks and residual-carrier downlinks. With a suppressed carrier, some signal processing that precedes the FFT causes a collapse of data modulation sidebands into a tone (located at the frequency of the phantom carrier) that can be identified by the FFT. Once a tone is found, FFTs are optionally computed for the adjacent bandwidth sections in order to verify that the true tone was found, as opposed to an alias from one of these adjacent bandwidth sections. Then a confirmation FFT, centered at the detected tone, may be computed if it is thought necessary to verify that the tone was not a strong signal that was just passing through. Such a set of FFTs produces an accurate measure of the carrier frequency.

When necessary, a set of FFTs can also be computed for determining the subcarrier frequency and symbol rate. Sometimes however, it is not necessary to measure the subcarrier frequency and symbol rate, since their predicts are usually quite accurate. Next, the numerically controlled oscillator (NCO) in the carrier loop is set with the aid of the information from the FFTs, and the carrier loop is closed (enabled). In the subcarrier loop and symbol loop, the NCOs are set and the loops closed (enabled). The loop closures may be selected to occur in parallel or in series. When the loops are initially closed, the loop gain normalizations are set in

accord with available predictions; but when phase-lock is indicated by the lock detectors, the coherent AGCs are enabled, allowing loop gain normalizations to be based on the actual received signal. This means that the power predicts are only required for acquisition.

#### 4.1 *FFT*

The FFT is an optional part of the acquisition process. It is only needed when the signal's frequency uncertainty is greater than one-half the initial loop bandwidth of the tracking loop. Often, only the carrier loop requires the computation of FFTs. The subcarrier and symbol frequencies are usually well enough known that they need not be measured with FFTs.

An FFT takes a sequence of data points as its input. The sample frequency of these data points, here denoted  $f_s$ , depends in general on the type of data being processed and the symbol rate. Permissible values of  $f_s$  are given in Table 3.  $R_{SYM}$  is the symbol rate and  $R_{QSYM}$  is the quaternary channel symbol rate for QPSK/OQPSK.

For the residual-carrier FFT,  $f_s$  is independent of the tracking loop update rate and is selectable by the user from one of the values given in Table 3. (The most commonly used values are 10 kHz, 50 kHz, and 100 kHz.)

For the suppressed-carrier FFT,  $f_s$  is selectable by the user from the same set of values as for the residual-carrier case. However,  $f_s$  cannot exceed the symbol rate,  $R_{SYM}$ .

For the QPSK/OQPSK FFT,  $f_s$  is selectable by the user from the same set of values as for the residual-carrier case. However,  $f_s$  cannot exceed the symbol rate,  $R_{QSYM}$ .

Table 3. FFT Sample Frequencies

<b>Data Type</b>	<b>Sample Frequency</b>
Residual Carrier	2, 5, 10, 20, 50, 100, 200, 500, 1000, or 2000 kHz
Suppressed Carrier	Same as above if $f_s < R_{SYM}$ ; else $R_{SYM}$
QPSK and OQPSK	Same as above if $f_s < R_{QSYM}$ ; else $R_{QSYM}$
Subcarrier	minimum of 500 Hz and $R_{SYM}$
Symbol	minimum of 500 Hz and $R_{SYM}$

In general, a number of FFTs may need to be computed before the signal is found. The search bandwidth is explored in sections, with one FFT computed for each section. A section is selected by an appropriate setting of the NCO. This setting determines the center of the section. The bandwidth of each section is determined by the data type and by  $f_s$ , as shown in Table 4.

Table 4. FFT Section Bandwidths

Data Type	Section Bandwidth	Section Bandwidth Limits
Residual Carrier	$f_s$	$-f_s/2 \rightarrow +f_s/2$
Suppressed Carrier	$f_s/2$	$-f_s/4 \rightarrow +f_s/4$
QPSK and OQPSK	$f_s/4$	$-f_s/8 \rightarrow +f_s/8$
Subcarrier	$f_s/2$	$-f_s/4 \rightarrow +f_s/4$
Symbol	$f_s/2$	$-f_s/4 \rightarrow +f_s/4$

The tone representing the carrier (or subcarrier or symbol rate) will be considered detected within a given section when the corresponding FFT indicates the presence of a tone for which the power level falls within an acceptance range centered on the predicted tone power. The acceptance range is characterized by a lower limit delta,  $\delta_{lower}$  in decibels and an upper limit delta,  $\delta_{upper}$  in decibels. The user will select the two parameters  $\delta_{lower}$  and  $\delta_{upper}$ .

Even after a tone is initially detected, more FFTs will, in general, be computed. An FFT for each of two adjacent sections is computed in order to check for aliases. Such an alias check is, however, optional; if the frequency predictions are quite good, the alias checks are unnecessary.

There is also an optional confirmation check. This consists of one FFT that is computed with the NCO set to the tone value detected in the previous FFTs. It is used to verify that the detected tone was not a noise spur (for weak signal acquisitions) and that the tone was not a very strong signal that was simply passing through.

The number of data points that should be selected for input to a particular FFT computation will depend on the predicted tone power. The algorithm that should be used in determining the number of data points is summarized here.

$$\text{Number of Data Points} = 2^M \tag{11}$$

$M$ , the base 2 logarithm of the number of data points, is given by

$$M = \max \left\{ 9, \left\lceil 4.817 - 3.581 \cdot \log_{10} \left( \frac{P_{CTP}}{N_0} \cdot \frac{1}{f_s} \right) \right\rceil \right\} \tag{12}$$

where  $\log_{10}(\ast)$  is the base 10 logarithm and  $\lceil \cdot \rceil$  is the ceiling function. The ceiling function equals the smallest integer not less than its argument. The smallest permissible value for  $M$  is 9, corresponding to  $2^9$  (512) data points.  $P_{CTP}/N_0$  is the computed tone power to noise spectral density ratio as calculated with Equation (13) for residual-carrier FFT or with Equation (14) for all other FFTs (see below). Figures 2 and 3 illustrate the dependence of the integer  $M$  on  $P_{CTP}/N_0$  for  $f_s = 2000$  Hz and  $f_s = 20$  Hz, respectively.

For the FFT that measures the carrier frequency of a residual-carrier downlink,  $P_{CTP}/N_0$  is given by

$$\frac{P_{CTP}}{N_0} = \left( 10^{\delta_{lower}/10} \right) \cdot \frac{P_C}{N_0} \cdot \text{sinc}^2 \left( \frac{1}{2F_{ZP}} \right), \quad \text{residual - carrier FFT} \quad (13)$$

where  $\delta_{lower}$  is a (negative) number representing the delta, in decibels, between the lower limit on acceptance and the predicted tone power level.  $P_C/N_0$  is the residual carrier power-to-noise spectral density ratio. The  $\text{sinc}(\ast)$  function is:  $\text{sinc}(x) = \sin(\pi x)/(\pi x)$ .  $F_{ZP}$  is the zero pad factor. When  $F_{ZP} = 1$ , there is no zero padding in the FFT. When  $F_{ZP} = 2$ , there are as many zeros padded to the end of the data points as there are data points. The size of the sequence that is input to the FFT equals  $F_{ZP}$  times the number of data points.

For all other FFTs (i.e., for all FFTs except that for the carrier frequency of a residual-carrier downlink),  $P_{CTP}/N_0$  is given by

$$\frac{P_{CTP}}{N_0} = \left( 10^{\delta_{lower}/10} \right) \cdot \frac{R_{SYM}(E_S/N_0)}{\alpha_1 + \alpha_2(E_S/N_0)^{-1}} \cdot \frac{P_C}{N_0} \cdot \text{sinc}^2 \left( \frac{1}{2F_{ZP}} \right), \quad \text{all other FFTs} \quad (14)$$

where  $R_{SYM}$  is the symbol rate, and  $E_S/N_0$  is the predicted energy per symbol to noise spectral density ratio. The coefficients  $\alpha_1$  and  $\alpha_2$  depend on the particular FFT. Table 5 lists these values. For example, for an FFT that is computed in order to identify the symbol rate, the coefficients  $\alpha_1$  and  $\alpha_2$  are 390 and 880, respectively, when there is a squarewave subcarrier present. For all loops besides the residual-carrier loop, the data modulation sidebands are employed. That is the reason Equation (14) is more complicated than Equation (13). Equation (14) is valid under the assumption that all loops are slipping (i.e., that none of the loops have acquired phase-lock) as the data points are being collected. If some loops have acquired phase-lock before the data points are collected for subsequent FFTs, then the  $P_{CTP}/N_0$  given in Equation (14) will be somewhat pessimistic for these subsequent FFTs. Equations (13) and (14) are based on modifications to the theory presented in Reference 4. (The modifications are necessary since the theory of Reference 4 is for the Fast Acquisition algorithm, which is not described in this module.)

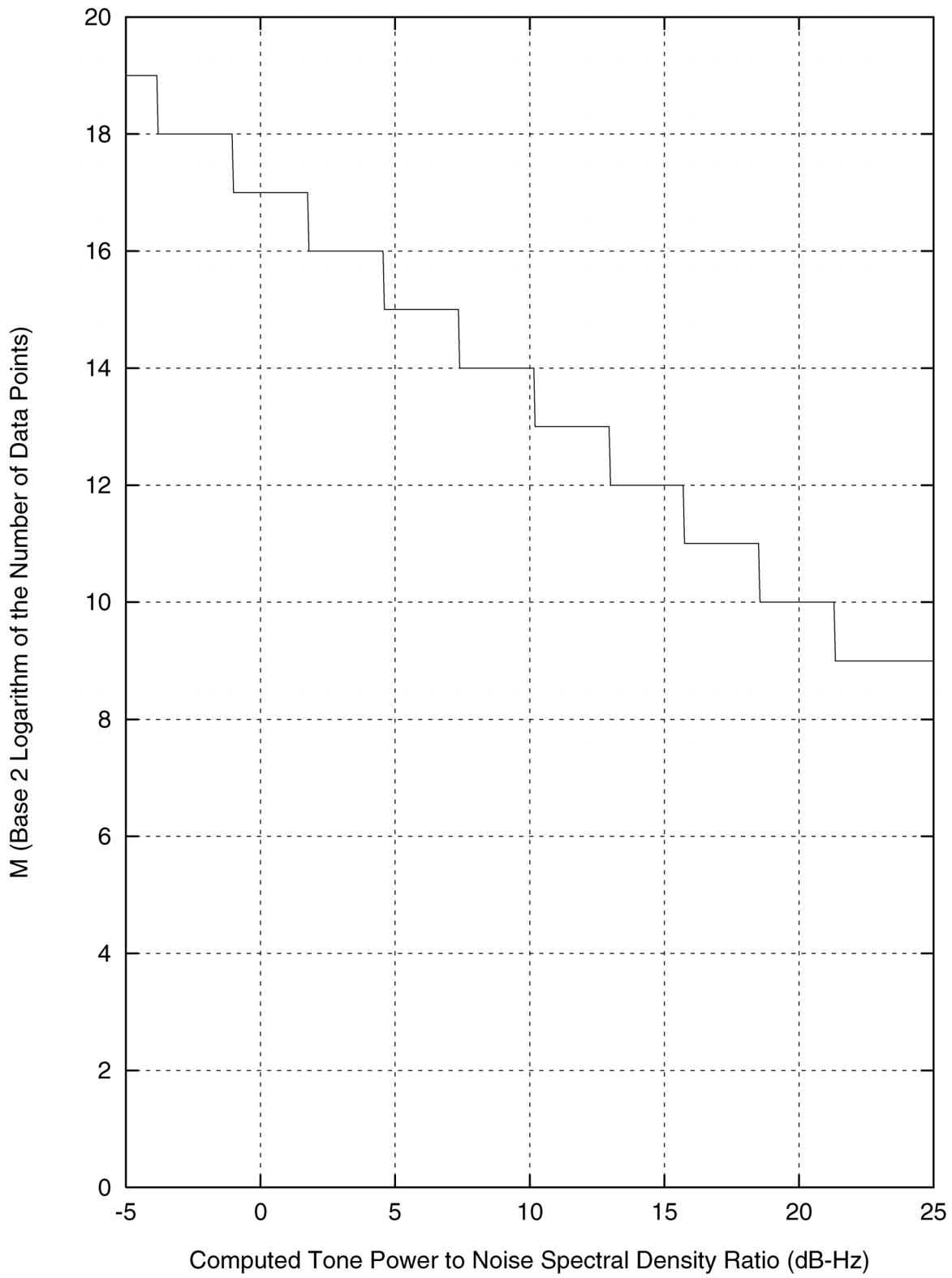


Figure 2. Number of Data Points for FFT; Sample Rate = 2000 Hz

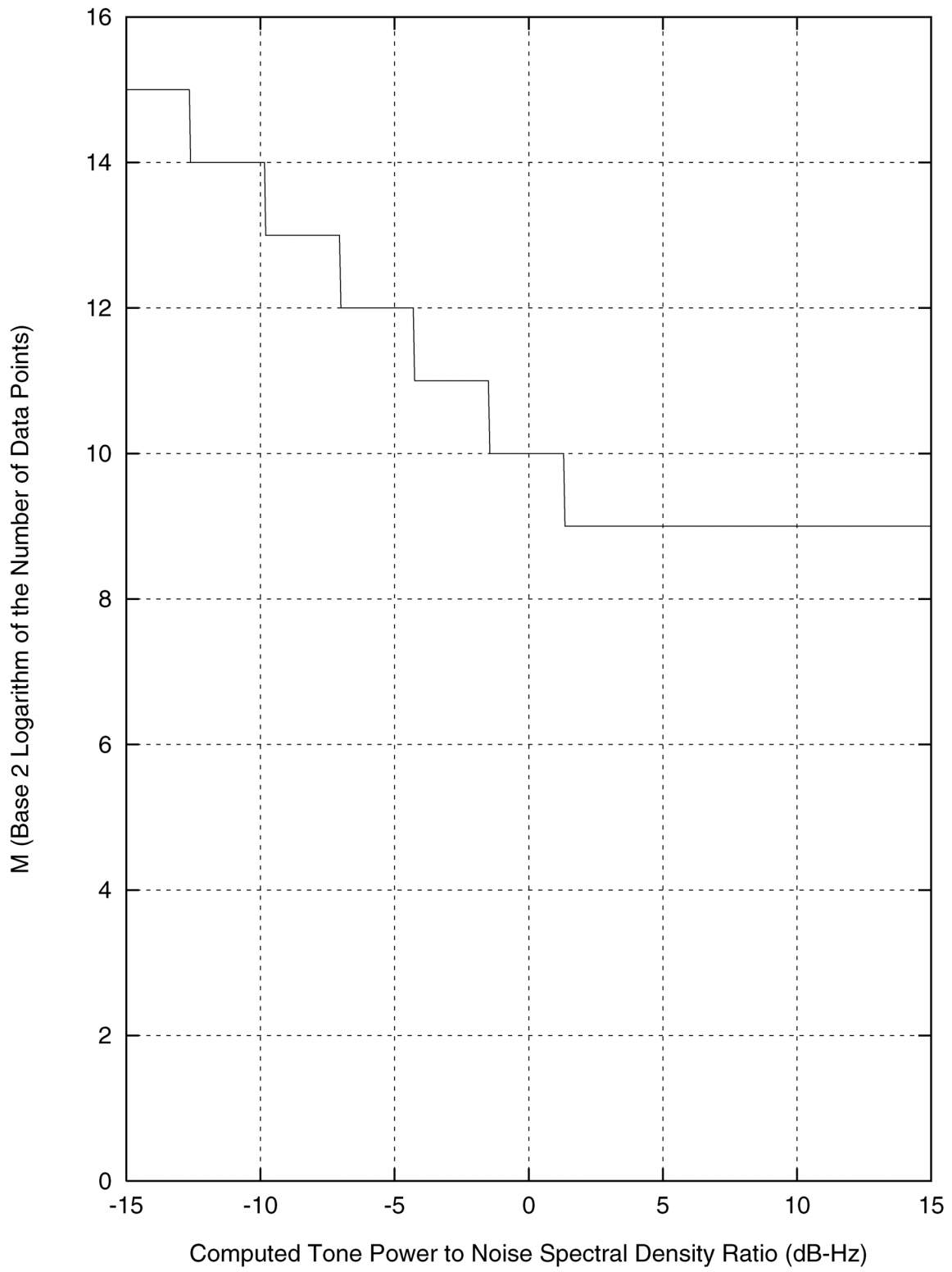


Figure 3. Number of Data Points for FFT; Sample Rate = 20 Hz

Table 5. Coefficients  $\alpha_1$  and  $\alpha_2$  in the Calculation of  $P_{CTP}/N_0$

FFT	Subcarrier	$\alpha_1$	$\alpha_2$
Suppressed Carrier	none	6	4.5
Suppressed Carrier	square	18	41
QPSK and OQPSK	none	46	145
Subcarrier	square	18	41
Subcarrier	sine	12	18
Symbol	none	130	100
Symbol	square	390	880
Symbol	sine	260	390

## 4.2 Loop Locking

Once the carrier frequency has been found, the NCO in the carrier loop is set to the detected frequency and the carrier loop is closed (enabled). The loop starts at an initial bandwidth. The loop phase error, initially large, diminishes with time through the natural feedback action of the loop. Once phase-lock is declared at this bandwidth, the loop bandwidth is gradually reduced to its final value — the desired operational value — in a manner consistent with the retention of phase-lock. When the final bandwidth has been achieved and the degradation to effective signal level resulting from transient phase errors just drops below 0.1 dB, the loop is considered to be acquired. The initial and final bandwidths are controlled by the user, as are the parameters that control the rate at which the bandwidth is narrowed. Starting with loop closure, the time it takes for the lock detector to indicate phase-lock at the final bandwidth is approximately ten times the reciprocal of the final bandwidth. For purposes of estimating acquisition time, however, it is recommended that twenty times the reciprocal of the final loop bandwidth be used. This admits the possibility that phase-lock is not indicated in the first lock detection period. The final step in the procedure is for the coherent AGC loop to be enabled, providing an accurate estimate of the loop normalization constant.

The locking of the subcarrier and symbol loops is a similar process to that described in the previous paragraph for the carrier loop. The subcarrier and symbol loops may either be closed (enabled) at the same time that the carrier loop is closed (enabled) or be closed after the carrier loop has indicated phase-lock. It is the user's choice. In the former case, all three loops are simultaneously trying to achieve phase-lock. For the (squarewave) subcarrier and symbol loops, there is also a transition window, which has an initial value, a final value, and a parameter that controls the rate of narrowing.

### 4.3 *Acquisition Time*

The total receiver acquisition time is estimated as a sum of two components: the time required for the FFT stage of the acquisition process and the time required for locking the loops.

There is a time associated with the collection of enough data points as required for each FFT. For a given FFT, this time equals the number of data points divided by the sample frequency.

$$\text{Time for each FFT} = \frac{2^M}{f_S} \quad (15)$$

where  $M$  is given by Equation (12). For the carrier FFT, the time required to actually compute an FFT is often small compared with the time it takes to collect the data points for input to that FFT. (The time it takes to pad an input sequence with zeros is also small.) Hence, it is often a good approximation to use Equation (15) to estimate the time it takes to produce one FFT.

It is necessary to consider how many FFTs might be required and to sum together the individual FFT times in order to estimate the time spent on the FFT stage of the acquisition process. Consideration must be given to whether subcarrier or symbol FFTs will be required. Often, it is not necessary to compute FFTs in support of subcarrier and symbol acquisition. In the best possible scenario, in which carrier frequency, subcarrier frequency and symbol rate are all very accurately characterized by predicts, no FFTs are required. In a more typical scenario, however, at least two FFTs will be required for the carrier: an initial FFT and a confirmation FFT. In some cases, more FFTs will be required for carrier acquisition: the search bandwidth may be larger than a single section bandwidth and alias checking may be required.

A second component of receiver acquisition time is the time required for the loops to lock once their NCOs have been set. For each loop, phase-lock will be achieved and duly indicated by the lock detector in a time that may be estimated as

$$\text{Time for each loop} = \frac{20}{B} \quad (16)$$

where  $B$  represents the final loop bandwidth of the loop in question (carrier, subcarrier, or symbol). The numerator in this estimate is twenty, rather than ten, allowing for the possibility that phase-lock is not indicated in the first lock detection period. Figure 4 illustrates this dependence. If the loops are acquired in parallel, the loop-locking component of receiver acquisition time may be estimated from Equation (16) with the smallest of all loop bandwidths substituted for  $B$ . Typically, the smallest loop bandwidth is that of the symbol loop. If the loops are acquired in series, the loop-locking component of receiver acquisition time may be estimated as the sum of the individual loop-locking times, each of which may be estimated from Equation (16) with the substitution of the appropriate loop bandwidth. In general, the following factors will influence the user's choice of loop bandwidths:  $P_T/N_0$ , Doppler dynamics, oscillator stability, and acquisition time. For example, larger values of  $P_T/N_0$  will permit larger loop bandwidths (for more details, see paragraph 5).

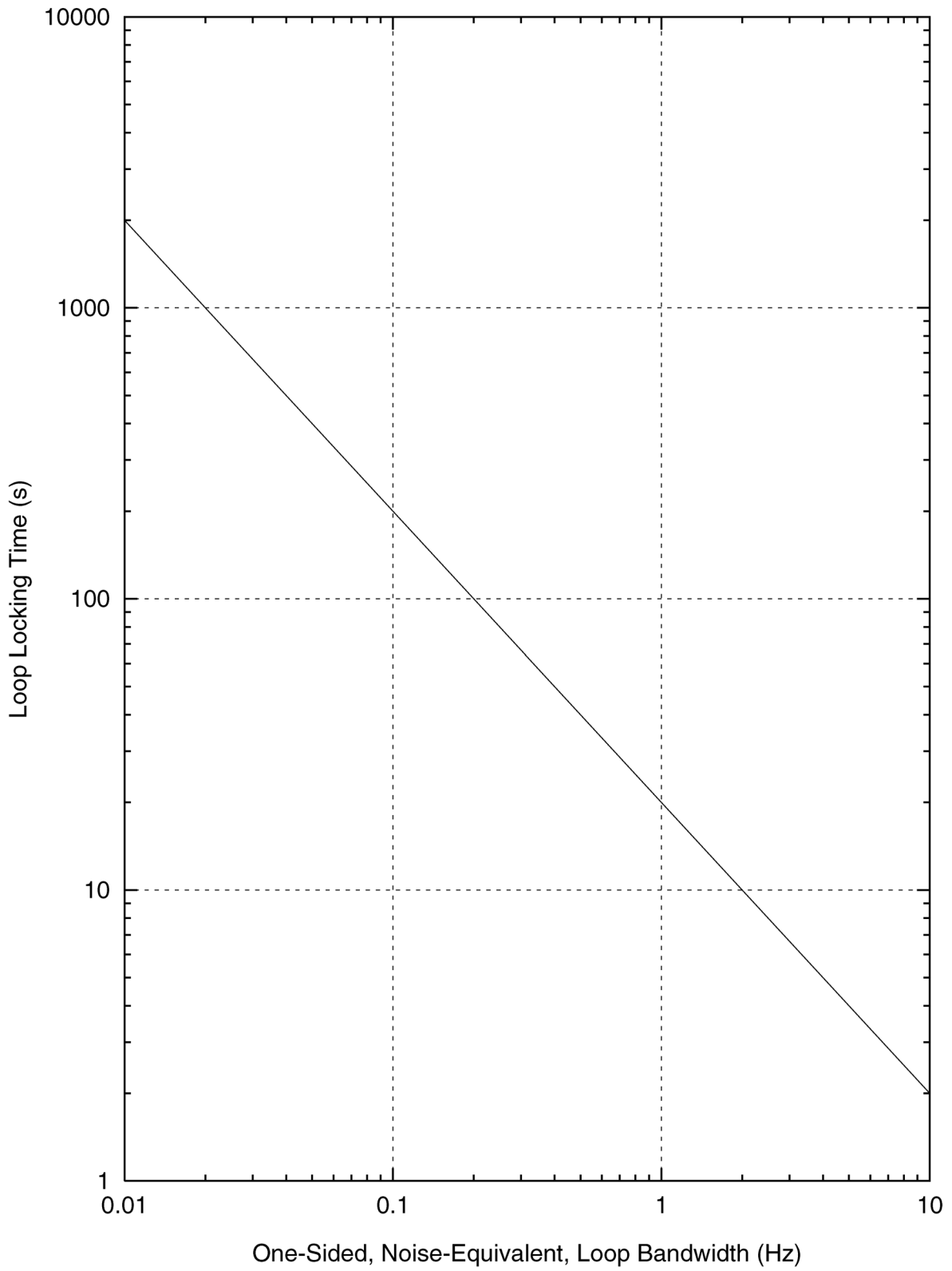


Figure 4. Loop Locking Time

For many applications, the receiver acquisition time will be one minute or less. This will be particularly true when the symbol rate is large and no particularly narrow loop bandwidths are employed. In such cases, it will not be necessary to estimate beforehand the receiver acquisition time. In other cases, particularly for small symbol rates and narrow loop bandwidths, it will take several minutes to accomplish receiver acquisition; and it may be important to characterize the receiver acquisition time with some degree of accuracy. Under such circumstances the discussion and equations of this paragraph should be used as a guide.

It would be very difficult to provide here a set of curves characterizing receiver acquisition time for all potential cases of interest. There are just too many possibilities. Not only are there a number of important variables (symbol rate, signal-to-noise ratio, loop bandwidths, quality of frequency predictions) with large dynamic ranges, but the flexibility of the Downlink Channel permits a wealth of different acquisition strategies. Alias-check FFTs and confirmation-check FFTs may or may not be used. Subcarrier FFTs and symbol rate FFTs may or may not be used. The loops may be acquired in parallel, in series, or in some other combination. (For example, the carrier loop might be acquired first, then the subcarrier and symbol loops might be acquired in parallel.) Although it is not practical to provide curves for all potential cases of interest, three sets of curves are provided in order to illustrate how receiver acquisition time varies with certain key parameters.

Figures 5, 6, and 7 show receiver acquisition time for a very specific set of assumptions. For all three of these figures, the frequency predicts are good enough that only two carrier FFTs (an initial FFT and a confirmation-check FFT) are necessary and that no subcarrier or symbol rate FFT is required. Furthermore, it is assumed that the loops are acquired in parallel. For these figures the receiver acquisition time is calculated as twice the "Time for each FFT", as given by Equation (15), plus  $20/B$ , where  $B$  is the smallest loop bandwidth (typically the symbol loop bandwidth). The integer  $M$  in Equation (15) is calculated from Equations (12) and (13) or (14).  $F_{ZP}$  is taken to be 1 (i.e., no zero padding) and  $\delta_{lower}$  taken to be  $-2$  dB.

Figure 5 shows the receiver acquisition time (in seconds) for a residual-carrier downlink as a function of  $P_C/N_0$  with  $B$ , the smallest loop bandwidth, as a parameter. The frequency predicts have to be reasonably good to achieve the acquisition times shown in this figure: the carrier must lie within the section bandwidth of the first FFT and the subcarrier frequency and symbol rate must be well enough known to obviate the need for their measurement.

Figure 6 shows the receiver acquisition time (in seconds) for a suppressed-carrier downlink as a function of  $R_{SYM}$  with  $B$ , the smallest loop bandwidth, as a parameter. The energy per symbol to noise spectral density ratio is  $-3$  dB. The frequency predicts have to be reasonably good to achieve the acquisition times shown in this figure: the collapsed carrier tone must lie within the section bandwidth of the first FFT, and the subcarrier frequency and symbol rate must be well enough known to obviate the need for their measurement.

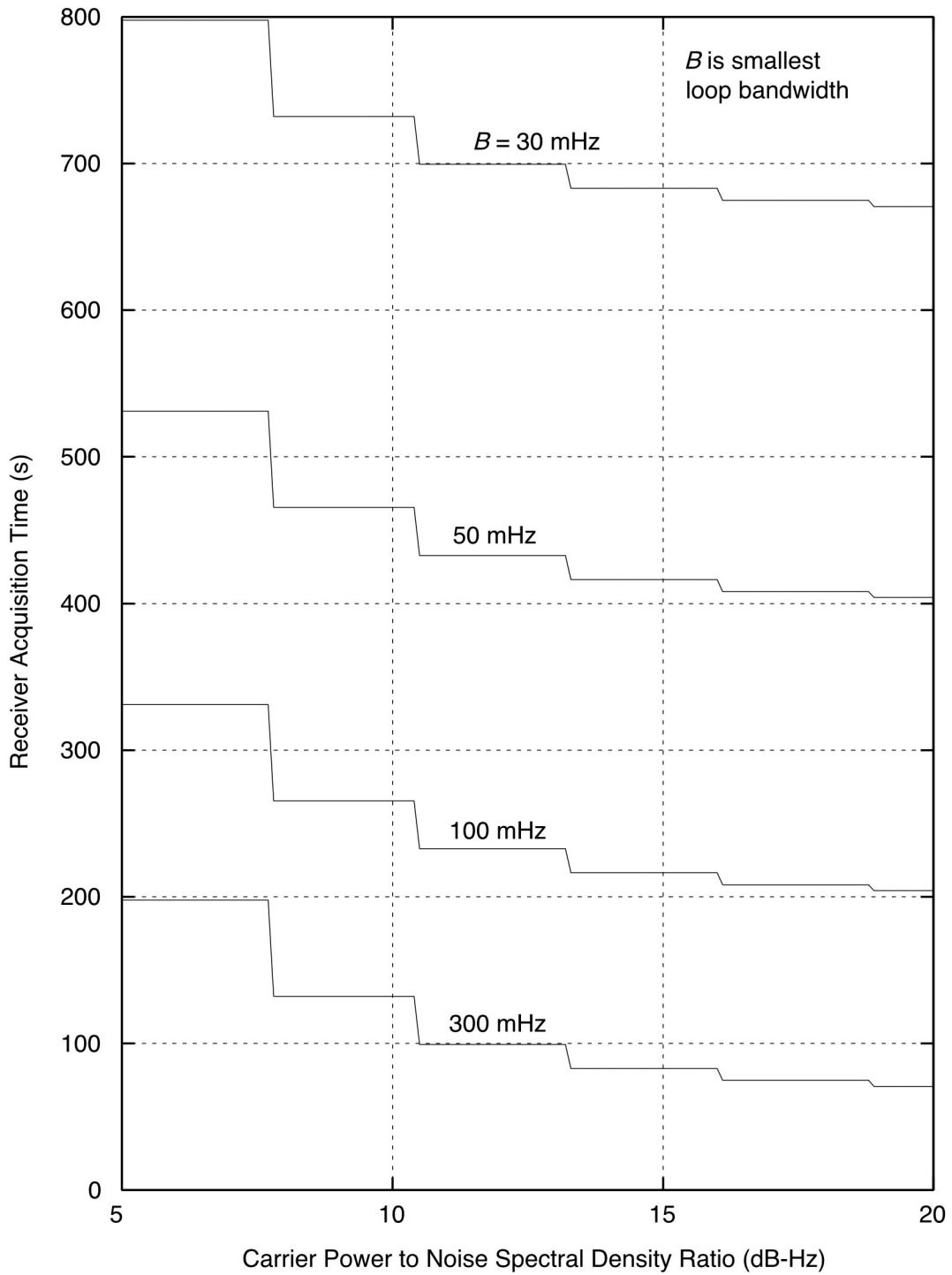


Figure 5. Receiver Acquisition Time; Residual Carrier

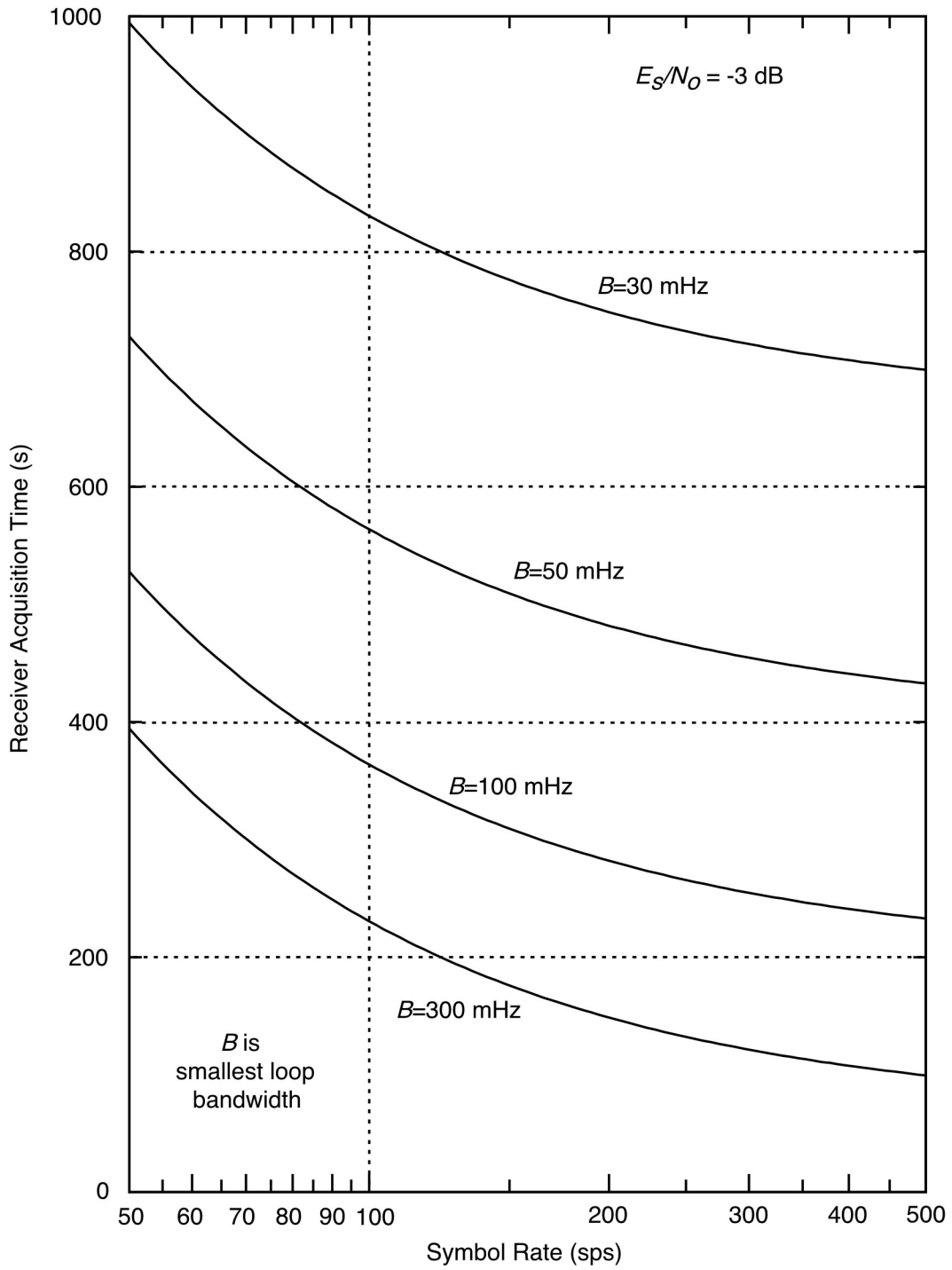


Figure 6. Receiver Acquisition Time; Suppressed Carrier,  $E_s/N_0 = -3$  dB

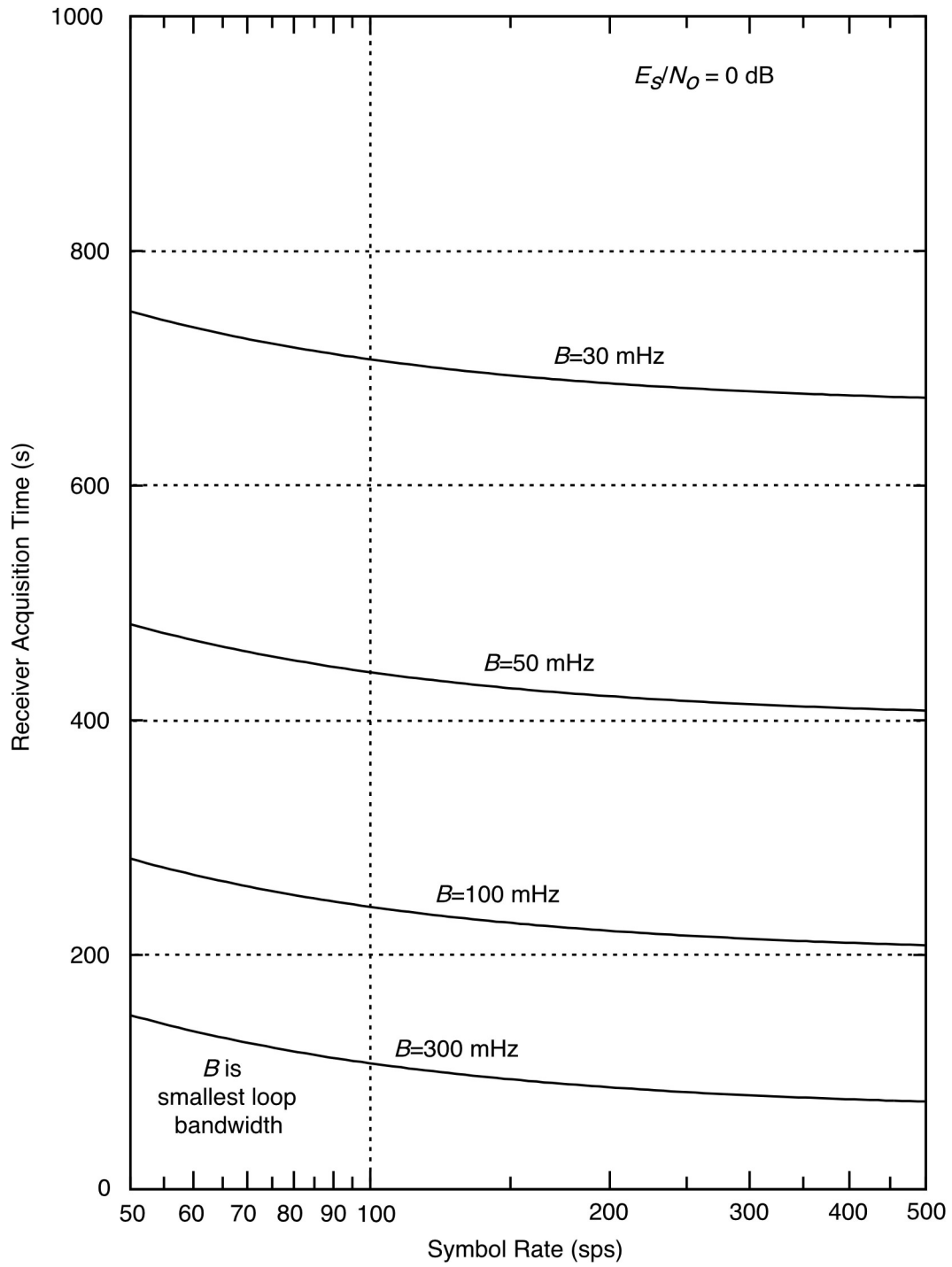


Figure 7. Receiver Acquisition Time; Suppressed Carrier,  $E_s/N_0 = 0$  dB

Figure 7 shows the receiver acquisition time (in seconds) for a suppressed-carrier downlink as a function of  $R_{SYM}$  with  $B$ , the smallest loop bandwidth, as a parameter. The energy per symbol to noise spectral density ratio is 0 dB. The frequency predicts have to be reasonably good to achieve the acquisition times shown in this figure: the collapsed carrier tone must lie within the section bandwidth of the first FFT, and the subcarrier frequency and symbol rate must be well enough known to obviate the need for their measurement.

A comparison of Figures 5, 6, and 7 reveals that the receiver acquisition time increases as the symbol rate decreases, the signal-to-noise ratio decreases, or the loop bandwidths decrease. Also, the receiver acquisition time for suppressed-carrier operation will generally be larger than for residual-carrier operation.

## 5 *Telemetry Performance*

In general, four signal-to-noise ratios affect telemetry performance: the energy per bit to noise spectral density ratio and the signal-to-noise ratios in each of the three synchronization loops (carrier, subcarrier, and symbol). In some cases (especially with a suppressed carrier) there will be no subcarrier present. In order for telemetry to be supported at a given bit rate,  $P_T/N_0$  must be large enough that these four (or three, if there is no subcarrier) signal-to-noise ratios are adequate. The following paragraphs offer guidance in this matter.

### 5.1 *Comparison of Residual Carrier and Suppressed Carrier*

The relative telemetry performance of residual-carrier operation and suppressed-carrier operation depends strongly on the bit rate. One scheme is said to have better telemetry performance than the other when it has a smaller required  $P_T/N_0$  for the support of a given bit rate at a given threshold FER. In general, residual carrier has the better telemetry performance for the very low bit rates and especially for low bit rates coupled with larger carrier loop bandwidths (as would be necessary in the presence of significant phase noise or uncompensated Doppler dynamics). For intermediate bit rates, suppressed carrier offers a significant telemetry performance advantage over residual carrier. For high bit rates, suppressed carrier offers a telemetry performance advantage, but it is only about 0.1 dB. Of course, there will be times in which the decision between residual carrier and suppressed carrier is made on grounds having nothing to do with telemetry performance. For example, a residual carrier is sometimes needed for a radio science experiment. Also, in some applications it will important to minimize acquisition time. Then, the choice of residual carrier or suppressed carrier will be based on whichever scheme offers the quicker acquisition.

Figure 8 shows a typical case. It compares the required  $P_T/N_0$  as a function of bit rate  $R_{BIT}$  for residual-carrier and suppressed-carrier operation in the case where a (1784, 1/3) turbo code is employed and the threshold FER is  $1 \times 10^{-4}$ . Three carrier loop bandwidths are considered: 0.5 Hz, 1 Hz, and 2 Hz.

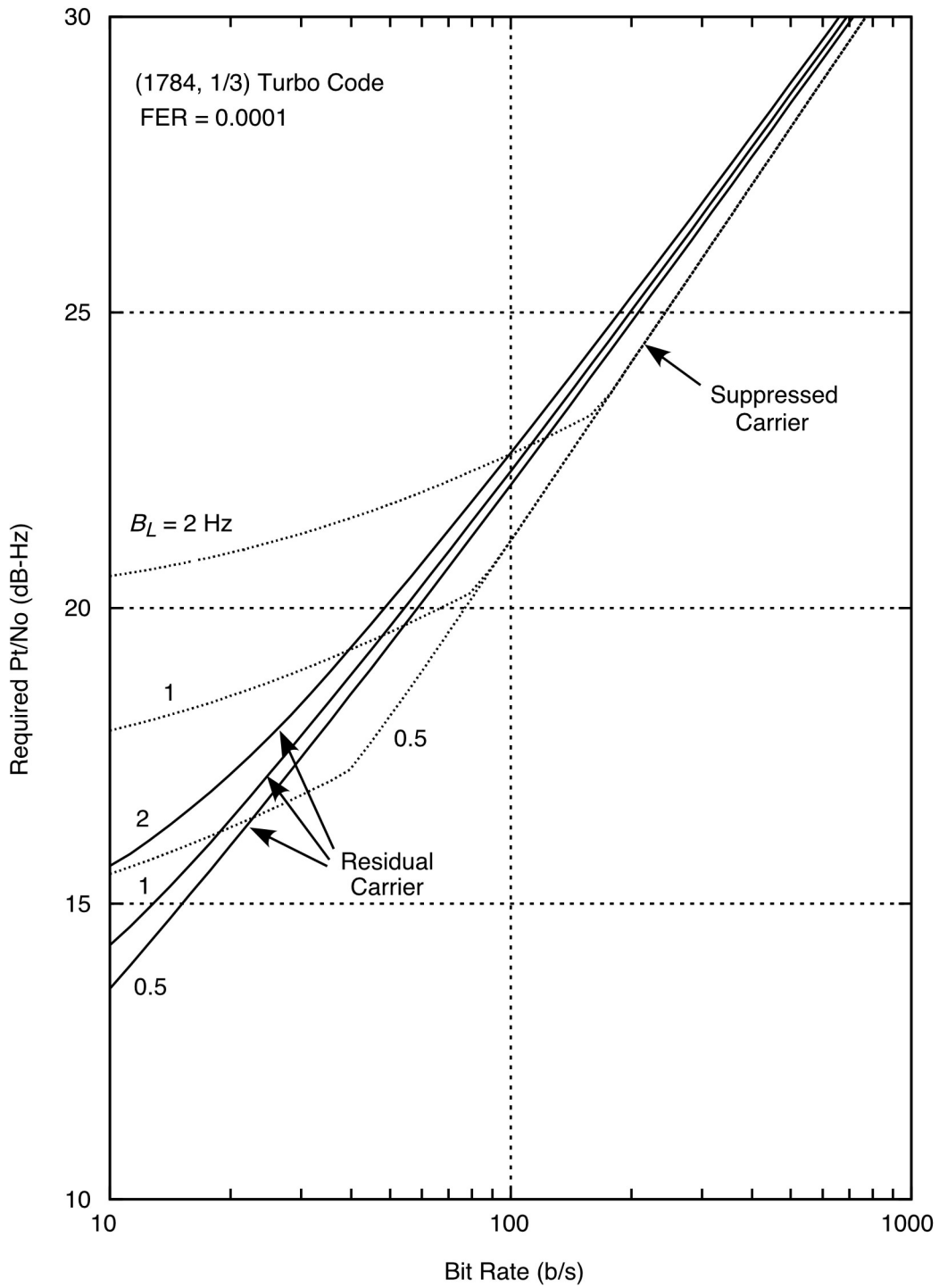


Figure 8. Comparison of Residual Carrier and Suppressed Carrier

For Figure 8, it has been assumed that there is no additional phase noise present in the carrier loop beyond that resulting from thermal noise. The required  $P_T/N_0$  is, in this case, the minimum  $P_T/N_0$  that simultaneously meets each of the following four constraints. First, the carrier loop signal-to-noise ratio ( $\rho_L$ , see paragraph 5.3) must be at least 10 dB if tracking a residual carrier or at least 17 dB if tracking a suppressed carrier. Second, the squarewave subcarrier loop signal-to-noise ratio ( $\rho_{SUB}$ , see paragraph 5.4) must be at least 20 dB. Third, the symbol loop signal-to-noise ratio ( $\rho_{SYM}$ , see paragraph 5.5) must be at least 15 dB. Fourth, the product  $\eta_{SYS} \cdot E_b/N_0$  must be at least 0.8 dB, where  $\eta_{SYS}$  is system loss. For each residual-carrier performance curve, it is assumed that at each point on the curve the optimum modulation index is used. The subcarrier loop bandwidth and window factor are assumed to be 50 mHz and 0.25, respectively. The symbol loop bandwidth and window factor are assumed to be 50 mHz and 0.25, respectively.

For the case represented in Figure 8 with  $B_L = 0.5$  Hz, residual carrier offers better telemetry performance than suppressed carrier for bit rates less than 20 bps, and suppressed carrier is better for bit rates greater than 20 bps. With  $B_L = 1$  Hz, the performances of residual carrier and suppressed carrier cross at 50 bps. With  $B_L = 2$  Hz, they cross at 100 bps. These numbers are specific to the example considered here. However, the essential qualitative features of the curves shown in Figure 8 are true in general. Residual carrier is better at low bit rates, suppressed carrier is better at intermediate bit rates, and there is not much difference at high bit rates. The bit rate for which the two performance curves cross increases with carrier loop bandwidth.

The reason residual carrier performs better than suppressed carrier at the low bit rates is because a residual-carrier loop is not subject to half-cycle slips. A suppressed-carrier loop, on the other hand, can slip a half-cycle and therefore requires a higher carrier loop signal-to-noise ratio in order to guard against these damaging slips. (A residual-carrier loop can slip a whole cycle, but this is both less likely and less damaging than a half-cycle slip.)

In order to get the best performance from residual-carrier operation, it is necessary that the modulation index be optimal or, at least, near optimal. Each residual-carrier performance curve of Figure 8 is based on the assumption that the modulation index is optimized at each point on the curve. Figure 9 shows what happens if this is not the case. In Figure 9, the lower curve (with the better telemetry performance) is the same as the residual-carrier curve with  $B_L = 1$  Hz of Figure 8, with an optimized modulation index at each point on the curve. The upper curve of Figure 9 represents residual-carrier performance with  $B_L = 1$  Hz under all the same circumstances except that the modulation index is not optimized at each point on the curve; instead, a single modulation index of  $54^\circ$  (the optimum modulation index for a bit rate of 10 bps) is used for the entire curve. The two curves of Figure 9 coalesce at  $R_{BIT} = 10$  bps but, for  $R_{BIT}$  greater than 10 bps, a penalty is paid for not using the appropriate optimum modulation index. At  $R_{BIT} = 1000$  bps, the penalty is about 2 decibels.

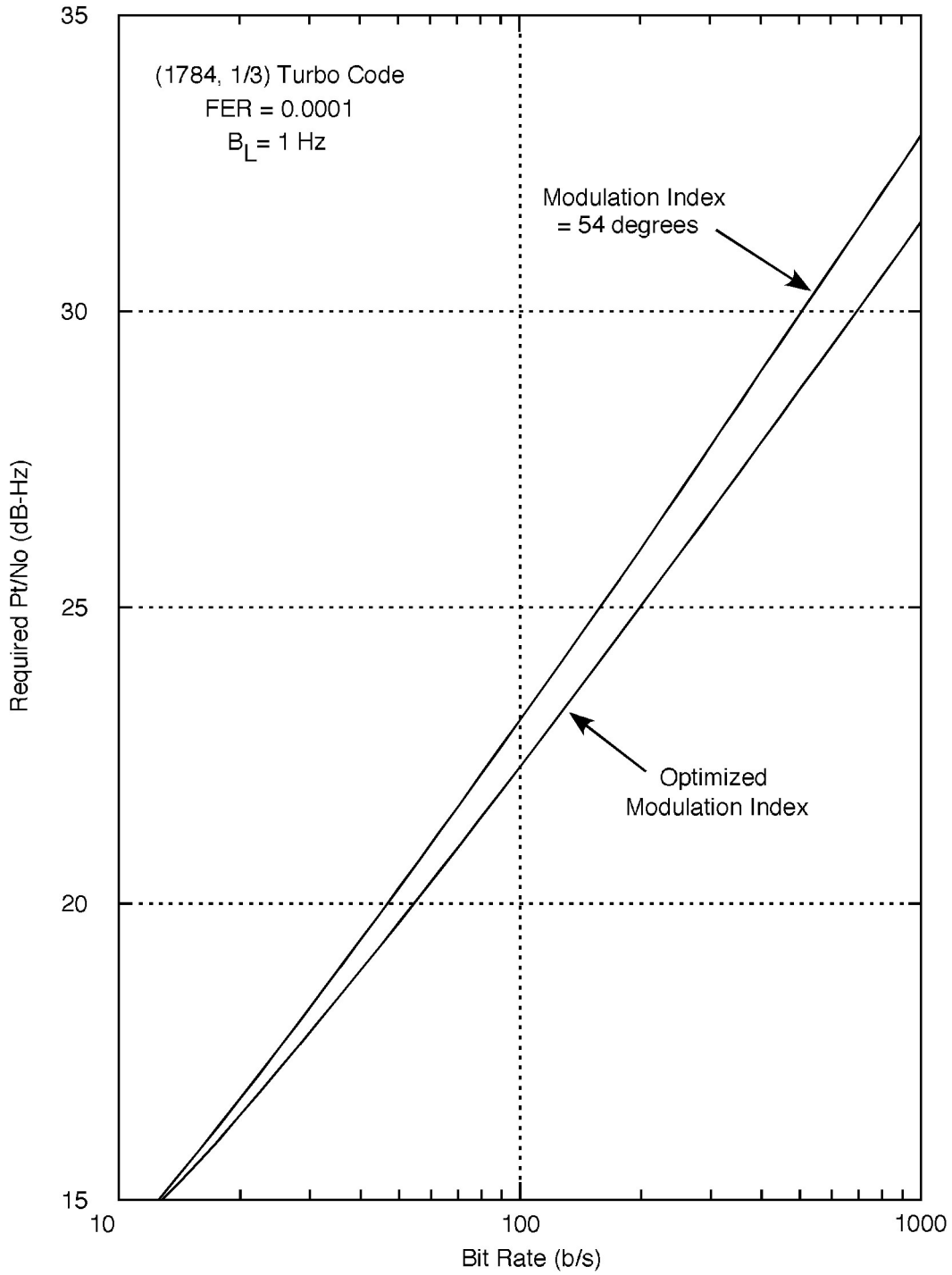


Figure 9. Comparison of Optimized and Non-optimized Modulation Index

## 5.2 Decoding Threshold and System Loss

Telemetry will not be properly decoded unless the product  $\eta_{SYS} \cdot E_b/N_0$  (the effective  $E_b/N_0$  after the available  $E_b/N_0$  has been reduced by system losses) is greater than or equal to the effective threshold energy per bit to noise spectral density ratio,  $f^{-1}(\text{BER})$  or  $f^{-1}(\text{FER})$ , that is required by the coding scheme.  $\eta_{SYS}$  is the system loss, BER is the threshold bit error rate, FER is the threshold frame error rate, and  $f(*)$  is the ideal functional dependence of probability of bit (or frame) error on bit SNR (see Appendix A).

Table 6 lists the effective threshold energy per bit to noise spectral density ratio,  $f^{-1}(\text{BER})$ , in decibels, that is required by an uncoded link and by each of three different convolutionally coded links. These baseline values are valid for residual carrier, suppressed-carrier BPSK, and QPSK or OQPSK.

Table 6. Baseline  $E_b/N_0$  for Uncoded and Convolutionally Coded Data, dB

Code	Threshold Bit Error Rate			
	$5 \times 10^{-3}$	$10^{-3}$	$10^{-4}$	$10^{-5}$
Uncoded	5.2	6.8	8.4	9.6
( $k=7, r=1/2$ )	2.3	3.0	3.8	4.5
( $k=15, r=1/4$ )	0.5	0.9	1.5	2.0
( $k=15, r=1/6$ )	0.3	0.7	1.3	1.8

Table 7 lists the effective threshold energy per bit to noise spectral density ratio,  $f^{-1}(\text{FER})$ , for a concatenated code (a Reed-Solomon outer code with one of two convolutional inner codes, the combination achieving a threshold frame error rate of  $10^{-5}$ ) using residual carrier, suppressed-carrier BPSK, QPSK and OQPSK. A frame error rate (as opposed to a bit error rate) is used because decoding failures of block-coded data result in the loss of the entire codeblock or data frame.

Table 7. Effective Threshold  $E_b/N_0$  for Concatenated Codes, dB

Concatenated Code	FER	$10 \log [f^{-1}(\text{FER})]$
RS with ( $k=7, r=1/2$ ) convolutional	$1 \times 10^{-5}$	2.38 dB
RS with ( $k=15, r=1/4$ ) convolutional	$1 \times 10^{-5}$	1.24 dB
RS with ( $k=15, r=1/6$ ) convolutional	$1 \times 10^{-5}$	1.04 dB

Table 8 lists the effective threshold energy per bit to noise spectral density ratio,  $f^{-1}(\text{FER})$ , for a turbo-coded link in order to achieve a frame error rate of  $1 \times 10^{-4}$  using residual carrier, suppressed-carrier BPSK, QPSK or OQPSK. A frame error rate is used because turbo decoding failures result in the loss of the entire codeblock or data frame. The threshold FER specified with each turbo code is considered to be representative of what should be expected from a telecommunications link using that code.

Table 8. Effective Threshold  $E_b/N_0$  for Turbo Codes, dB

Turbo Code	$10 \log [f^{-1}(\text{FER})]$	Turbo Code	$10 \log [f^{-1}(\text{FER})]$
( 1784, 1/2)	1.5 dB	( 7136, 1/2)	1.1 dB
( 1784, 1/3)	0.8 dB	( 7136, 1/3)	0.4 dB
( 1784, 1/4)	0.6 dB	( 7136, 1/4)	0.3 dB
( 1784, 1/6)	0.3 dB	( 7136, 1/6)	0.0 dB
( 3568, 1/2)	1.3 dB	( 8920, 1/2)	1.1 dB
( 3568, 1/3)	0.6 dB	( 8920, 1/3)	0.4 dB
( 3568, 1/4)	0.4 dB	( 8920, 1/4)	0.2 dB
( 3568, 1/6)	0.1 dB	( 8920, 1/6)	-0.1 dB

The system loss  $\eta_{SYS}$  ( $0 < \eta_{SYS} < 0.93$ ) is a composite factor used in communication link budgets to account for the following influences on telemetry efficiency: imperfect carrier, subcarrier, and symbol synchronization, and waveform distortion.

$$\eta_{SYS} = \min\{0.93, \eta_{RADIO} \cdot \eta_{SUB} \cdot \eta_{SYM} \cdot \eta_{WD}\} \quad (17)$$

where  $\eta_{RADIO}$  is radio loss,  $\eta_{SUB}$  is subcarrier demodulation loss,  $\eta_{SYM}$  is symbol synchronization loss, and  $\eta_{WD}$  is waveform distortion loss. The models for the four losses are given in paragraphs 5.3.5 (Radio Loss), 5.4 (Subcarrier Synchronization), 5.5 (Symbol Synchronization) and 5.6 (Waveform Distortion). The component losses are estimated separately and the results multiplied (or their decibel equivalents added) to get the composite system loss. If the product of the component losses is not less than 0.93, then  $\eta_{SYS}$  should be estimated as 0.93 (i.e.,  $-10 \log \eta_{SYS} = 0.3$  dB).

### 5.3 Carrier Synchronization

Three different algorithms are used for carrier synchronization, depending on whether the tracking is residual carrier, suppressed-carrier BPSK, or QPSK/OQPSK.

### 5.3.1 *Residual Carrier*

A residual-carrier signal can be tracked whether or not there is a subcarrier (squarewave or sinewave) present and whether the symbols are non-return-to-zero or Bi-phase. When tracking a residual carrier, the carrier loop signal-to-noise ratio is

$$\rho_L = \frac{P_C}{N_0 B_L}. \quad (18)$$

There is an additional loss to the carrier loop signal-to-noise ratio when tracking a residual carrier with non-return-to-zero symbols in the absence of a subcarrier. This loss is due to the presence of data sidebands overlaying the residual carrier in the frequency domain and therefore increasing the effective noise level for carrier synchronization.  $\rho_L$ , in this case, must be calculated as (Reference 5)

$$\rho_L = \frac{P_C}{N_0 B_L} \cdot \frac{1}{1 + 2 E_S / N_0}. \quad (19)$$

The model of Equation (19) is valid when the data bits are balanced. If the data bits are unbalanced (an unequal number of logical ones and zeroes), non-return-to-zero, and directly modulate the carrier (that is, no subcarrier), there will be a phase bias in the residual-carrier tracking loop that causes an additional loss in telemetry demodulation. This loss can be as great as 2 dB.

Imperfect carrier synchronization results in a higher bit error probability for the recovered telemetry data than would be the case if perfect tracking could be achieved. Radio loss is a measure of this discrepancy between the ideal and what is achieved in practice. Figures 10 through 19 show the effect of radio loss with residual carrier. Figure 10 is for uncoded telemetry. Figures 11, 12, and 13 are for convolutionally coded ( $k=7, r=1/2$ ), ( $k=15, r=1/4$ ) and ( $k=15, r=1/6$ ) telemetry. Figures 14 and 15 are for concatenated codes using a Reed-Solomon outer code with either a ( $k=7, r=1/2$ ) or ( $k=15, r=1/6$ ) convolutional inner code. Figures 16, 17, 18, and 19 are for turbo-coded (1784, 1/2), (1784, 1/3), (8920, 1/4) and (8920, 1/6) telemetry. Turbo codes have an error floor in their performance that is not shown in these figures. The error floor is different for each code but, for each of the turbo codes shown here, the error floor lies below a frame error rate of  $10^{-5}$  and therefore is not visible in the figure. Great care must be taken in evaluating the performance of these codes for frame error rates of less than  $10^{-5}$ .

For the last six figures (14 through 19) the ordinate is Frame Error Rate rather than Bit Error Rate. For all figures, it has been assumed that subcarrier synchronization, symbol synchronization, and waveform symmetry are perfect and that transmitter and solar phase noise is negligible. Furthermore, it has been assumed that the bit rate is very large compared with the carrier loop bandwidth. The purpose of these six figures is to show the effect of imperfect carrier synchronization (due to thermal noise and static phase error) on telemetry performance. Appendix B summarizes the theory upon which the curves of Figures 10 through 19 are based.

The radio loss as a positive, decibel quantity (i.e.,  $-10\log\eta_{RADIO}$ ) is simply the horizontal distance between the baseline curve and the curve that represents performance in the presence of imperfect carrier synchronization. In comparing several curves from any one figure, it is evident that radio loss is a function of both  $\rho_L$  and the threshold BER (FER). In comparing different figures, it is evident that radio loss is a function of the coding scheme.

In each of Figures 10 through 19, there are three curves, corresponding to static phase errors of 0, 3, and 5 degrees, for each value of  $\rho_L$ . Static phase error is caused by uncompensated Doppler dynamics (Appendix C).

With residual-carrier tracking it is important to make an optimal selection of the modulation index. In general, the optimum value for modulation index is a function of the bit rate, the carrier loop bandwidth, the coding scheme, and the threshold BER. Figure 20 shows the optimum modulation index for uncoded telemetry. Figures 21 and 22 show the optimum modulation index for convolutionally coded ( $k=7, r=1/2$ ) and ( $k=15, r=1/6$ ) telemetry, respectively. The optimum modulation index for convolutionally coded ( $k=15, r=1/4$ ) and ( $k=15, r=1/6$ ) are approximately the same. Figure 23 shows modulation indices that are approximately optimum for use with any of the sixteen turbo codes listed in Table 8. For concatenated codes, it is recommended that the optimum modulation for the inner (convolutional) code be selected. Figures 20 through 23 are all based on the assumption that the carrier loop phase error variance is determined by thermal noise. If significant external phase noise is present, such as phase noise from the transmitter or phase scintillations from the solar corona, the optimum modulation index must be reconsidered.

The curves of Figures 20 through 23 are defined by two constraints:  $\rho_L$  should be greater than or equal to 10 dB and the product  $\eta_{RADIO} \cdot E_b/N_0$  should be greater than the threshold effective energy per bit to noise spectral density ratio. Moreover, for effective residual-carrier tracking the modulation index must be no larger than 80 degrees.

Sometimes, it is important to take transmitter and solar phase noise into account. This is especially true for operation close to the Sun or for one-way or two-way noncoherent operation with an Auxiliary Oscillator (or some oscillator, serving as the source of the downlink carrier, that has relatively poor frequency stability).

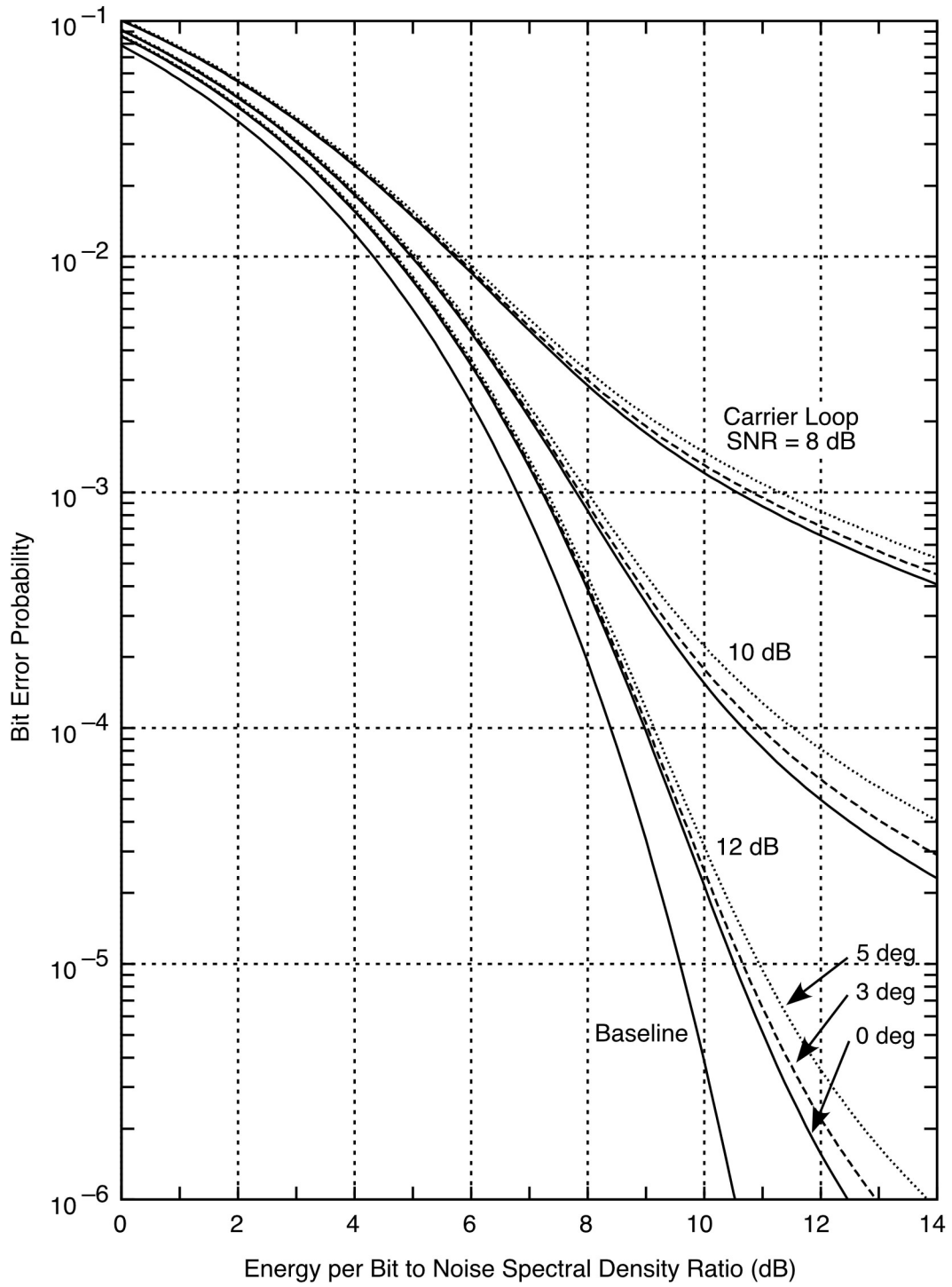


Figure 10. Telemetry Performance; Uncoded, Residual Carrier

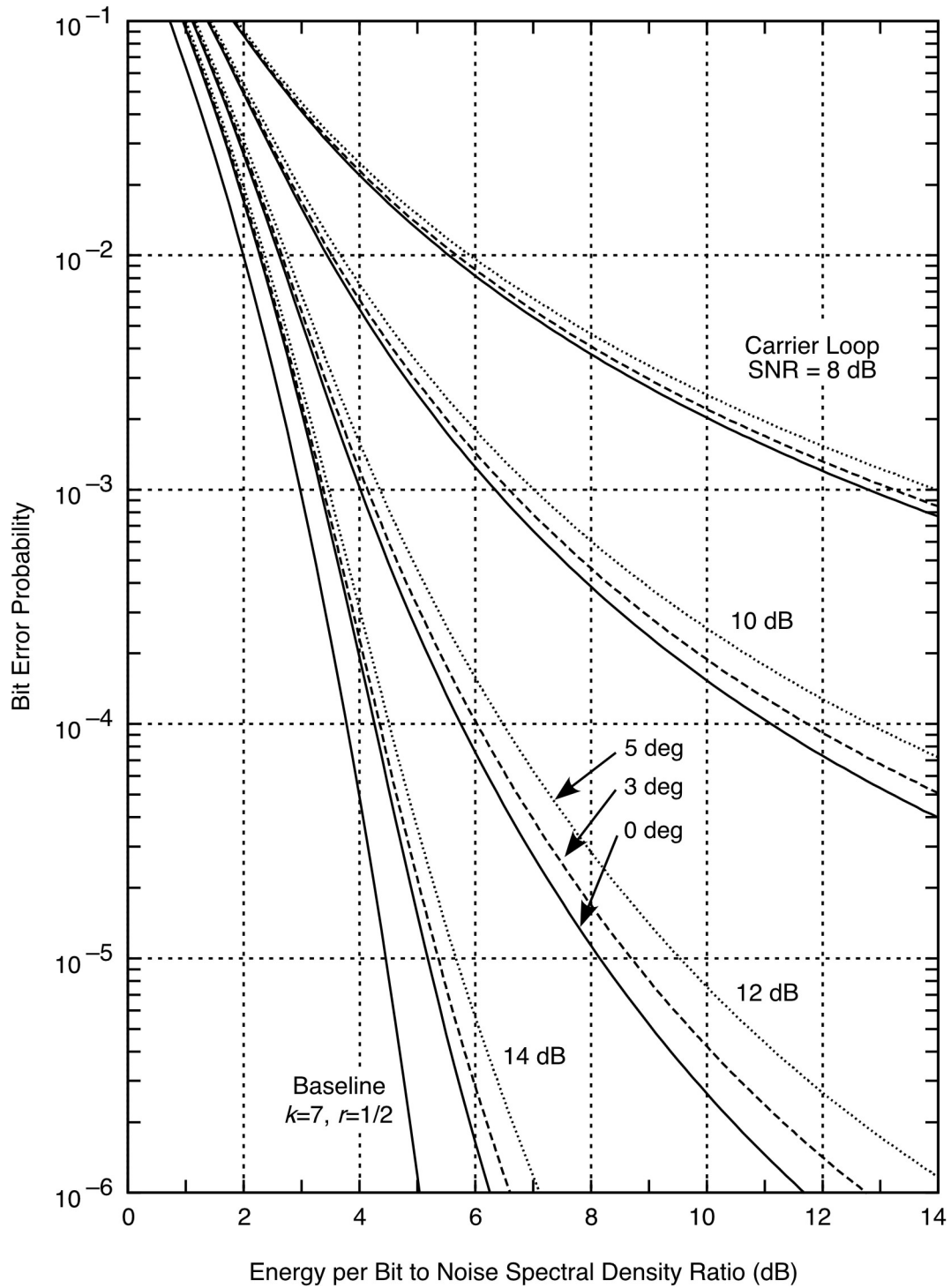


Figure 11. Telemetry Performance; ( $k=7, r=1/2$ ) Convolutional Code with Residual Carrier

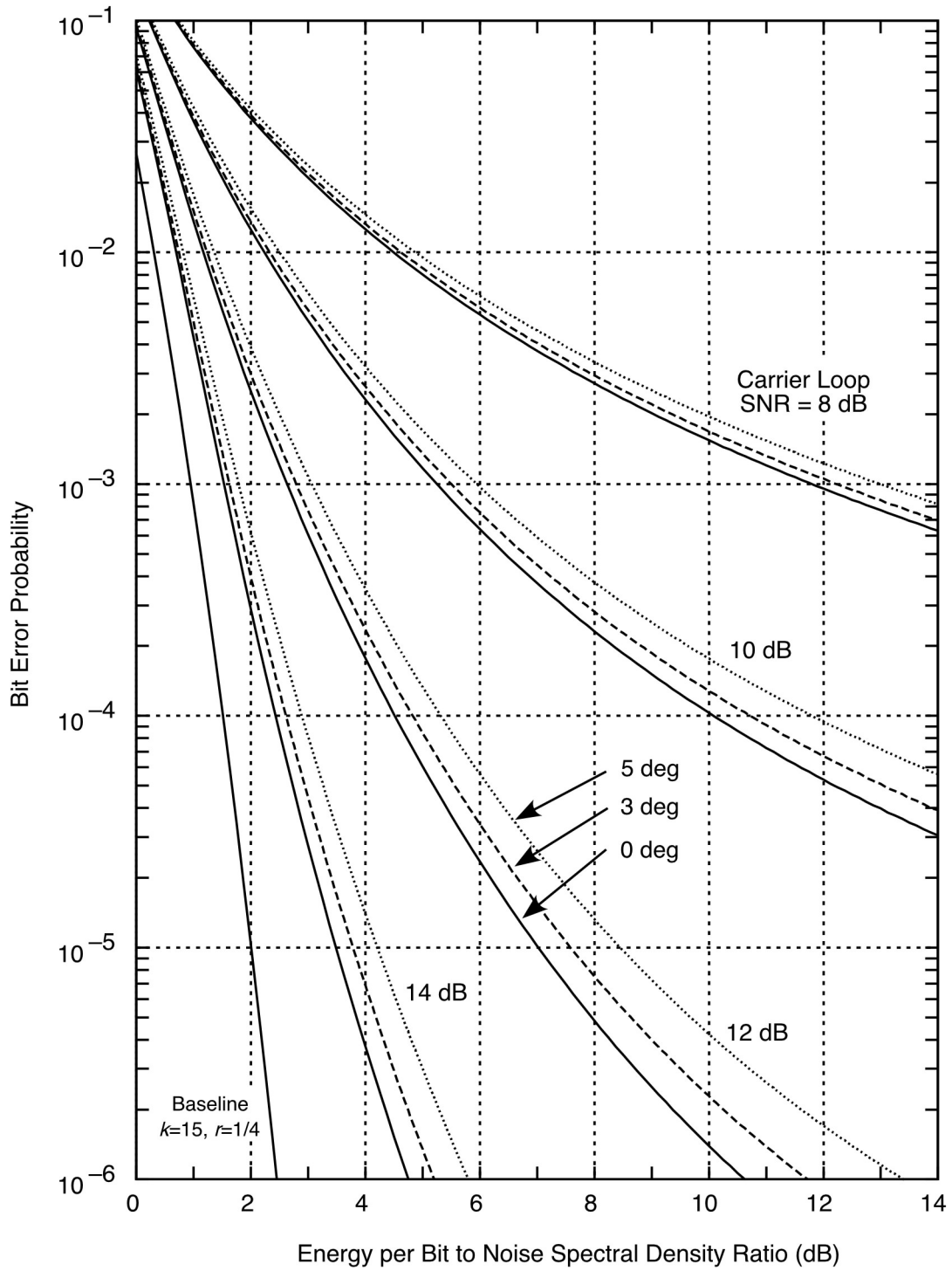


Figure 12. Telemetry Performance; ( $k=15, r=1/4$ ) Convolutional Code with Residual Carrier

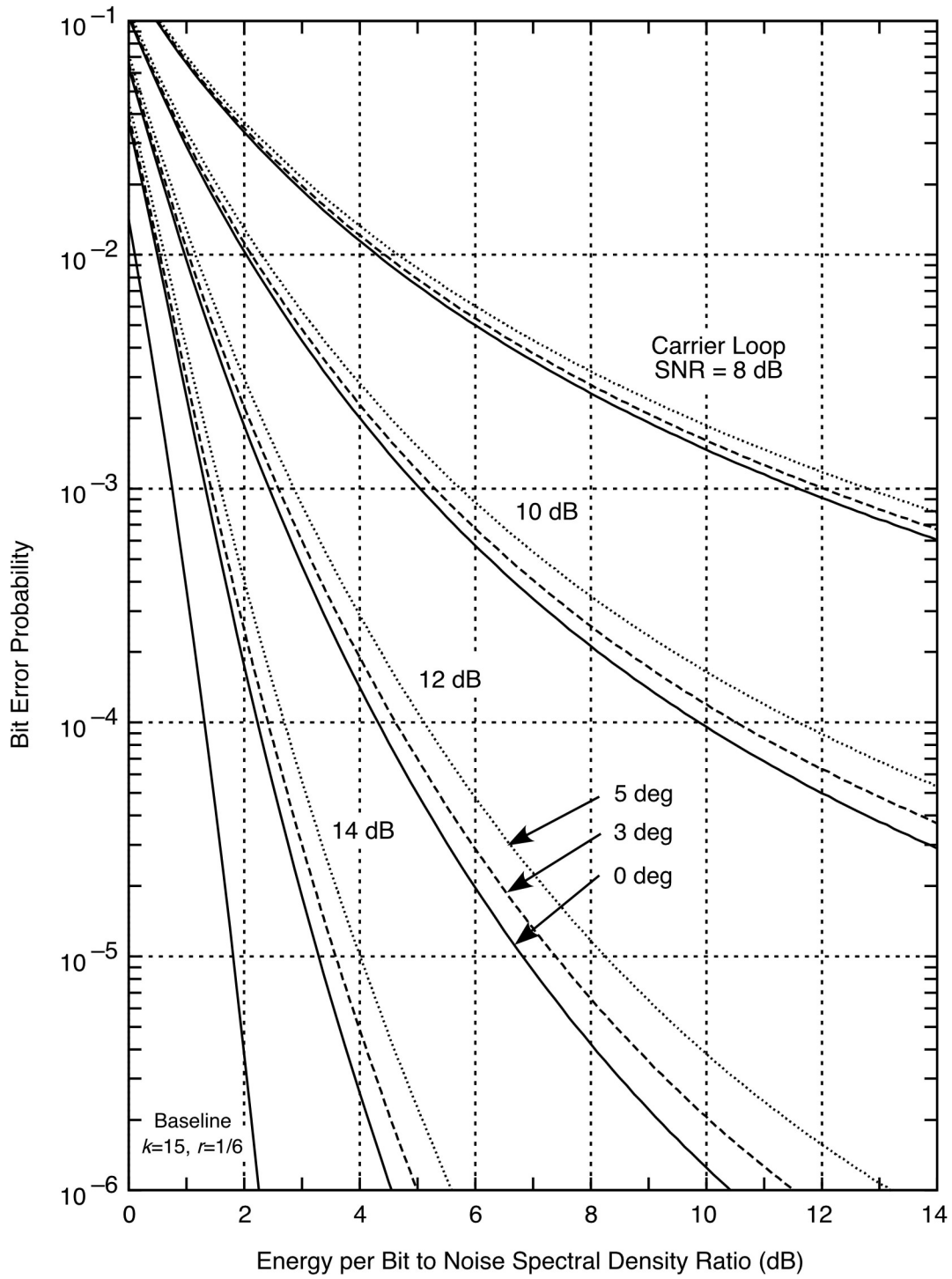


Figure 13. Telemetry Performance; ( $k=15, r=1/6$ ) Convolutional Code with Residual Carrier

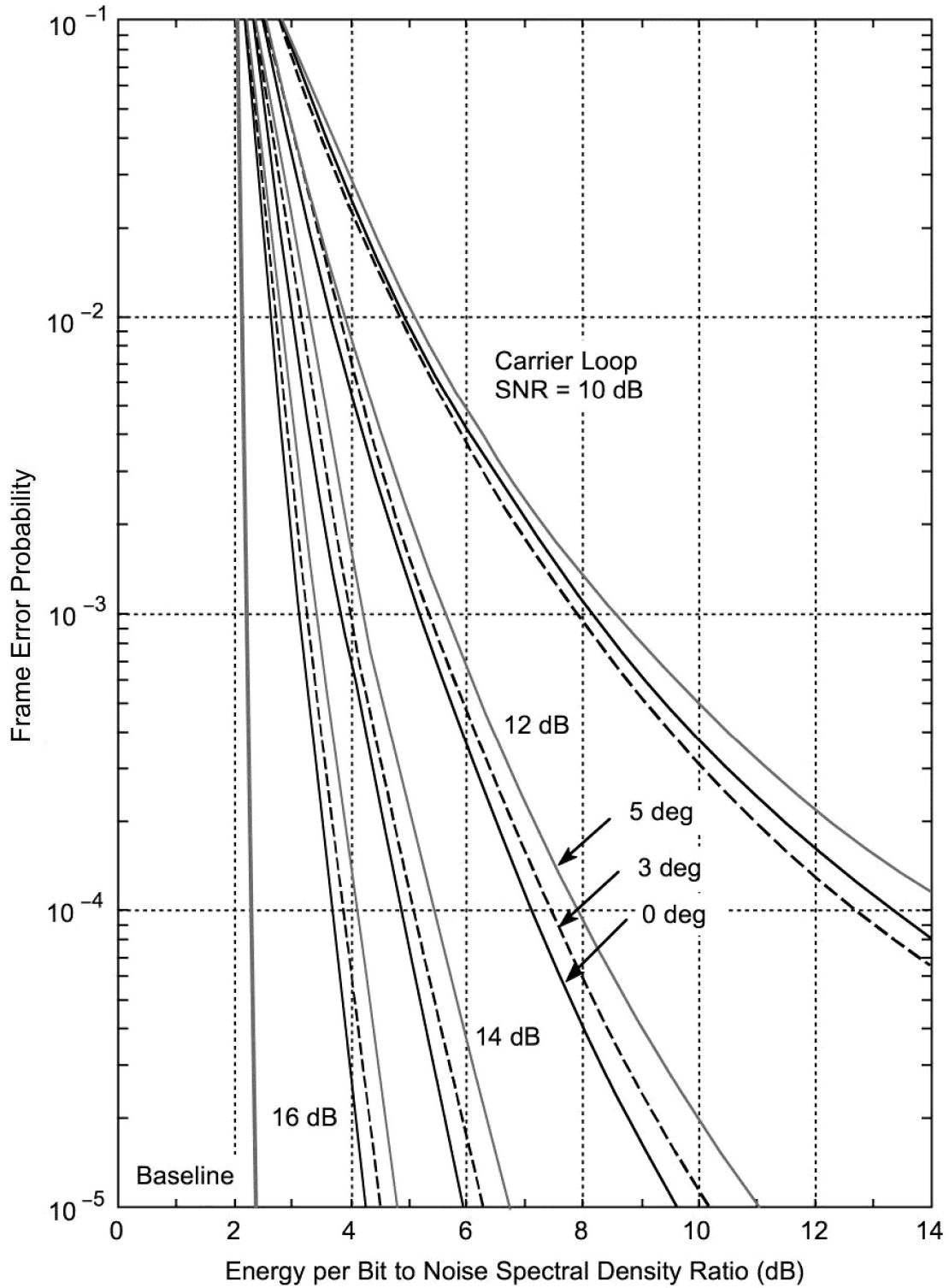


Figure 14. Telemetry Performance; Concatenated RS and  $(k=7, r=1/2)$ , Convolutional Code with Residual Carrier.

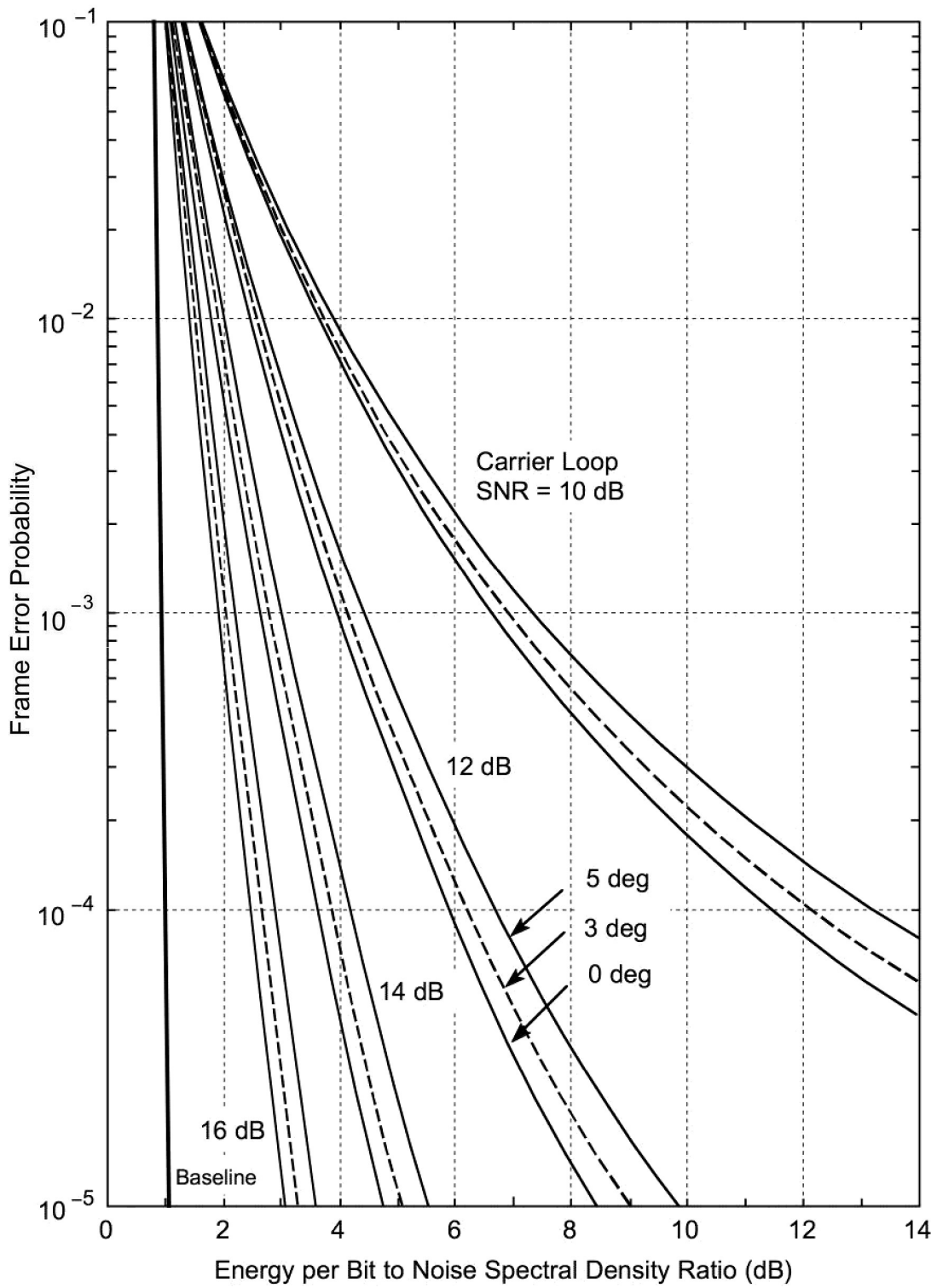


Figure 15. Telemetry Performance; Concatenated RS and  $(k=15, r=1/6)$  Convolutional Code with Residual Carrier.

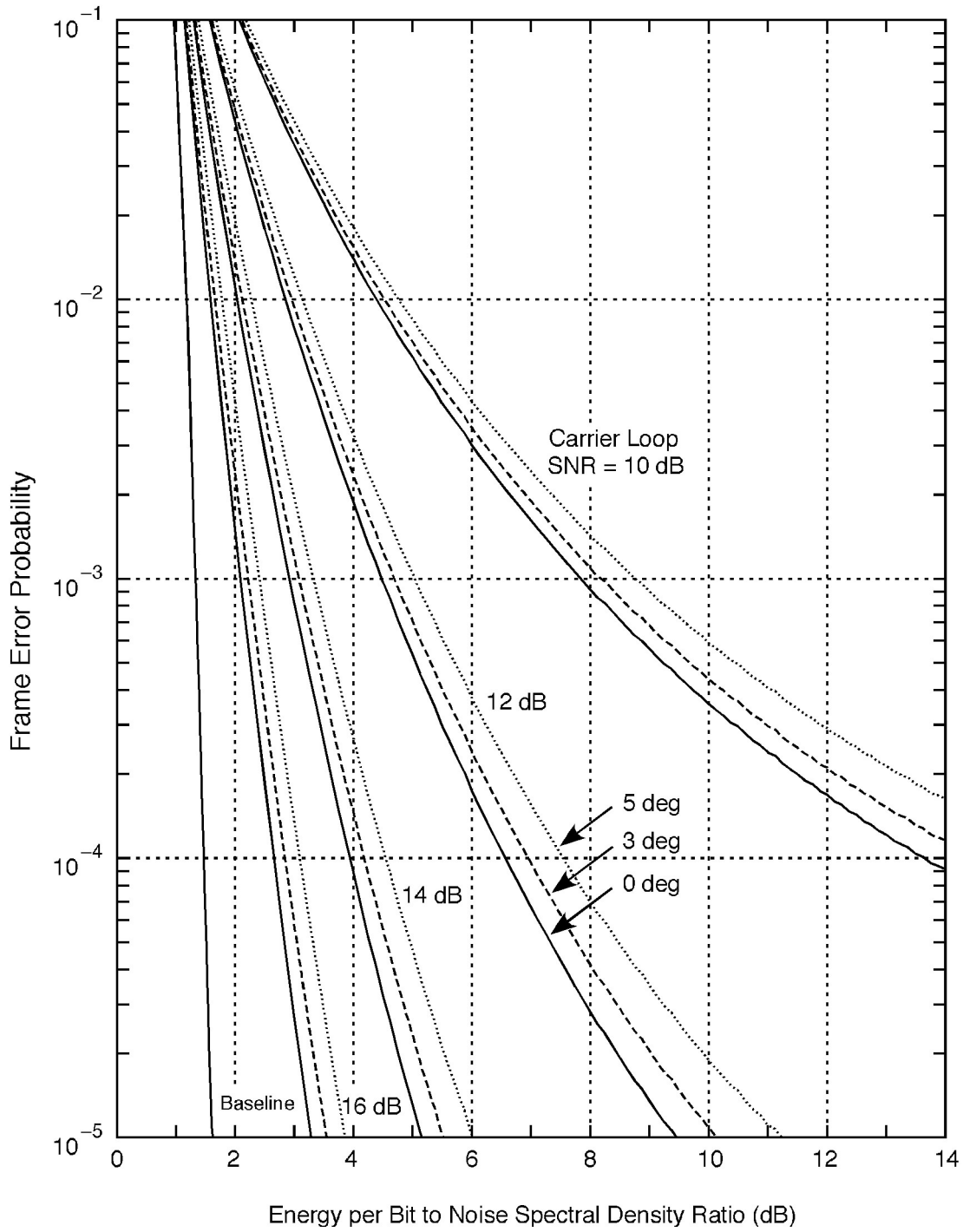


Figure 16. Telemetry Performance; (1784, 1/2) Turbo Code with Residual Carrier

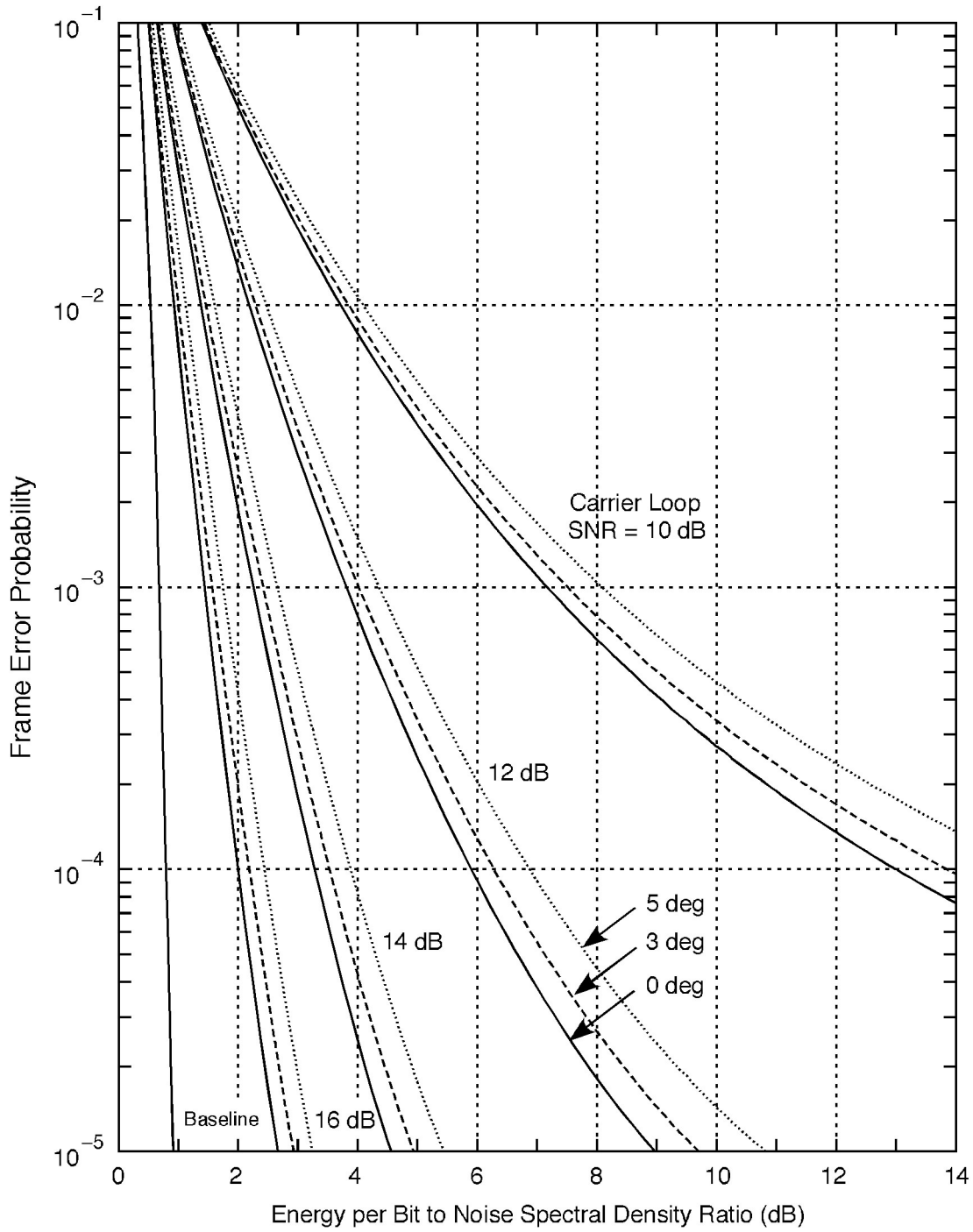


Figure 17. Telemetry Performance; (1784, 1/3) Turbo Code with Residual Carrier

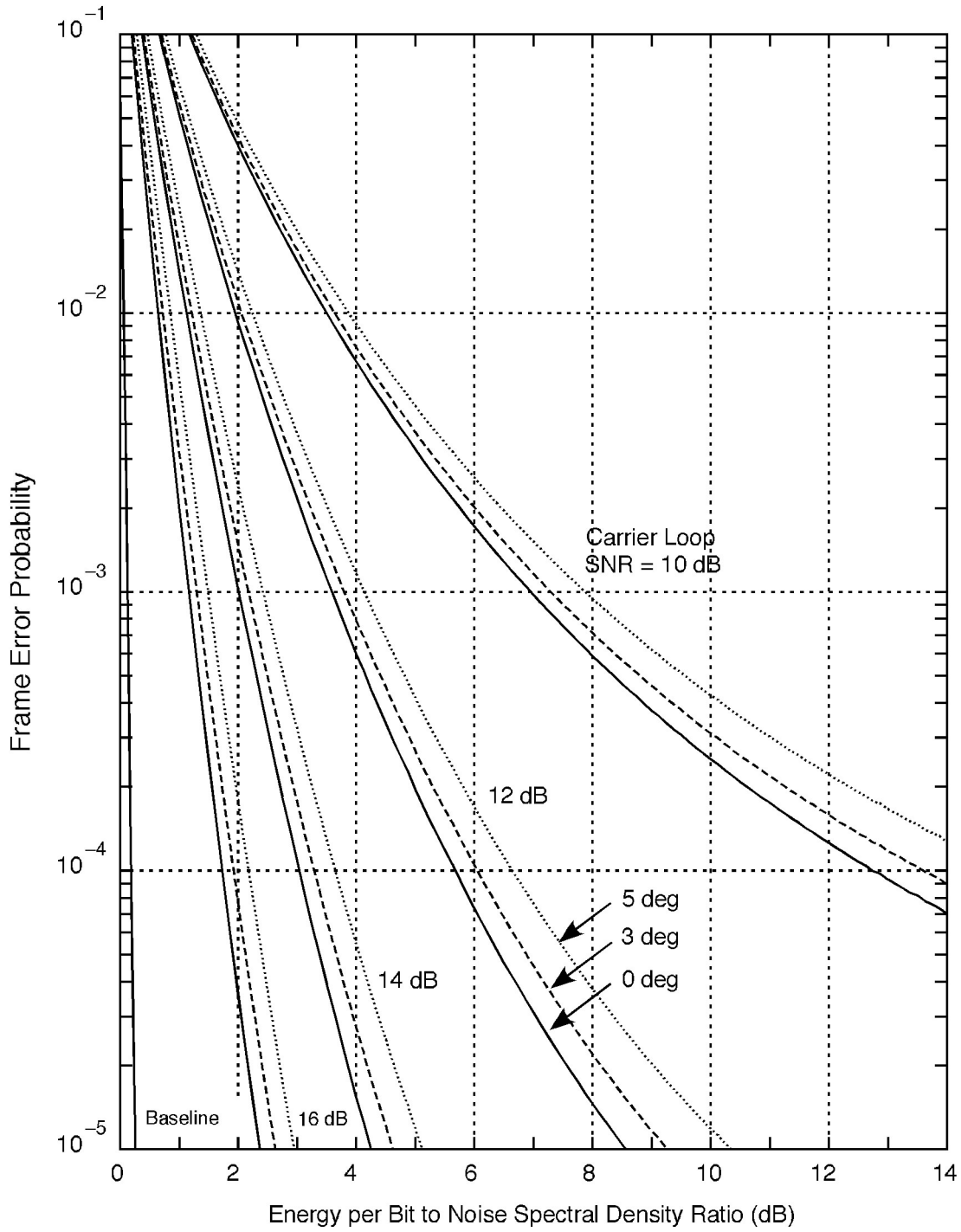


Figure 18. Telemetry Performance; (8920, 1/4) Turbo Code with Residual Carrier

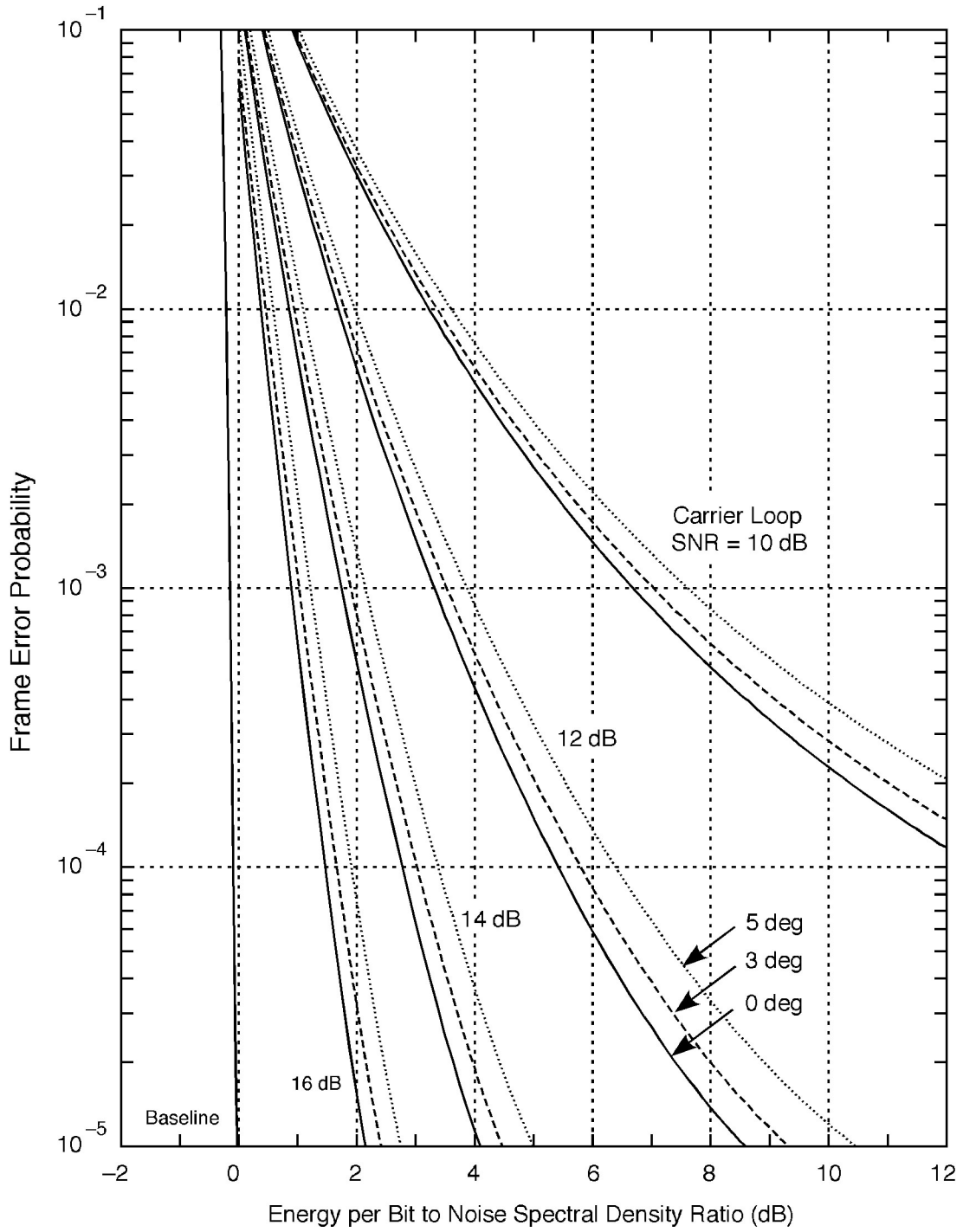


Figure 19. Telemetry Performance; (8920, 1/6) Turbo Code with Residual Carrier

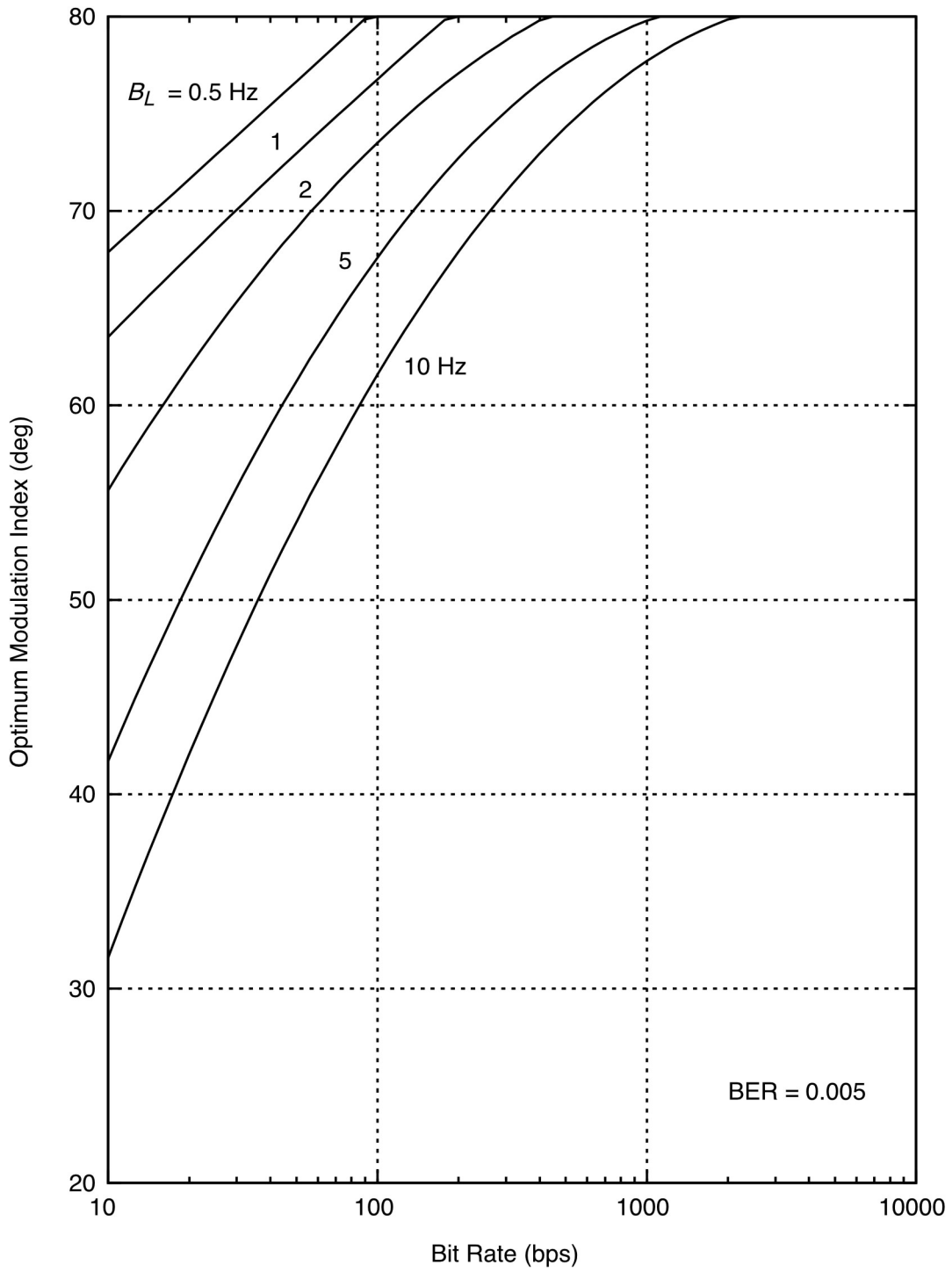


Figure 20. Optimum Modulation Index; Uncoded

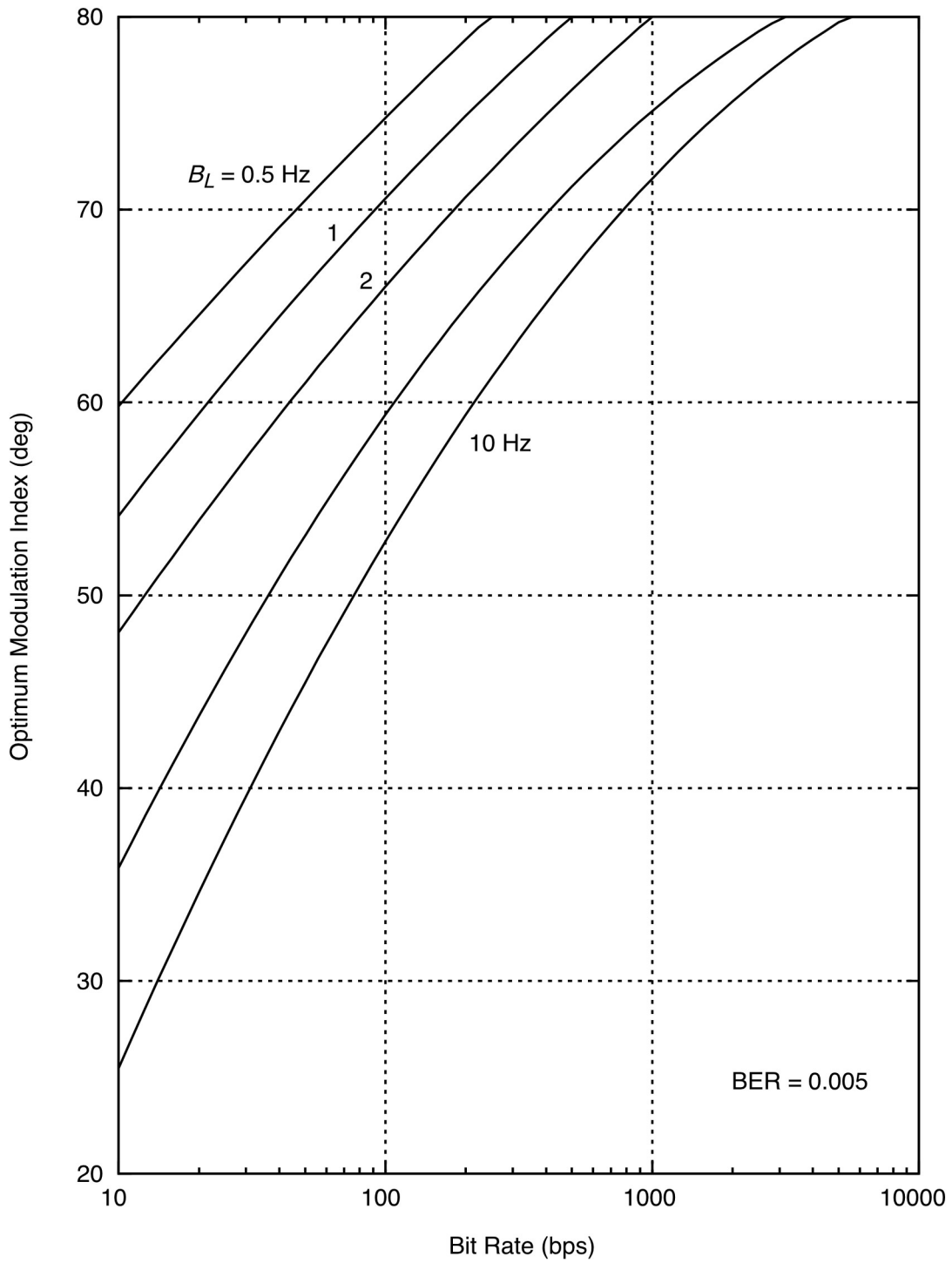


Figure 21. Optimum Modulation Index; ( $k=7, r=1/2$ ) Convolutional Code

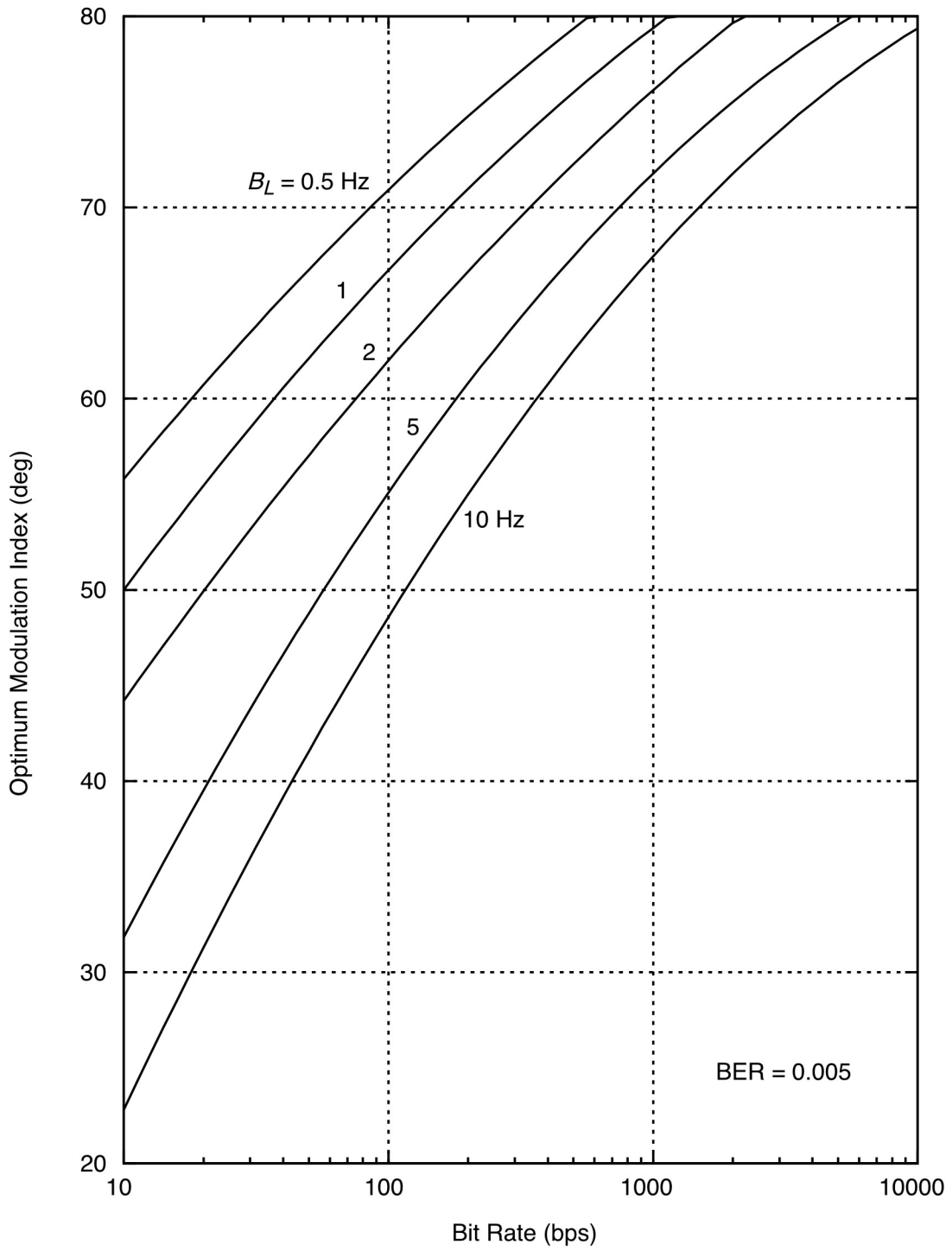


Figure 22. Optimum Modulation Index; ( $k=15, r=1/6$ ) Convolutional Code

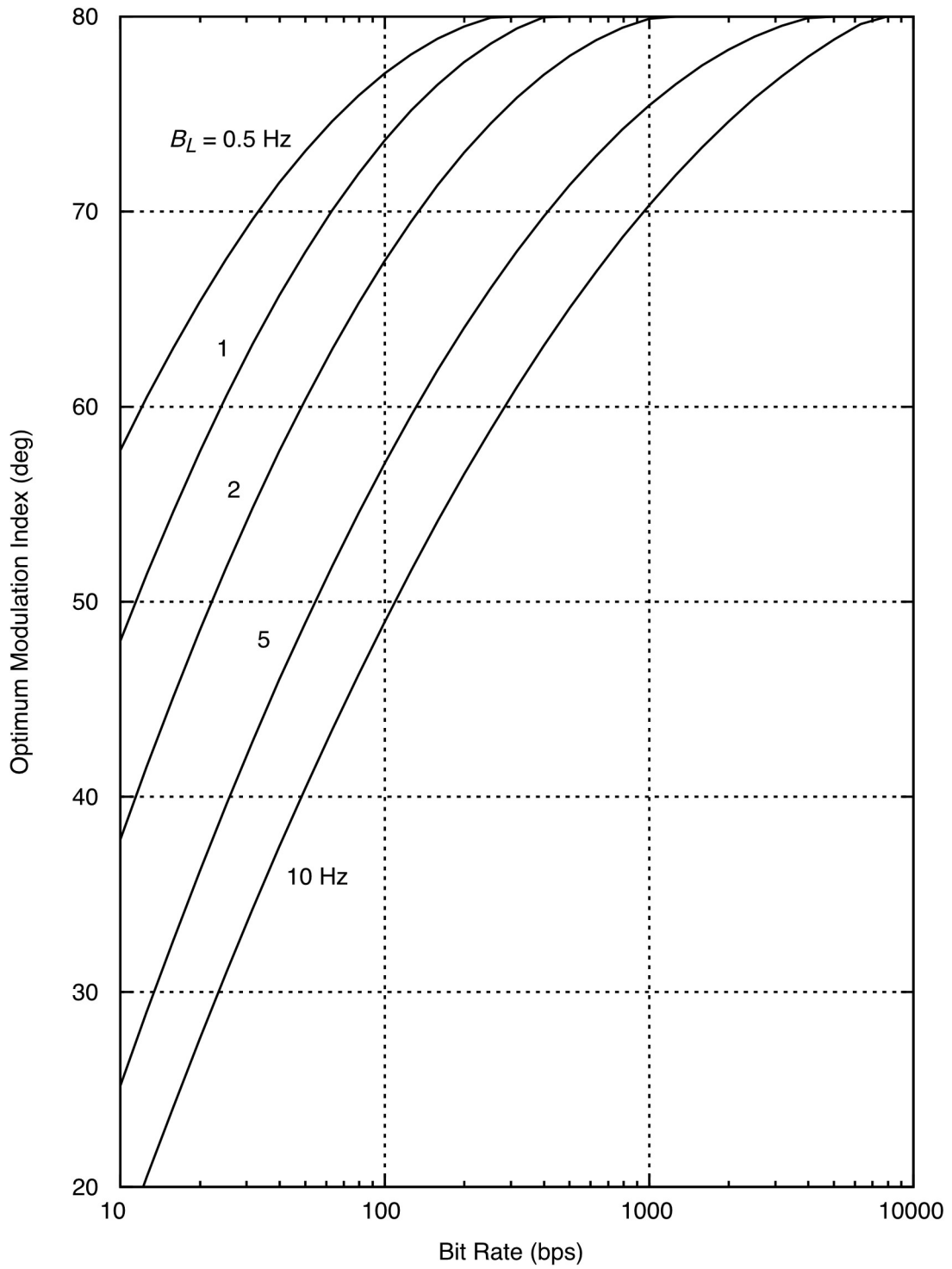


Figure 23. Optimum Modulation Index; Turbo Codes

Radio loss may, more generally, be regarded as a function of the carrier phase error variance  $\sigma_\phi^2$ .

$$\sigma_\phi^2 = \frac{1}{\rho_L} + \sigma_T^2 + \sigma_S^2, \text{ rad}^2 \quad (20)$$

where  $\sigma_T^2$  is the contribution of the transmitter phase noise to the phase error variance in the carrier loop and  $\sigma_S^2$  is the contribution of solar phase noise. The contribution of thermal noise to phase error variance in the carrier loop equals the reciprocal of the carrier loop SNR; this is the first term on the right-hand side of Equation (20).  $\sigma_T^2$  is a function of  $B_L$  and the statistical properties of the transmitter phase noise. Appendix D offers suggestions for estimating  $\sigma_T^2$ . If the Sun-Earth-probe angle is small,  $\sigma_S^2$  will be significant and must be taken into account. Appendix E provides estimates of  $\sigma_S^2$  as a function of Sun-Earth-probe angle and  $B_L$ .

In general, as a first step in estimating radio loss, the carrier phase error variance  $\sigma_\phi^2$  should be calculated using Equation (20). Then, radio loss will be calculated as a function of  $\sigma_\phi^2$ .

It is recommended that the following constraint on residual-carrier tracking be observed.

$$\sigma_\phi^2 \leq 0.10 \text{ rad}^2 \quad (21)$$

This recommendation is based on simulations of cycle clipping in a phase-locked loop (Reference 12). In the absence of transmitter or solar phase noise, this becomes  $\rho_L \geq 10.0$  (10 dB). In general, with transmitter or solar phase noise present,  $\rho_L$  needs to be larger yet.

The contributions of transmitter phase noise and of solar phase noise to the carrier phase error variance are computed as described in Appendices D and E, respectively. These computed contributions, together with Equations (20) and (21), define the minimum-acceptable carrier loop SNR for residual-carrier tracking.

### 5.3.2 *Suppressed-Carrier BPSK*

Suppressed-carrier BPSK is tracked with a Costas loop. This loop has different statistical properties than does the residual-carrier loop; thus, radio loss will be different in this case.

When tracking suppressed-carrier BPSK, the carrier loop signal-to-noise ratio is

$$\rho_L = \frac{S_L P_T}{N_0 B_L} \quad (22)$$

where  $S_L$  is the squaring loss of the Costas loop (Reference 6).

$$S_L = \frac{2 \frac{E_S}{N_0}}{1 + 2 \frac{E_S}{N_0}} \quad (23)$$

Radio loss can be regarded as a function of the carrier phase error variance  $\sigma_\phi^2$ .

$$\sigma_\phi^2 = \frac{1}{\rho_L} + \sigma_T^2 + \sigma_S^2, \text{ rad}^2. \quad (24)$$

As before,  $\sigma_T^2$  and  $\sigma_S^2$  are the contributions of transmitter and solar phase noise, respectively, to the phase error variance in the carrier loop (see Appendices D and E).

It is recommended that the following constraint on suppressed-carrier BPSK tracking be observed.

$$\sigma_\phi^2 \leq 0.02, \text{ rad}^2 \quad (25)$$

Violating this recommendation will lead to (at least) an occasional half-cycle slip. In the absence of transmitter or solar phase noise, inequality (25) corresponds to  $\rho_L \geq 50.0$  (17dB), see Reference 7. In general, with transmitter or solar phase noise present,  $\rho_L$  needs to be larger yet.

### 5.3.3 *QPSK and OQPSK*

A QPSK or OQPSK signal is tracked by a loop designed for this purpose. The squaring loss is different than for the Costas loop used for suppressed-carrier BPSK.

When tracking a QPSK or OQPSK signal, the carrier loop signal-to-noise ratio is

$$\rho_L = \frac{S_{LQ} P_T}{N_0 B_L} \quad (26)$$

where  $S_{LQ}$  is the squaring loss of the QPSK/OQPSK loop.

$$S_{LQ} = \frac{1}{1 + \frac{9}{2 \frac{E_{SQ}}{N_0}} + \frac{6}{\left(\frac{E_{SQ}}{N_0}\right)^2} + \frac{3}{2 \left(\frac{E_{SQ}}{N_0}\right)^3}} \quad (27)$$

Radio loss can be regarded as a function of the carrier phase error variance  $\sigma_\phi^2$ .

$$\sigma_\phi^2 = \frac{1}{\rho_L} + \sigma_T^2 + \sigma_S^2, \text{ rad}^2 \quad (28)$$

As before,  $\sigma_T^2$  and  $\sigma_S^2$  are the contributions of transmitter and solar phase noise, respectively, to the phase error variance in the carrier loop (see Appendices D and E).

It is recommended that the following constraint on QPSK and OQPSK tracking be observed.

$$\sigma_\phi^2 \leq 0.005, \text{ rad}^2 \quad (29)$$

Violating this recommendation will lead to (at least) an occasional quarter-cycle slip. In the absence of transmitter or solar phase noise, inequality (29) corresponds to  $\rho_L \geq 200.0$  (23dB), see Reference 7. In general, with transmitter or solar phase noise present,  $\rho_L$  needs to be larger yet.

### 5.3.4 *Two/Three-Way Coherent*

When the spacecraft is tracked in a two-way (or three-way) phase-coherent mode, the carrier phase error variance  $\sigma_\phi^2$  in the ground receiver is increased by a portion of the phase noise (of thermal origin) introduced onto the downlink by the spacecraft transponder.

$$\sigma_\phi^2 = \frac{1}{\rho_L} + \frac{G^2(B_{TR} - B_L)}{P_C/N_0|_{U/L}} + \sigma_S^2, \text{ rad}^2 \quad (30)$$

where  $G$  is the spacecraft transponder ratio and  $P_C/N_0|_{U/L}$  is the uplink residual-carrier power-to-noise spectral density ratio.  $B_{TR}$  and  $B_L$  are the (one-sided) noise-equivalent carrier loop bandwidths of the transponder and ground receiver, respectively.

Equation (30) is a valid approximation only if  $B_{TR} > B_L$ .  $\sigma_S^2$  is the contribution of solar phase noise to the phase error variance in the carrier loop; it will generally be larger for coherent operation than for one-way or two-way noncoherent operation (see Appendix E).

### 5.3.5 *Radio Loss*

For all of the carrier tracking modes discussed above—residual carrier, suppressed-carrier BPSK, QPSK/OQPSK, and two/three-way coherent—a common framework is used for modeling radio loss, the loss due to imperfect carrier tracking. That framework is summarized in the paragraphs that follow. Radio loss is a function of carrier loop phase error variance  $\sigma_\phi^2$ . This variance must be calculated as described in the previous paragraphs. The radio loss models of this paragraph will be valid when  $\sigma_\phi^2$  satisfies the inequality:

$$\sigma_\phi^2 \leq \begin{cases} 0.1 \text{ rad}^2, & \text{Residual carrier} \\ 0.02 \text{ rad}^2, & \text{Suppressed - carrier BPSK} \\ 0.005 \text{ rad}^2, & \text{QPSK or OQPSK} \end{cases} \quad (31)$$

In the discussion that follows, a distinction is made between residual-carrier tracking and suppressed-carrier tracking where the latter includes both suppressed-carrier BPSK and QPSK/OQPSK.

Radio loss is modeled as an interpolation between a High-Rate Model (HRM) and a Low-Rate Model (LRM). This interpolation is

$$\eta_{RADIO}^* = a \cdot \eta_{HRM}^* + (1-a) \cdot \eta_{LRM}^* \quad (32)$$

where

$$\eta_{RADIO}^* = \text{positive decibel radio loss } (\eta_{RADIO}^* = -10 \log \eta_{RADIO})$$

$$\eta_{HRM}^* = \text{positive decibel HRM radio loss}$$

$$\eta_{LRM}^* = \text{positive decibel LRM radio loss}$$

$$a = \text{interpolation factor } (0 \leq a \leq 1)$$

The interpolation factor  $a$  depends on the code. For uncoded and convolutionally coded telemetry, the interpolation factor is given by

$$a = \frac{1}{4B_L T_{SYM}} \left[ 1 - \frac{1}{8B_L T_{SYM}} \left( 1 - e^{-8B_L T_{SYM}} \right) \right] \quad (33)$$

where  $B_L$  is the (one-sided, noise-equivalent) carrier loop bandwidth and  $T_{SYM}$  is the binary symbol period (the reciprocal of the binary symbol rate). For concatenated and turbo codes, the interpolation factor  $a$  is given by

$$a = \frac{1}{1 + c_1 (R/B_L)^{-c_2}} \quad (34)$$

where  $R$  is the bit rate. Computer simulations verify that Equation (34) yields an appropriate interpolation factor for concatenated and turbo codes (References 8 and 9). Table 9 gives the coefficients  $c_1$  and  $c_2$  for concatenated codes. The coefficients for turbo codes are provided in Table 10.

The HRM radio loss is modeled with a curve-fit of the form

$$\eta_{HRM}^* = c_{H0} \left[ \exp(c_{H1} \sigma_\phi^2) - 1 \right] \quad (35)$$

and the LRM radio loss is modeled with a curve-fit of the same form (but with different coefficients)

$$\eta_{LRM}^* = c_{LO} \left[ \exp(c_{LI} \sigma_\phi^2) - 1 \right] \quad (36)$$

where  $\sigma_\phi^2$  is the carrier loop phase error variance in units of rad<sup>2</sup>.

Table 9. Interpolation Factor Coefficients  $c_1$  and  $c_2$  for Concatenated Codes

Concatenated Code	Tracking Mode	$c_1$	$c_2$
RS with ( $k=7, r=1/2$ ) Convolutional	Residual	31,000.	1.3
RS with ( $k=15, r=1/4$ ) or ( $k=15, r=1/6$ ) Convolutional	Residual	52,400.	1.3
RS with ( $k=7, r=1/2$ ) Convolutional	Suppressed	76,000.	1.3
RS with ( $k=15, r=1/4$ ) or ( $k=15, r=1/6$ ) Convolutional	Suppressed	129,000.	1.3

Table 10. Interpolation Factor Coefficients  $c_1$  and  $c_2$  for Turbo Codes

Turbo Code	$c_1$	$c_2$
(1784, 1/2), (1784, 1/3), (1784, 1/4), (1784, 1/6)	264.	0.84
(3568, 1/2), (3568, 1/3), (3568, 1/4), (3568, 1/6)	473.	0.84
(7136, 1/2), (7136, 1/3), (7136, 1/4), (7136, 1/6)	846.	0.84
(8920, 1/2), (8920, 1/3), (8920, 1/4), (8920, 1/6)	1020.	0.84

The HRM coefficients  $c_{HO}$  and  $c_{HI}$  of Equation (35) depend on the code, the threshold BER or FER, and the tracking mode. These coefficients are given in Table 11 for uncoded telemetry, in Table 12 for ( $k=7, r=1/2$ ) convolutionally coded telemetry, and in Table 13 for both ( $k=15, r=1/4$ ) and ( $k=15, r=1/6$ ) convolutionally coded telemetry. For concatenated codes, the coefficients at a threshold FER of  $1 \times 10^{-5}$  are given in Table 14. The coefficients for the turbo codes listed in Table 8 at a threshold FER of  $1 \times 10^{-4}$  are given in Table 15 for residual carrier tracking and in Table 16 for suppressed carrier tracking. The LRM coefficients  $c_{LO}$  and  $c_{LI}$  are independent of the code and are given in Table 17.

Table 11. HRM Coefficients  $c_{H0}$  and  $c_{H1}$  for Uncoded Telemetry

Tracking Mode	Threshold BER	$c_{H0}$	$c_{H1}$
Residual	$10^{-2}$	0.53	8.1
Residual	$5 \times 10^{-3}$	0.39	10.5
Residual	$10^{-3}$	0.21	17.5
Residual	$10^{-4}$	0.070	35.2
Residual	$10^{-5}$	0.030	55.5
Suppressed	$10^{-2}$	0.27	15.2
Suppressed	$5 \times 10^{-3}$	0.21	18.5
Suppressed	$10^{-3}$	0.12	29.3
Suppressed	$10^{-4}$	0.031	62.7
Suppressed	$10^{-5}$	0.000023	244.

Table 12. HRM Coefficients  $c_{H0}$  and  $c_{H1}$  for ( $k=7, r=1/2$ ) Convolutional Code

Tracking Mode	Threshold BER	$c_{H0}$	$c_{H1}$
Residual	$10^{-2}$	0.30	17.7
Residual	$5 \times 10^{-3}$	0.24	21.6
Residual	$10^{-3}$	0.21	28.7
Residual	$10^{-4}$	0.11	45.8
Residual	$10^{-5}$	0.066	64.7
Suppressed	$10^{-2}$	0.11	34.6
Suppressed	$5 \times 10^{-3}$	0.085	42.5
Suppressed	$10^{-3}$	0.041	65.2
Suppressed	$10^{-4}$	0.010	116.
Suppressed	$10^{-5}$	0.0030	174.

Table 13. HRM Coefficients  $c_{H0}$  and  $c_{H1}$  for  $k=15$  Convolutional Codes

Tracking Mode	Threshold BER	$c_{H0}$	$c_{H1}$
Residual	$10^{-2}$	0.45	16.6
Residual	$5 \times 10^{-3}$	0.45	18.8
Residual	$10^{-3}$	0.34	27.3
Residual	$10^{-4}$	0.21	43.1
Residual	$10^{-5}$	0.13	61.5
Suppressed	$10^{-2}$	0.13	38.4
Suppressed	$5 \times 10^{-3}$	0.098	46.9
Suppressed	$10^{-3}$	0.067	65.4
Suppressed	$10^{-4}$	0.044	93.4
Suppressed	$10^{-5}$	0.021	135.

Table 14. HRM Coefficients  $c_{H0}$  and  $c_{H1}$  for Concatenated Codes

Concatenated Code	Tracking Mode	$C_1$	$C_2$
RS with ( $k=7$ , $r=1/2$ ) Convolutional	Residual	2.07	25.4
RS with ( $k=15$ , $r=1/4$ ) or ( $k=15$ , $r=1/6$ ) Convolutional	Residual	2.92	20.6
RS with ( $k=7$ , $r=1/2$ ) Convolutional	Suppressed	0.88	52.1
RS with ( $k=15$ , $r=1/4$ ) or ( $k=15$ , $r=1/6$ ) Convolutional	Suppressed	1.14	46.5

Table 15. HRM Coefficients  $c_{H0}$  and  $c_{H1}$  for Turbo Codes, Residual Carrier

<b>Turbo Code</b>	<b><math>c_{H0}</math></b>	<b><math>c_{H1}</math></b>	<b>Turbo Code</b>	<b><math>c_{H0}</math></b>	<b><math>c_{H1}</math></b>
( 1784, 1/2)	2.14	19.4	( 7136, 1/2)	3.25	15.7
( 1784, 1/3)	2.60	17.2	( 7136, 1/3)	2.45	18.9
( 1784, 1/4)	1.41	24.7	( 7136, 1/4)	2.03	21.1
( 1784, 1/6)	1.74	22.2	( 7136, 1/6)	3.51	16.0
( 3568, 1/2)	2.75	16.9	( 8920, 1/2)	3.39	15.3
( 3568, 1/3)	2.01	21.1	( 8920, 1/3)	3.19	16.1
( 3568, 1/4)	2.36	20.9	( 8920, 1/4)	3.29	15.6
( 3568, 1/6)	2.32	19.6	( 8920, 1/6)	3.67	14.5

Table 16. HRM Coefficients  $c_{H0}$  and  $c_{H1}$  for Turbo Codes, Suppressed Carrier

<b>Turbo Code</b>	<b><math>c_{H0}</math></b>	<b><math>c_{H1}</math></b>
(1784, 1/2), (1784, 1/3), (1784, 1/4), (1784, 1/6)	0.025	182.0
(3568, 1/2), (3568, 1/3), (3568, 1/4), (3568, 1/6)	0.22	99.8
(7136, 1/2), (7136, 1/3), (7136, 1/4), (7136, 1/6)	0.54	61.9
(8920, 1/2), (8920, 1/3), (8920, 1/4), (8920, 1/6)	0.75	50.7

Table 17. LRM Coefficients  $c_{L0}$  and  $c_{L1}$  for All Codes

<b>Tracking Mode</b>	<b><math>c_{L0}</math></b>	<b><math>c_{L1}</math></b>
Residual Carrier	4.0	1.1
Suppressed Carrier	0.56	7.3

## 5.4 Subcarrier Synchronization

Subcarrier demodulation loss  $\eta_{SUB}$  ( $0 < \eta_{SUB} \leq 1$ ) is a contributor to system loss. It is the result of imperfect subcarrier synchronization. In general, the subcarrier demodulation loss is a function of subcarrier loop signal-to-noise ratio, the coding scheme, the threshold BER or FER, and the type of subcarrier (squarewave or sinewave).

The signal-to-noise ratio  $\rho_{SUB}$  in a subcarrier synchronization loop is given by (Reference 10)

$$\rho_{SUB} = \begin{cases} \left(\frac{2}{\pi}\right)^2 \cdot \frac{S_{SUB}}{W_{SUB}B_{SUB}} \cdot \frac{P_D}{N_0}, & \text{squarewave subcarrier} \\ \frac{S_{SUB}}{B_{SUB}} \cdot \frac{P_D}{N_0}, & \text{sinewave subcarrier} \end{cases} \quad (37)$$

where  $B_{SUB}$  is the (one-sided) noise-equivalent subcarrier loop bandwidth.  $S_{SUB}$  is the squaring loss of the subcarrier loop. For a squarewave subcarrier,  $P_D$  is the power in all the data modulation sidebands; whereas for a sinewave subcarrier,  $P_D$  is the power in the fundamental data modulation sidebands only. For a squarewave subcarrier,  $W_{SUB}$  is the subcarrier loop window factor ( $W_{SUB} = 2^{-n}$ , where  $n = 0, 1, 2, 3$ , or  $4$ ). A window is not used with sinewave subcarriers. The squaring loss  $S_{SUB}$  is, in the case of either squarewave or sinewave,

$$S_{SUB} = \frac{2 \frac{E_S}{N_0}}{1 + 2 \frac{E_S}{N_0}} \quad (38)$$

It is recommended that the following constraint on subcarrier tracking be observed.

$$\rho_{SUB} = \begin{cases} 100.0 & (20 \text{ dB}), \text{ squarewave subcarrier} \\ 50.0 & (17 \text{ dB}), \text{ sinewave subcarrier} \end{cases} \quad (39)$$

Subcarrier demodulation loss is modeled as an interpolation between a High-Rate Model (HRM) and a Low-Rate Model (LRM). This interpolation is

$$\eta_{SUB}^* = a \cdot \eta_{HSUB}^* + (1-a) \cdot \eta_{LSUB}^* \quad (40)$$

where

$$\eta_{SUB}^* = \text{positive decibel subcarrier demodulator loss} \\ \left( \eta_{SUB}^* = -10 \log \eta_{SUB} \right)$$

- $\eta^*_{HSUB}$  = positive decibel HRM subcarrier demodulator loss  
 $\eta^*_{LSUB}$  = positive decibel LRM subcarrier demodulator loss  
 $a$  = interpolation factor ( $0 \leq a \leq 1$ )

The interpolation factor depends on the code. For uncoded and convolutionally coded telemetry, the interpolation factor  $a$  is given by

$$a = \frac{1}{4B_{SUB}T_{SYM}} \left[ 1 - \frac{1}{8B_{SUB}T_{SYM}} \left( 1 - e^{-8B_{SUB}T_{SYM}} \right) \right] \quad (41)$$

where  $B_{SUB}$  is the subcarrier loop bandwidth and  $T_{SYM}$  is the symbol period (the reciprocal of symbol rate). For concatenated and turbo codes, the interpolation factor  $a$  is given by

$$a = \frac{1}{1 + c_1 \left( R/B_{SUB} \right)^{-c_2}} \quad (42)$$

where  $R$  is the bit rate. The coefficients  $c_1$  and  $c_2$  depend on the code. Table 18 gives these coefficients for concatenated codes. The coefficients for turbo codes were provided in Table 10.

Table 18. Interpolation Factor Coefficients  $c_1$  and  $c_2$  for Concatenated Codes

Concatenated Code	$c_1$	$c_2$
RS with ( $k=7, r=1/2$ ) Convolutional	76,000.	1.3
RS with ( $k=15, r=1/4$ ) or ( $k=15, r=1/6$ ) Convolutional	129,000.	1.3

The HRM subcarrier demodulation loss is modeled with a curve-fit whose form depends on whether the subcarrier is squarewave or sinewave.

$$\eta^*_{HSUB} = \begin{cases} c_0 (\rho_{SUB})^{c_1}, & \text{squarewave} \\ c_0 \left( e^{c_1/\rho_{SUB}} - 1 \right), & \text{sinewave} \end{cases} \quad (43)$$

The HRM coefficients  $c_0$  and  $c_1$  of Equation (43) depend on the code and the threshold BER as well as the type of subcarrier (squarewave or sinewave). Table 19 provides the coefficients for uncoded and convolutionally coded telemetry using a squarewave subcarrier. Table 20 provides the same information for a sinewave subcarrier. The coefficients given in Tables 19 and 20 for the ( $k=15, r=1/6$ ) convolutional code also apply to the ( $k=15, r=1/4$ ) code. Tables 21 and 22 provide the coefficients for concatenated codes using squarewave and sinewave

subcarriers at a threshold FER (from Table 7) of  $1 \times 10^{-5}$ . Tables 23 and 24 provide the coefficients for turbo codes listed in Table 8 at a threshold FER of  $1 \times 10^{-4}$  for residual carrier and suppressed carrier.

The LRM subcarrier demodulation loss is independent of the code and is modeled with a curve-fit of the form

$$\eta_{LSUB}^* = \begin{cases} 4.6(\rho_{SUB})^{-0.50}, & \text{squarewave} \\ 5.8(\rho_{SUB})^{-1.07}, & \text{sinewave} \end{cases} \quad (44)$$

Table 19. Subcarrier Demodulation HRM Loss Coefficients for Uncoded and Convolutionally Coded Data using Squarewave Subcarriers

Code	Threshold BER	Subcarrier Demodulation Loss Coefficient $c_0$	Subcarrier Demodulation Loss Coefficient $c_1$
Uncoded	$10^{-2}$	6.3	-0.55
Uncoded	$5 \times 10^{-3}$	6.6	-0.56
Uncoded	$10^{-3}$	7.7	-0.58
Uncoded	$10^{-4}$	9.8	-0.61
Uncoded	$10^{-5}$	13.	-0.66
( $k=7, r=1/2$ )	$10^{-2}$	12.	-0.65
( $k=7, r=1/2$ )	$5 \times 10^{-3}$	13.	-0.66
( $k=7, r=1/2$ )	$10^{-3}$	16.	-0.69
( $k=7, r=1/2$ )	$10^{-4}$	21.	-0.74
( $k=7, r=1/2$ )	$10^{-5}$	29.	-0.78
( $k=15, r=1/6$ )	$10^{-2}$	22.	-0.73
( $k=15, r=1/6$ )	$5 \times 10^{-3}$	25.	-0.76
( $k=15, r=1/6$ )	$10^{-3}$	31.	-0.79
( $k=15, r=1/6$ )	$10^{-4}$	40.	-0.83
( $k=15, r=1/6$ )	$10^{-5}$	53.	-0.87

Table 20. Subcarrier Demodulation HRM Loss Coefficients for Uncoded and Convolutionally Coded Data using Sinewave Subcarriers

<b>Code</b>	<b>Threshold BER</b>	<b>Subcarrier Demodulation Loss Coefficient <math>c_0</math></b>	<b>Subcarrier Demodulation Loss Coefficient <math>c_1</math></b>
Uncoded	$10^{-2}$	0.27	15.2
Uncoded	$5 \times 10^{-3}$	0.21	18.5
Uncoded	$10^{-3}$	0.12	29.3
Uncoded	$10^{-4}$	0.031	62.7
Uncoded	$10^{-5}$	0.000023	244.
( $k=7, r=1/2$ )	$10^{-2}$	0.11	34.6
( $k=7, r=1/2$ )	$5 \times 10^{-3}$	0.085	42.5
( $k=7, r=1/2$ )	$10^{-3}$	0.041	65.2
( $k=7, r=1/2$ )	$10^{-4}$	0.010	116.
( $k=7, r=1/2$ )	$10^{-5}$	0.0030	174
( $k=15, r=1/6$ )	$10^{-2}$	0.13	38.4
( $k=15, r=1/6$ )	$5 \times 10^{-3}$	0.098	46.9
( $k=15, r=1/6$ )	$10^{-3}$	0.067	65.4
( $k=15, r=1/6$ )	$10^{-4}$	0.044	93.4
( $k=15, r=1/6$ )	$10^{-5}$	0.021	135.

Table 21. Subcarrier Demodulation HRM Loss Coefficients for Concatenated Codes Using Squarewave Subcarriers

<b>Concatenated Code</b>	<b>Subcarrier Demodulation Loss Coefficient <math>c_0</math></b>	<b>Subcarrier Demodulation Loss Coefficient <math>c_1</math></b>
RS with ( $k=7, r=1/2$ ) Convolutional	56.	-0.69
RS with ( $k=15, r=1/4$ ) or ( $k=15, r=1/6$ ) Convolutional	50.	-0.65

Table 22. Subcarrier Demodulation HRM Loss Coefficients for Concatenated Codes Using Sinewave Subcarriers

Concatenated Code	Subcarrier Demodulation Loss Coefficient $c_0$	Subcarrier Demodulation Loss Coefficient $c_1$
RS with $(k=7, r=1/2)$ Convolutional	1260.	-1.70
RS with $(k=15, r=1/4)$ or $(k=15, r=1/6)$ Convolutional	643.	-1.51

Table 23. Subcarrier Demodulation HRM Loss Coefficients for Turbo Codes Using Squarewave Subcarriers

Turbo Codes	Subcarrier Demodulation Loss Coefficient $c_0$	Subcarrier Demodulation Loss Coefficient $c_1$
$(1784, 1/2)$ , $(1784, 1/3)$ , $(1784, 1/4)$ , $(1784, 1/6)$	62	-0.76
$(3568, 1/2)$ , $(3568, 1/3)$ , $(3568, 1/4)$ , $(3568, 1/6)$	53	-0.71
$(7136, 1/2)$ , $(7136, 1/3)$ , $(7136, 1/4)$ , $(7136, 1/6)$	48	-0.67
$(8920, 1/2)$ , $(8920, 1/3)$ , $(8920, 1/4)$ , $(8920, 1/6)$	46	-0.66

Table 24. Subcarrier Demodulation HRM Loss Coefficients for Turbo Codes Using Sinewave Subcarriers

Turbo Codes	Subcarrier Demodulation Loss Coefficient $c_0$	Subcarrier Demodulation Loss Coefficient $c_1$
(1784, 1/2), (1784, 1/3), (1784, 1/4), (1784, 1/6)	6490	-2.23
(3568, 1/2), (3568, 1/3), (3568, 1/4), (3568, 1/6)	2450	-1.97
(7136, 1/2), (7136, 1/3), (7136, 1/4), (7136, 1/6)	881	-1.67
(8920, 1/2), (8920, 1/3), (8920, 1/4), (8920, 1/6)	768	-1.63

## 5.5 Symbol Synchronization

Imperfect symbol synchronization results in a finite symbol synchronization loss,  $\eta_{SYM}$  ( $0 < \eta_{SYM} \leq 1$ ), which is a contributor to system loss. The symbol synchronization loss is a function of symbol loop signal-to-noise ratio.

The signal-to-noise ratio  $\rho_{SYM}$  in the symbol synchronization loop is given by (Reference 11)

$$\rho_{SYM} = \frac{2}{(2\pi)^2} \cdot \frac{S_{SYM}}{W_{SYM} B_{SYM}} \cdot \frac{P_D}{N_0} \quad (45)$$

where  $B_{SYM}$  is the (one-sided) noise-equivalent symbol loop bandwidth,  $W_{SYM}$  is the symbol loop window factor ( $W_{SYM} = 2^{-n}$ , where  $n = 0, 1, 2, 3$ , or  $4$ ), and  $S_{SYM}$  is the squaring loss of the symbol loop. In the case of QPSK/OQPSK, the  $P_D/N_0$  of Equation (45) should be interpreted as  $1/2$  ( $P_T/N_0$ ), since only the power in one of the two quadrature channels assists the symbol synchronization process.  $S_{SYM}$  takes on values from 0 to 1 and asymptotically equals 1 for large values of  $E_s/N_0$ . Figure 24 shows  $S_{SYM}$  (dB) as a function of  $E_s/N_0$ . Appendix G gives equations for calculating  $S_{SYM}$ .

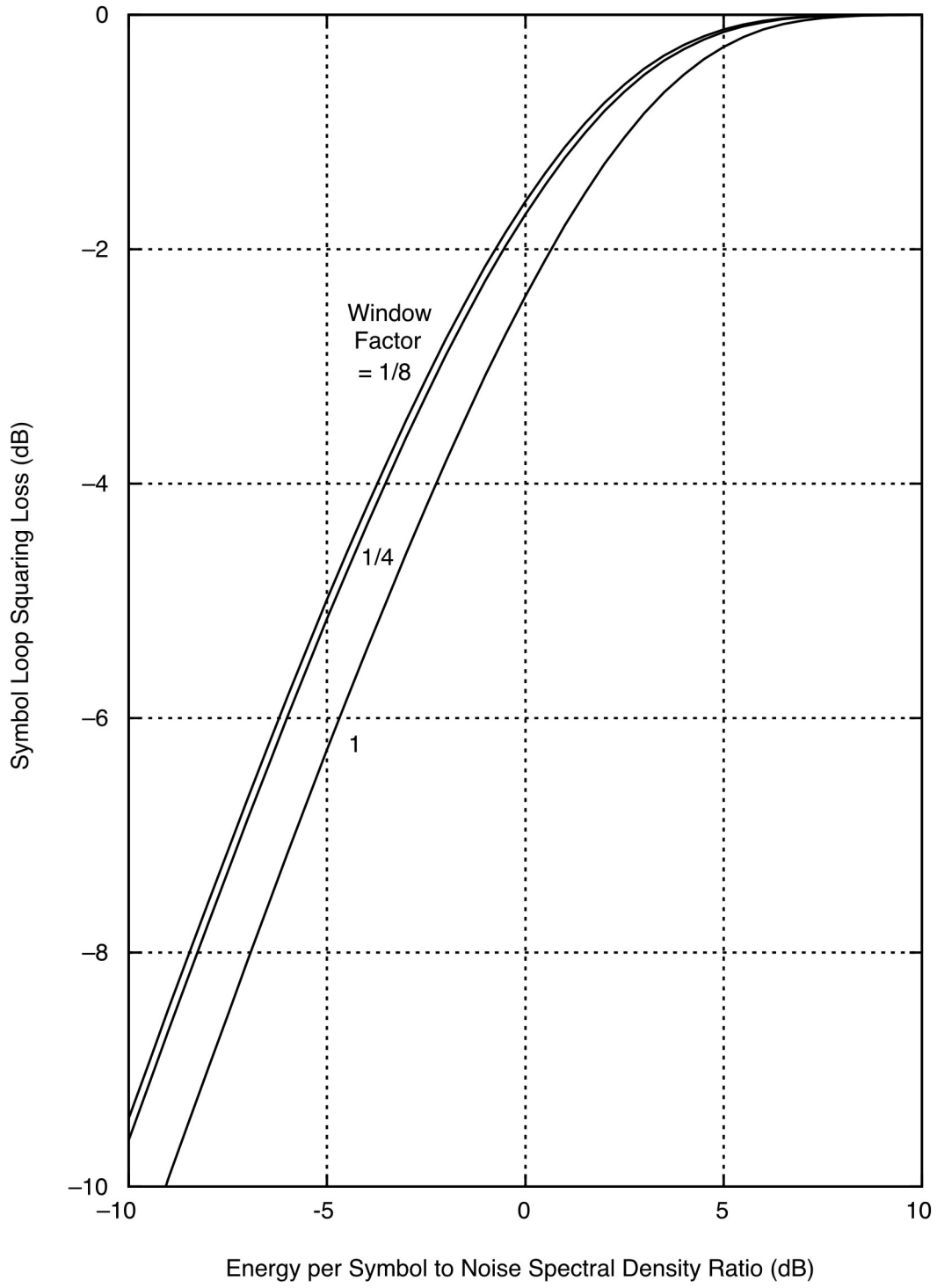


Figure 24. Symbol Loop Squaring Loss

It is recommended that the following constraint on symbol synchronization be observed.

$$\rho_{SYM} \geq 31.6 \text{ (15 dB)} \quad (46)$$

The inequality (46) is based on the assumption that the symbol transition density is approximately 0.5 or higher. If the symbol transition density is closer to 0.25, then it is recommended that  $\rho_{SYM}$  be at least 18 dB.

Symbol synchronization loss is modeled as an interpolation between a High-Rate Model (HRM) and a Low-Rate Model (LRM). This interpolation is

$$\eta_{SYM}^* = a \cdot \eta_{HSYM}^* + (1-a) \cdot \eta_{LSYM}^* \quad (47)$$

where

$$\begin{aligned} \eta_{SYM}^* &= \text{positive decibel symbol synchronizer loss } \left( \eta_{SYM}^* = -10 \log \eta_{SYM} \right) \\ \eta_{HSYM}^* &= \text{positive decibel HRM symbol synchronizer loss} \\ \eta_{LSYM}^* &= \text{positive decibel LRM symbol synchronizer loss} \\ a &= \text{interpolation factor } (0 \leq a \leq 1) \end{aligned}$$

The interpolation factor depends on the code. For uncoded and convolutionally coded telemetry, the interpolation factor  $a$  is given by

$$a = \frac{1}{4B_{SYM}T_{SYM}} \left[ 1 - \frac{1}{8B_{SYM}T_{SYM}} \left( 1 - e^{-8B_{SYM}T_{SYM}} \right) \right] \quad (48)$$

where  $B_{SYM}$  is the symbol loop bandwidth and  $T_{SYM}$  is the symbol period (the reciprocal of symbol rate). For concatenated and turbo codes, the interpolation factor  $a$  is given by

$$a = \frac{1}{1 + c_1 \left( R/B_{SYM} \right)^{-c_2}} \quad (49)$$

where  $R$  is the bit rate. The coefficients  $c_1$  and  $c_2$  were provided in Table 18 for concatenated codes and in Table 10 for turbo codes.

The HRM symbol synchronization loss is modeled with a curve-fit of the form

$$\eta_{HSYM}^* = c_0 \left( \rho_{SYM} \right)^{c_1} \quad (50)$$

where the HRM coefficients  $c_0$  and  $c_1$  depend on the code. For uncoded and convolutionally coded telemetry, the coefficients of Equation (50) are  $c_0 = 2.2$  and  $c_1 = -0.62$ . In fact, an

excellent approximation for  $\eta_{SYM}^*$  may be obtained in this case (without the need for an interpolation) as follows

$$\eta_{SYM}^* = 2.2(\rho_{SYM})^{-0.62}. \quad (51)$$

The HRM coefficients  $c_0$  and  $c_1$  of Equation (50) are given in Table 25 for concatenated codes at a threshold FER of  $1 \times 10^{-5}$  and in Table 26 for the turbo codes listed in Table 8 at a threshold FER of  $1 \times 10^{-4}$ .

Table 25. Symbol Synchronization HRM Loss Coefficients for Concatenated Codes

Concatenated Code	Symbol Synchronization Loss Coefficient $c_0$	Symbol Synchronization Loss Coefficient $c_1$
RS with $(k=7, r=1/2)$ Convolutional	9.7	-0.77
RS with $(k=15, r=1/4)$ or $(k=15, r=1/6)$ Convolutional	8.2	-0.68

Table 26. Symbol Synchronization HRM Loss Coefficients for Turbo Codes

Turbo Codes	Symbol Synchronization Loss Coefficient $c_0$	Symbol Synchronization Loss Coefficient $c_1$
$(1784, 1/2), (1784, 1/3),$ $(1784, 1/4), (1784, 1/6)$	6.6	-0.75
$(3568, 1/2), (3568, 1/3),$ $(3568, 1/4), (3568, 1/6)$	7.3	-0.75
$(7136, 1/2), (7136, 1/3),$ $(7136, 1/4), (7136, 1/6)$	7.4	-0.69
$(8920, 1/2), (8920, 1/3),$ $(8920, 1/4), (8920, 1/6)$	6.8	-0.66

The LRM symbol synchronization loss is independent of the code and can be modeled with a curve-fit of the same form (but with different coefficients)

$$\eta_{LSYM}^* = 2.27(\rho_{SYM})^{-0.50} \quad (52)$$

## 5.6 *Waveform Distortion*

Deviations of either the subcarrier waveform or the symbol waveform from ideal will adversely affect telemetry performance. In general, waveform distortion loss  $\eta_{WD}$  (fractional and dimensionless) is the composite loss factor that incorporates both of these deviations.  $\eta_{WD}$ , in turn, is a contributor to the system loss  $\eta_{SYS}$ .

In the case of no subcarrier, only the symbol waveform deviation is of concern.

$$\eta_{WD} = 1 - 2 \left( \frac{\Delta T_{SYM}}{T_{SYM}} \right) + 2 \left( \frac{\Delta T_{SYM}}{T_{SYM}} \right)^2 \quad (53)$$

$T_{SYM}$  is the symbol period in seconds. The parameter  $\Delta T_{SYM}$  is a measure of the finite risetime is recommended that  $\Delta T_{SYM}$  be less than 2 percent.

In the case of a squarewave subcarrier,

$$\eta_{WD} = \left[ 1 - \frac{2\Delta T_{SUB}}{T_{SUB}} \right]^2 \cdot \left[ 1 - 2 \left( \frac{\Delta T_{SYM}}{T_{SYM}} \right) + 2 \left( \frac{\Delta T_{SYM}}{T_{SYM}} \right)^2 \right] \quad (54)$$

where  $T_{SUB}$  is the subcarrier period in seconds and  $\Delta T_{SUB}$  its asymmetry. Equation (54) is not applicable in the case of a sinewave subcarrier. The waveform distortion loss associated with a sinewave subcarrier should normally be negligible.

## 5.7 *Amplitude Scintillation at Small Sun-Earth-Probe (SEP) Angles*

When the Sun-Earth-Probe (SEP) angle is small and the spacecraft is beyond the sun, Rician fading of the signal occurs due to multipath propagation of the downlink signal within the solar corona. This is called amplitude scintillation. The effect is worse at lower carrier frequencies. For small SEP angles, the BER or FER increases dramatically as a result of amplitude scintillation. Appendix I summarizes the theory of amplitude scintillation. Figures 25, 26, and 27 illustrate the degradation to FER for a (1784, 1/3) turbo code due to amplitude scintillation for the cases of S-band, X-band and Ka-band, respectively.

Turbo codes have an error floor in their performance that are not shown in Figures 25 through 27. The error floor is different for each turbo code but, for each of the turbo codes shown here, the error floor lies below a frame error rate of  $10^{-5}$  and therefore is not visible in the figures. Great care must be taken in evaluating the performance of these codes for frame error rates less than  $10^{-5}$ .

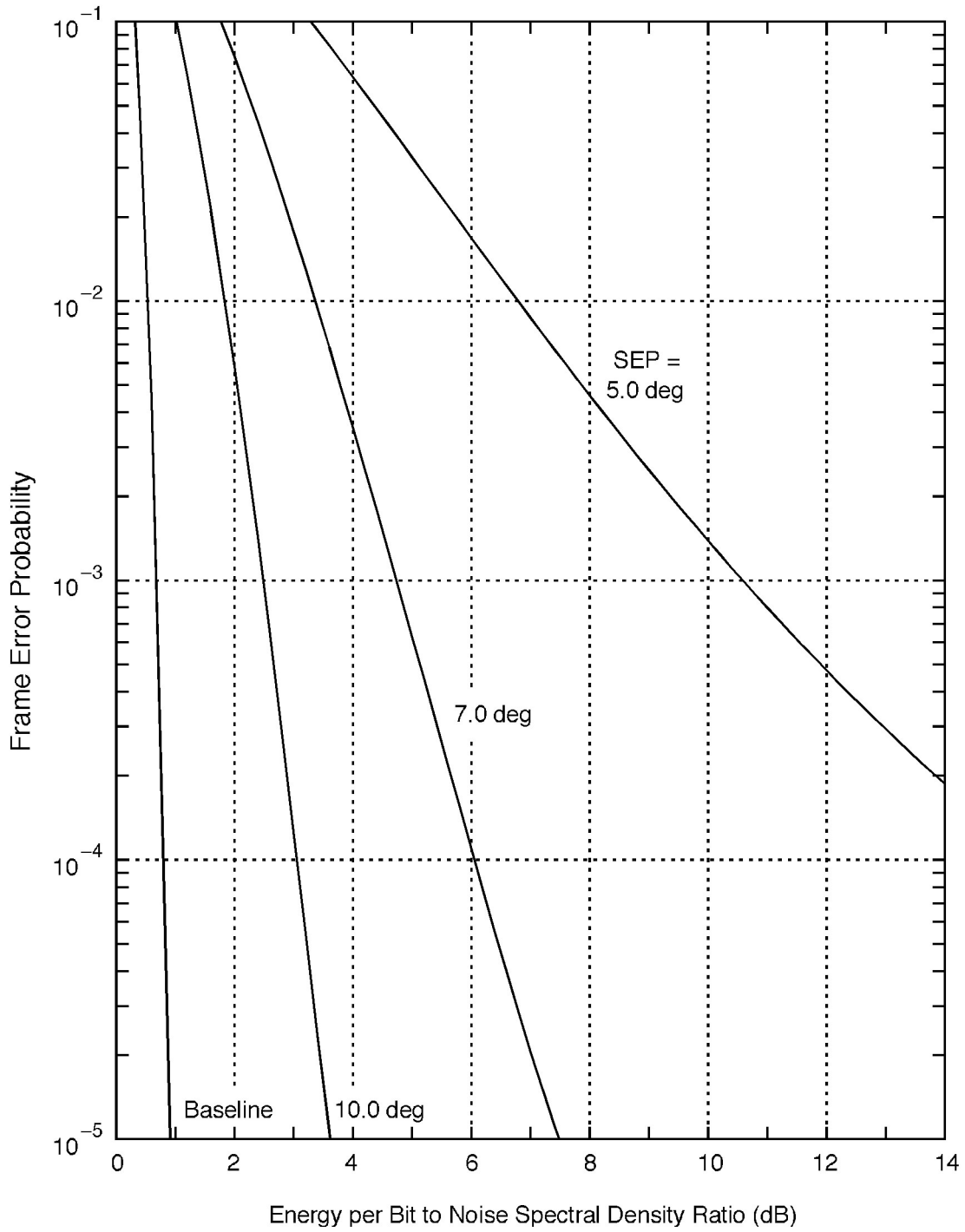


Figure 25. (1784, 1/3) Turbo Code Performance at S-Band With Amplitude Scintillation

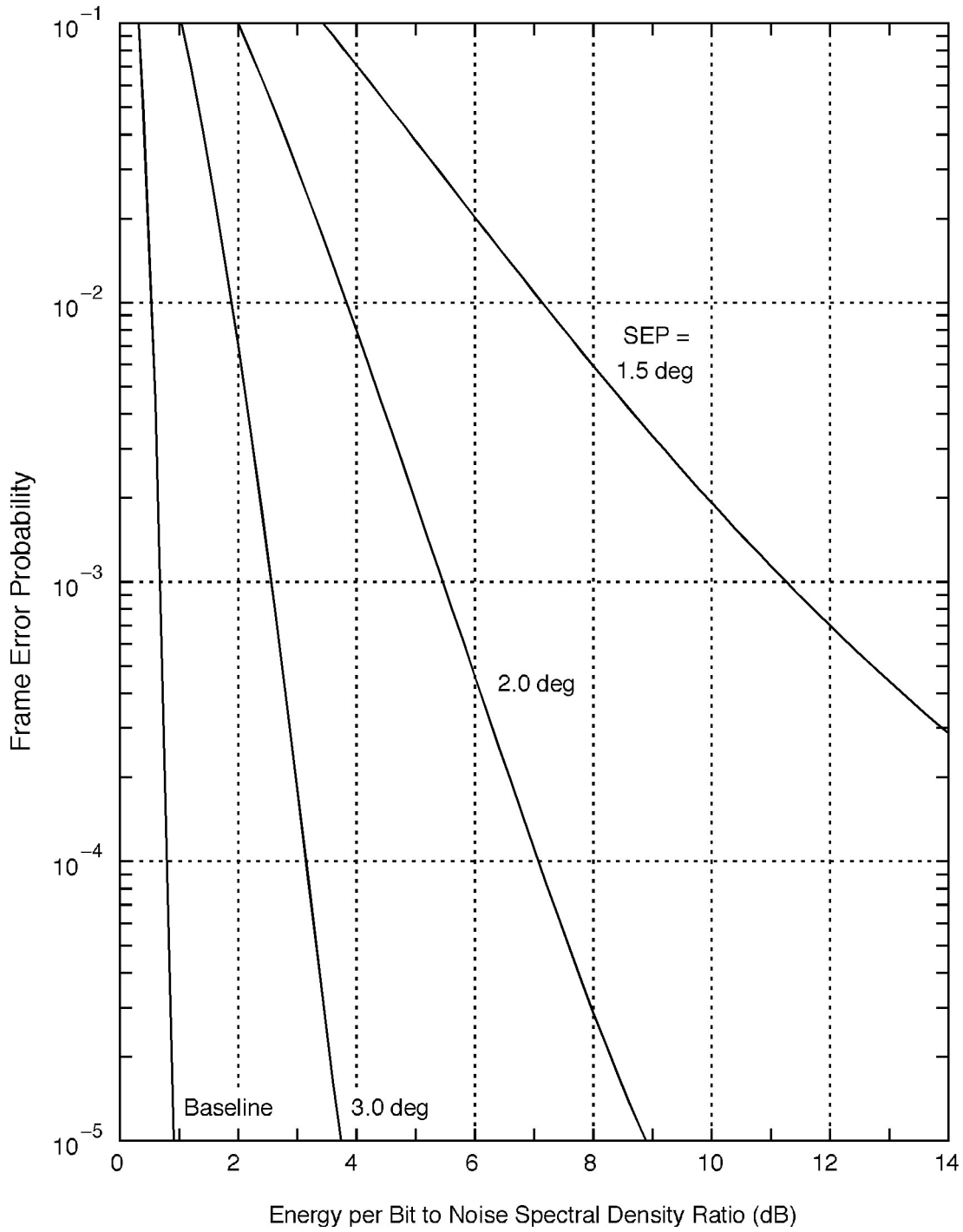


Figure 26. (1784, 1/3) Turbo Code Performance at X-Band With Amplitude Scintillation

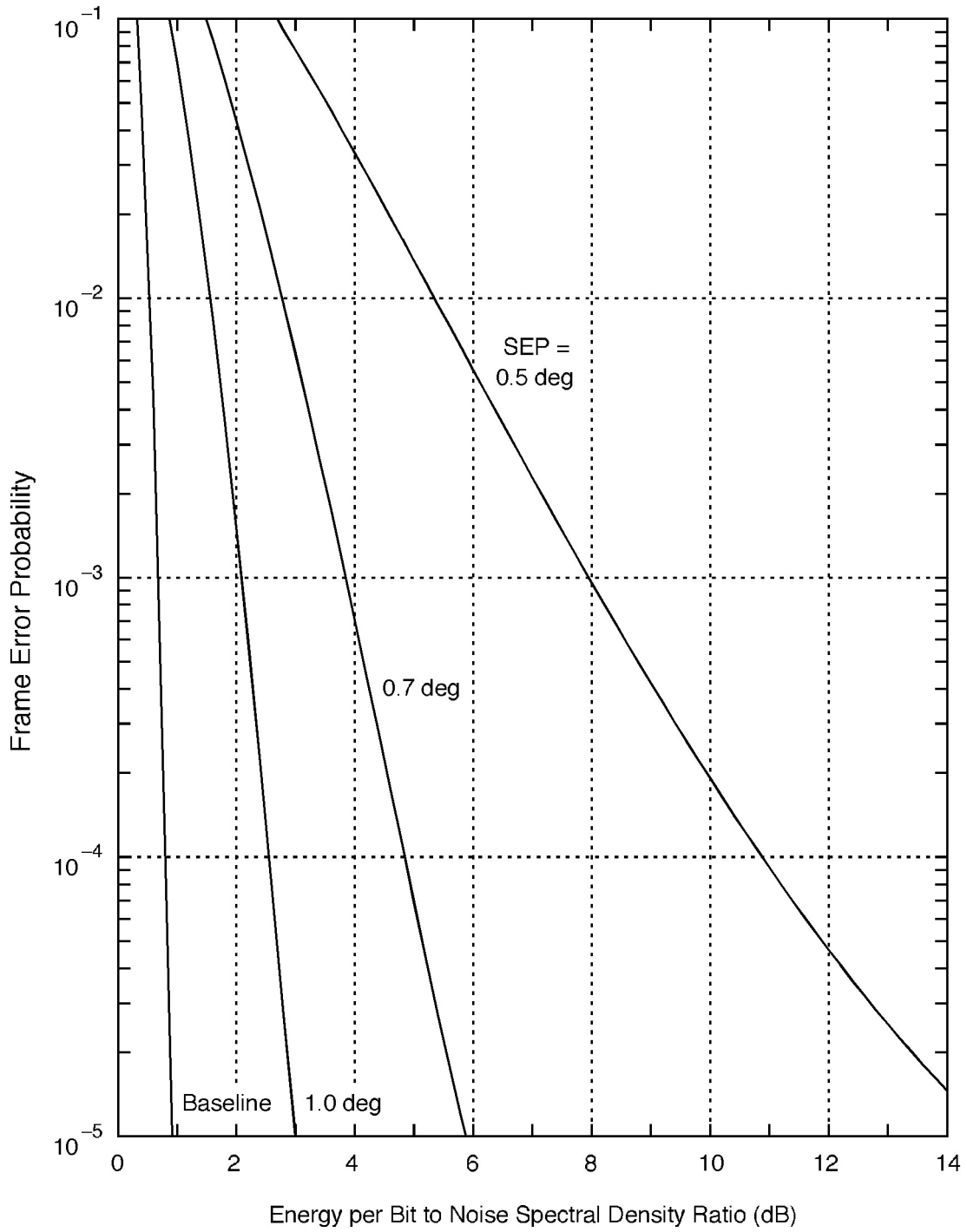


Figure 27. (1784, 1/3) Turbo Code Performance at Ka-Band With Amplitude Scintillation

## ***Appendix A*** ***Baseline BER and FER Performance***

The baseline performance is the Bit Error Rate (BER) or Frame Error Rate (FER) when synchronization is perfect (i.e., with a system loss of 0 dB). For uncoded and convolutionally coded telemetry, BER is the appropriate figure of merit. For concatenated and turbo codes, FER is the appropriate figure of merit.

### ***A.1 Uncoded and Convolutionally Coded Telemetry***

For uncoded and convolutionally coded telemetry, the functional dependence of BER on  $E_b/N_0$  in the ideal case of no system loss is here denoted

$$\text{Baseline: } \text{BER} = f(E_b/N_0) \quad (\text{A-1})$$

In Equation (A-1),  $E_b/N_0$  is a dimensionless quantity (i.e., it is the true ratio of bit energy to noise spectral density). This performance is never achieved in practice. Nonetheless, this idealized performance is a useful reference (baseline) from which to measure actual performance. For uncoded telemetry,

$$f(x) = \frac{1}{2} \text{erfc}(\sqrt{x}) \quad (\text{A-2})$$

where

$$\text{erfc}(x) = 1 - \text{erf}(x) = 1 - \frac{2}{\sqrt{\pi}} \int_0^x e^{-y^2} dy \quad (\text{A-3})$$

For convolutionally coded telemetry, the baseline telemetry performance is approximated as

$$f(x) = \min\left\{\frac{1}{2}, \exp(a_0 - a_1 x)\right\} \quad (\text{A-4})$$

where the coefficients  $a_0$  and  $a_1$  depend on the particular convolutional code, as indicated in Table A-1.

Table A-1. Coefficients  $a_0$  and  $a_1$  for Equation (A-4)

<b>Code</b>	<b><math>a_0</math></b>	<b><math>a_1</math></b>
$(k = 7, r = 1/2)$	4.4514	5.7230
$(k = 15, r = 1/4)$	9.8070	13.431
$(k = 15, r = 1/6)$	9.8070	14.064

## A.2 *Concatenated and Turbo-Coded Telemetry*

For concatenated and turbo codes, the functional dependence of FER on  $E_b/N_0$  in the ideal case of no system loss is here denoted

$$\text{Baseline: } FER = f(E_b/N_0) \quad (\text{A-5})$$

In Equation (A-5),  $E_b/N_0$  is a dimensionless quantity (i.e., it is the true ratio of bit energy to noise spectral density). This performance is never achieved in practice. Nonetheless, this idealized performance is a useful reference (baseline) from which to measure actual performance.

The baseline telemetry performance for concatenated codes is approximated as

$$f(x) = \min\{1, \exp(a_0 - a_1 x)\} \quad (\text{A-6})$$

where the coefficients  $a_0$  and  $a_1$  depend on the particular code, as indicated in Table A-2.

Table A-2. Coefficients  $a_0$  and  $a_1$  for Equation (A-6), Concatenated Codes

<b>Concatenated Code</b>	<b><math>a_0</math></b>	<b><math>a_1</math></b>
RS with ( $k=7, r=1/2$ ) Convolutional	105.0019	67.4242
RS with ( $k=15, r=1/4$ ) Convolutional	158.2971	127.5629
RS with ( $k=15, r=1/6$ ) Convolutional	158.2971	133.5748

Simulations performed at JPL have characterized the baseline performance of the turbo codes. Tables A-3 through A-6 give the simulation data for these codes. This results were obtained by using 10 decoding iterations per frame. In this module, the baseline performance of the turbo codes is based on interpolations of the simulation data given below.

Table A-3. Rate 1/2 Turbo Code Baseline Data

$E_b/N_0$	Turbo Code			
	(1784, 1/2)	(3568, 1/2)	(7136, 1/2)	(8920, 1/2)
0.4		1.0000E+00		
0.5		—		1.0000E+00
0.6	7.5000E-01	8.0000E-01		8.8496E-01
0.7	—	—	5.5266E-01	5.9524E-01
0.8	3.8931E-01	2.6247E-01	1.8382E-01	1.8939E-01
0.9	—	—	2.5046E-02	2.0309E-02
1.0	7.5529E-02	2.2411E-02	1.4271E-03	8.4691E-04
1.1	—	—	7.7270E-05	3.5650E-05
1.2	7.9605E-03	3.1980E-04	7.6700E-06	1.5510E-05
1.3	—	—		1.2280E-05
1.4	3.2503E-04	4.0800E-06		6.7700E-06
1.5	—	—		
1.6	1.1620E-05	1.5800E-06		
1.7	—	—		
1.8	3.7500E-06	5.8000E-07		
1.9	—	—		
2.0	2.2500E-06	6.0000E-08		
2.1	—	—		
2.2	7.5000E-07	1.1000E-07		

Table A-4. Rate 1/3 Turbo Code Baseline Data

$E_b/N_0$	Turbo Code			
	(1784, 1/3)	(3568, 1/3)	(7136, 1/3)	(8920, 1/3)
-0.4	9.9020E-01			
-0.3	—			
-0.2	9.0090E-01			
-0.1	—			
0.0	6.8493E-01			8.3333E-01
0.1	—		4.3328E-01	4.9505E-01
0.2	2.9762E-01	1.8065E-01	1.0761E-01	9.7752E-02
0.3	—	5.1557E-02	1.0989E-02	8.9847E-03
0.4	4.7174E-02	9.0463E-03	4.4099E-04	2.0755E-04
0.5	—	9.5734E-04	1.0050E-05	2.8730E-05
0.6	4.4583E-03	4.1120E-05		1.4360E-05
0.7	—	4.5100E-06		1.1490E-05
0.8	9.2350E-05			
0.9	—			
1.0	1.9100E-06			

Table A-5. Rate 1/4 Turbo Code Baseline Data

$E_b/N_0$	Turbo Code			
	(1784, 1/4)	(3568, 1/4)	(7136, 1/4)	(8920, 1/4)
-0.4				
-0.3				9.9010E-01
-0.2				8.4746E-01
-0.1			3.3866E-01	3.7594E-01
0.0	2.3810E-01	1.3508E-01	6.7147E-02	7.3260E-02
0.1	1.4006E-01	3.1327E-02	5.5659E-03	2.9790E-03
0.2	3.8865E-02	4.1032E-03	2.9471E-04	5.4510E-05
0.3	9.9325E-03	4.9503E-04	1.0723E-04	2.5700E-06
0.4	2.1765E-03	6.0170E-05		2.0300E-06
0.5	4.9670E-04			1.7100E-06
0.6	7.7840E-05			7.8000E-07
0.7	1.0430E-05			
0.8	3.1900E-06			
0.9	1.7100E-06			
1.0	9.7000E-07			
1.1	5.1000E-07			
1.2	6.6000E-07			

Table A-6. Rate 1/6 Turbo Code Baseline Data

$E_b/N_0$	Turbo Code			
	(1784, 1/6)	(3568, 1/6)	(7136, 1/6)	(8920, 1/6)
-0.50				9.0909E-01
-0.45				7.2464E-01
-0.40			4.7659E-01	4.7619E-01
-0.35			—	2.8653E-01
-0.30	2.7855E-01		1.1924E-01	9.9701E-02
-0.25	—		—	3.2362E-02
-0.20	1.4793E-01	4.8632E-02	1.2559E-02	6.6542E-03
-0.15	—	—	—	1.1703E-03
-0.10	5.1203E-02	7.2787E-03	6.4147E-04	1.3089E-04
-0.05	—	—	—	1.6310E-05
0.0	1.1990E-02	9.2768E-04	4.5750E-05	5.5200E-06
0.05	—	—		4.3200E-06
0.10	3.5388E-03	5.9720E-05		2.4000E-06
0.15	—	—		
0.20	5.8113E-04	9.6500E-06		
0.25	—			
0.30	5.7830E-05			
0.35	—			
0.40	9.9500E-06			
0.45	—			
0.50	2.3400E-06			

## **Appendix B**

### **High-Rate Model (HRM) Radio Loss**

The High-Rate Model (HRM) is discussed in this appendix in terms of Bit Error Rate (BER); but for concatenated and turbo codes, Frame Error Rate (FER) is the proper figure of merit. So for these codes, the reader should regard BER in the following equations as being a stand-in for FER.

The HRM radio loss,  $\eta_{HRM}$  (fractional and dimensionless), is given by

$$\eta_{HRM} = \frac{f^{-1}(BER)}{E_b/N_0} \quad (B-1)$$

where  $f(*)$  is the ideal functional dependence of probability of bit (frame) error on bit SNR (see Appendix A), corresponding to zero decibels of system loss. In the above equation,  $E_b/N_0$  is the actual bit SNR needed to achieve a given threshold BER in the presence of imperfect carrier synchronization; it is the solution of the following equation (Reference 12)

$$BER = \int_{-\pi/2}^{\pi/2} f\left(\frac{E_b}{N_0} \cos^2 \phi\right) p_\phi(\phi) d\phi \quad (B-2)$$

where  $p_\phi(\phi)$  is the probability density function of the carrier loop phase error  $\phi$  and BER is, as before, the threshold bit error rate.

When tracking a residual carrier,

$$p_\phi(\phi) = \frac{\exp\left[\frac{\cos \phi}{\sigma_\phi^2}\right]}{\int_{-\pi/2}^{\pi/2} \exp\left[\frac{\cos \psi}{\sigma_\phi^2}\right] d\psi}, \quad |\phi| \leq \pi/2 \quad (B-3)$$

When tracking suppressed carrier BPSK,

$$p_\phi(\phi) = \frac{\exp\left[\frac{\cos \phi}{4\sigma_\phi^2}\right]}{\int_{-\pi/2}^{\pi/2} \exp\left[\frac{\cos 2\psi}{4\sigma_\phi^2}\right] d\psi}, \quad |\phi| \leq \pi/2 \quad (B-4)$$

For either case,  $p_\phi(\phi)$  is assumed to be zero for  $|\phi| > \pi/2$ . The parameter  $\sigma_\phi^2$  is the carrier loop phase error variance. The presence of  $f(*)$  in Equation (B-2) means that the HRM radio loss depends on the coding scheme; it also depends on the threshold BER.

When there is a static phase error caused by Doppler dynamics,  $p_\phi(\phi)$  has a different form. For a residual-carrier loop

$$p_\phi(\phi) = \frac{\exp\left[\frac{\cos\phi + \phi \sin \xi_{spe}}{\sigma_\phi^2}\right]}{\int_{-\pi/2}^{\pi/2} \exp\left[\frac{\cos\psi + \psi \sin \xi_{spe}}{\sigma_\phi^2}\right] d\psi}, \quad |\phi| \leq \pi/2 \quad (\text{B-5})$$

where  $\xi_{spe}$  is the static phase error.

## *Appendix C*

### *Static Phase Error*

The carrier loop, either as type 2 or type 3, has a very large tracking range; even a Doppler offset of several megahertz can be tracked. With a finite Doppler rate, however, there will be a static phase error in a type 2 loop.

Table C-1 shows the static phase error in the carrier that results from various Doppler dynamics for several different loops. These equations are based on the work reported in Reference 13 where standard underdamped and supercritically damped loops are defined.  $B_L$  is the (one-sided) noise-equivalent loop bandwidth of the carrier loop. The Doppler dynamics are here defined by the parameters  $\alpha$ ,  $\beta$ , and  $t$  where  $\alpha$  is the Doppler Rate (Hz/s),  $\beta$  is the Doppler Acceleration (Hz/s<sup>2</sup>), and  $t$  is the time since the beginning of the Doppler acceleration. (If the Doppler acceleration begins before carrier lock,  $t$  is the time since the loop acquired lock.)

The equations of Table C-1 are valid for either residual-carrier or suppressed-carrier BPSK, QPSK or OQPSK. In the presence of a persistent Doppler acceleration, a type 2 loop will periodically slip cycles.

Table C-1. Static Phase Error (rad)

Loop	Constant Range-Rate	Constant Derivative of Range-Rate	Constant Second Derivative of Range-Rate
	Constant Doppler Offset	Constant Doppler Rate	Constant Doppler Acceleration
type 2, standard underdamped	0	$\frac{9\pi}{16B_L^2} \cdot \alpha$	$\left(\frac{9\pi\beta}{16B_L^2}\right)t - \frac{27\pi\beta}{64B_L^3}$
type 2, supercritically damped	0	$\frac{25\pi}{32B_L^2} \cdot \alpha$	$\left(\frac{25\pi\beta}{32B_L^2}\right)t - \frac{125\pi\beta}{128B_L}$
type 3, standard underdamped	0	0	$\frac{12167\pi}{8000B_L^3} \beta$
type 3, supercritically damped	0	0	$\frac{35937\pi}{16384B_L^3} \beta$

## ***Appendix D*** ***Transmitter Phase Noise***

Transmitter phase noise contributes to the phase error in the receiver's carrier loop. This contribution is a zero-mean random process, and its variance equals

$$\sigma_{\phi}^2 = \int_0^{\infty} S_{\theta}(f) |1 - H(j2\pi f)|^2 df, \text{ rad}^2 \quad (\text{D-1})$$

where  $S_{\theta}(f)$  is the one-sided power spectral density of the transmitter phase noise and  $H(j2\pi f)$  is the phase transfer function of the carrier loop.  $S_{\theta}(f)$ , with units of  $\text{rad}^2/\text{Hz}$ , is related to  $L_{\theta}(f)$ , the modulation sideband power spectral density relative to the carrier power, measured in the units  $\text{dBc}/\text{Hz}$  (Reference 14).

$$L_{\theta}(f) = 10 \log \left( \frac{1}{2} S_{\theta}(f) \right) \quad (\text{D-2})$$

For example, if the transmitter phase noise is flicker-of-frequency (i.e.,  $L_{\theta}(f)$  decreases with Fourier frequency  $f$  at a rate of 30 decibels per decade) in the frequency range of interest, and if  $L_{\theta}(1 \text{ Hz}) = -45 \text{ dBc}/\text{Hz}$ , then  $S_{\theta}(f)$  may be modeled as  $S_3/f^3$  with  $S_3$  given by  $2 \times 10^{-45/10} = 0.000063$ .

For a type 2 loop, the phase transfer function  $H(j2\pi f)$  is given by (Reference 13):

$$H(j2\pi f) = \frac{(j2\pi f)K_1 + K_2}{(j2\pi f)^2 + (j2\pi f)K_1 + K_2} \quad (\text{D-3})$$

where

$$K_1 = \frac{8}{3} B_L, \quad K_2 = \frac{1}{2} K_1^2, \quad (\text{standard underdamped})$$

$$K_1 = \frac{16}{5} B_L, \quad K_2 = \frac{1}{4} K_1^2, \quad (\text{supercritically damped})$$

For a type 3 loop, the phase transfer function  $H(j2\pi f)$  is given by (Reference 13):

$$H(j2\pi f) = \frac{(j2\pi f)^2 K_1 + (j2\pi f)K_2 + K_3}{(j2\pi f)^3 + (j2\pi f)^2 K_1 + (j2\pi f)K_2 + K_3} \quad (\text{D-4})$$

where

$$K_1 = \frac{60}{23} B_L, \quad K_2 = \frac{4}{9} K_1^2, \quad K_3 = \frac{2}{27} K_1^3, \quad (\text{standard underdamped})$$

$$K_1 = \frac{32}{11} B_L, \quad K_2 = \frac{1}{3} K_1^2, \quad K_3 = \frac{1}{27} K_1^3 \quad (\text{supercritically damped})$$

Table D-1 lists solutions to Equation (D-1) for several types of carrier loop and for two types of phase noise. These expressions are valid for residual-carrier, suppressed-carrier BPSK, or QPSK/OQPSK.  $B_L$  is the (one-sided) noise-equivalent carrier loop bandwidth.

Table D-1. Carrier Phase Error Variance,  $\sigma_\phi^2$  (rad<sup>2</sup>)

	<b>type 2 standard underdamped</b>	<b>type 2 supercritically damped</b>	<b>type 3 standard underdamped</b>	<b>type 3 supercritically damped</b>
$S_\theta(f) = \frac{S_2}{f^2}$	$\frac{3\pi^2}{8B_L} S_2$	$\frac{5\pi^2}{16B_L} S_2$	$\frac{23\pi^2}{50B_L} S_2$	$\frac{99\pi^2}{256B_L} S_2$
$S_\theta(f) = \frac{S_3}{f^3}$	$\frac{9\pi^3}{32B_L^2} S_3$	$\frac{25\pi^2}{32B_L^2} S_3$	$\frac{529\pi^2(\pi - \ln 2)}{1000B_L^2} S_3$	$\frac{1089\pi^3}{1024B_L^2} S_3$

## ***Appendix E*** ***Solar Phase Noise***

When the Sun-Earth-probe angle is small and the spacecraft is beyond the Sun, microwave carriers pick up phase scintillations in passing through the solar corona. There is a resulting contribution to phase error in the carrier loop. The magnitude of the effect is highly variable, depending on the activity of the sun. Equation (E-1) below, based on the work reported in Reference 15, offers a coarse estimate of the average solar contribution, in units of rad<sup>2</sup>, to carrier loop phase error variance. This equation is valid for residual-carrier, suppressed-carrier BPSK or QPSK/OQPSK, but only for sun-earth-probe angles between 5° and 27°.

$$\sigma_S^2 = \frac{C_{band} \cdot C_{loop}}{(\sin \beta)^{2.45} \cdot B_L^{1.65}}, \quad 5^\circ \leq \beta \leq 27^\circ \quad (\text{E-1})$$

In Equation (E-1),  $\beta$  is the Sun-Earth-probe angle and  $B_L$  is the (one-sided) noise-equivalent carrier loop bandwidth.  $C_{band}$  is a constant for a given set of operating bands.

For one-way or two-way noncoherent operation,

$$C_{band} = \begin{cases} 2.6 \times 10^{-5}, & \text{S - down} \\ 1.9 \times 10^{-6}, & \text{X - down} \\ 1.3 \times 10^{-7}, & \text{Ka - down} \end{cases} \quad (\text{E-2})$$

For coherent operation,

$$C_{band} = \begin{cases} 6.1 \times 10^{-5}, & \text{S - up / S - down} \\ 4.8 \times 10^{-4}, & \text{S - up / X - down} \\ 5.5 \times 10^{-6}, & \text{X - up / X - down} \\ 5.2 \times 10^{-5}, & \text{X - up / Ka - down} \\ 1.9 \times 10^{-6}, & \text{Ka - up / X - down} \\ 2.3 \times 10^{-7}, & \text{Ka - up / Ka - down} \end{cases} \quad (\text{E-3})$$

where  $C_{loop}$  is a constant for a given carrier loop.

$$C_{loop} = \begin{cases} 5.9, & \text{standard underdamped type 2 loop} \\ 5.0, & \text{supercritically damped type 2 loop} \\ 8.2, & \text{standard underdamped type 3 loop} \\ 6.7, & \text{supercritically damped type 3 loop} \end{cases} \quad (\text{E-4})$$

## ***Appendix F*** ***Subcarrier Demodulation Loss***

The subcarrier demodulation loss is discussed in this appendix in terms of Bit Error Rate (BER); but for concatenated and turbo codes, Frame Error Rate (FER) is the proper figure of merit. So for these codes, the reader should regard BER in the following equations as being a stand-in for FER.

The subcarrier demodulation loss  $\eta_{SUB}$  (fractional and dimensionless) is

$$\eta_{SUB} = \frac{f^{-1}(BER)}{E_b / N_0} \quad (\text{F-1})$$

where  $f(*)$  is the ideal functional dependence of probability of bit (frame) error on bit SNR (see Appendix A), corresponding to zero decibels of system loss. In Equation (F-1)  $E_b/N_0$  is the actual bit SNR needed to achieve a given threshold BER in the presence of imperfect subcarrier synchronization (with the assumption of perfect carrier and symbol synchronization); in the case of a squarewave subcarrier, it is the solution of the following equation

$$BER = \int_{-\pi/2}^{\pi/2} f\left(\frac{E_b}{N_0} \left[1 - \frac{2}{\pi} |\phi|\right]^2\right) p_\phi(\phi) d\phi \quad (\text{F-2})$$

where BER is, as before, the threshold bit error rate. The probability density function  $p_\phi(\phi)$  of squarewave subcarrier loop phase error  $\phi$  is modeled as having a Gaussian form within the limits  $|\phi| \leq \pi/2$  and as zero outside those limits.

$$p_\phi(\phi) = \frac{\exp(-\rho_{SUB}\phi^2/2)}{\int_{-\pi/2}^{\pi/2} \exp(-\rho_{SUB}\psi^2/2) d\psi} \quad (\text{F-3})$$

where  $\rho_{SUB}$  is the squarewave subcarrier loop signal-to-noise ratio as computed from Equation (37). Equations (F-1), (F-2), and (F-3) define the subcarrier demodulation loss for a squarewave subcarrier. The presence of  $f(*)$  in Equation (F-2) means that the subcarrier demodulation loss depends on the coding scheme; it also depends on the threshold BER.

For a sinewave subcarrier, the subcarrier demodulation loss is governed by Equations (B-1), (B-2), and (B-4), which also characterize the HRM radio loss with suppressed carrier, except that  $\sigma_\phi^2$  is replaced by  $1/\rho_{SUB}$ , where  $\rho_{SUB}$  is the sinewave subcarrier signal-to-noise ratio as defined in Equation (37).

## **Appendix G**

### **Symbol Loop Squaring Loss**

Symbol loop squaring loss  $S_{SYM}$  is given by (Reference 11)

$$S_{SYM} = \frac{\left[ \operatorname{erf}\left(\sqrt{E_S/N_0}\right) - \frac{W_{SYM}}{2} \sqrt{\frac{E_S/N_0}{\pi}} \exp(-E_S/N_0) \right]^2}{1 + \frac{W_{SYM}}{2} E_S/N_0 - \frac{W_{SYM}}{2} \left[ \frac{1}{\sqrt{\pi}} \exp(-E_S/N_0) + \sqrt{E_S/N_0} \operatorname{erf}\left(\sqrt{E_S/N_0}\right) \right]^2} \quad (\text{G-1})$$

where the error function is given by

$$\operatorname{erf}(x) = \frac{2}{\sqrt{\pi}} \int_0^x e^{-y^2} dy \quad (\text{G-2})$$

$E_S/N_0$  is the ratio of the energy in one binary symbol to the one-sided noise spectral density. In the case of suppressed-carrier BPSK, this is  $(P_T/N_0)T_{SYM}$ , where  $T_{SYM}$  is the binary symbol period. In the case of QPSK/OQPSK, only half the total power is available for symbol synchronization but the quaternary symbol period is double the binary symbol period. So for QPSK/OQPSK, the same  $E_S/N_0$  should be used as with suppressed-carrier BPSK, since

$$\frac{1}{2} (P_T/N_0) \cdot 2T_{SYM} = (P_T/N_0) \cdot T_{SYM} \quad (\text{G-3})$$

## **Appendix H**

### **Symbol Synchronization Loss**

The symbol synchronization loss is discussed in this appendix in terms of Bit Error Rate (BER); but for concatenated and turbo codes, Frame Error Rate (FER) is the proper figure of merit. So, for these codes, the reader should regard BER in the following equations as being a stand-in for FER.

The symbol synchronization loss  $\eta_{SYM}$  (fractional and dimensionless) is

$$\eta_{SYM} = \frac{f^{-1}(BER)}{E_b/N_0} \quad (H-1)$$

where  $f(*)$  is the ideal functional dependence of probability of bit (frame) error on bit SNR (see Appendix A), corresponding to zero decibels of system loss. In Equation (H-1)  $E_b/N_0$  is the actual bit SNR needed to achieve a given threshold BER in the presence of imperfect symbol synchronization (with the assumption of perfect carrier and subcarrier synchronization); it is the solution of the following equation

$$BER = \int_{-\pi/2}^{\pi/2} f \left( \frac{E_b}{N_0} \left[ \frac{1}{2} \left\{ 1 + \left( 1 - \frac{|\phi|}{\pi} \right)^2 \right\} \right] \right) p_\phi(\phi) d\phi \quad (H-2)$$

where BER is, as before, the threshold bit error rate. The probability density function  $p_\phi(\phi)$  of symbol loop phase error  $\phi$  is modeled as having a Gaussian form within the limits  $|\phi| \leq \pi/2$  and as zero outside those limits.

$$p_\phi(\phi) = \frac{\exp(-\rho_{SYM}\phi^2/2)}{\int_{-\pi/2}^{\pi/2} \exp(-\rho_{SYM}\psi^2/2) d\psi} \quad (H-3)$$

In Equation (H-3)  $\rho_{SYM}$  is the symbol loop signal-to-noise ratio as computed from Equation (45).

## ***Appendix I*** ***Rician Fading at Small Sun-Earth-Probe (SEP) Angles***

The discussion in this appendix is in terms of Bit Error Rate (BER); but for concatenated and turbo codes, Frame Error Rate (FER) is the proper figure of merit. So for these codes, the reader should regard BER in the following equations as being a stand-in for FER.

The BER of a signal subjected to Rician fading is given by

$$BER = \int_0^{\infty} f(x^2 E_b/N_0) p_r(x) dx \quad (I-1)$$

where  $f(*)$  is the ideal functional dependence of probability of bit (frame) error on bit SNR (see Appendix A) in the absence of amplitude scintillation and system loss. Equation (I-1) represents an averaging over the random, normalized amplitude factor  $r$ , which is governed by the Rician probability density function

$$p_r(x) = 2x(1+K)\exp(-K)\exp[-(1+K)x^2] I_0(2x\sqrt{K(1+K)}), \quad r \geq 0 \quad (I-2)$$

where  $I_0(*)$  is the modified Bessel function of the first kind of order zero and  $K$  is the Rice factor ( $K > 0$ ). A smaller Rice factor indicates more severe fading. This Rice factor  $K$  is related to the scintillation index  $m$  by

$$K = \left( \frac{1}{m^2} - 1 \right) + \sqrt{\left( \frac{1}{m^2} - 1 \right)^2 + \left( \frac{1}{m^2} - 1 \right)} \quad (I-3)$$

A coarse approximation for the scintillation index is given by

$$m = \begin{cases} \frac{0.01}{(\sin \beta)^{1.55}}, & \text{S - band} \\ \frac{0.0016}{(\sin \beta)^{1.55}}, & \text{X - band} \\ \frac{0.00024}{(\sin \beta)^{1.55}}, & \text{Ka - band} \end{cases} \quad (I-4)$$

where  $\beta$  is the SEP angle. Equation (I-4) is based on the observations reported in Reference 16. In general, Equation (I-1) must be evaluated numerically.

## ***Appendix J*** ***References***

- (1) J. B. Berner and K. M. Ware, "An Extremely Sensitive Digital Receiver for Deep Space Satellite Communications," *Eleventh Annual International Phoenix Conference on Computers and Communications*, pp. 577-584, Scottsdale, Arizona, April 1-3, 1992.
- (2) J. P. Costas, "Synchronous Communications," *Proceedings of the IRE*, Vol. 44, pp. 1713-1718, December 1956.
- (3) P. W. Kinman and J. B. Berner, "Two-Way Ranging During Early Mission Phase," *2003 IEEE Aerospace Conference*, Big Sky, MT, March 8-15, 2003.
- (4) M. Aung, W. J. Hurd, C. M. Buu, J. B. Berner, S. A. Stephens, and J. M. Gevargiz, "The Block V Receiver Fast Acquisition Algorithm for the Galileo S-Band Mission," *TDA Progress Report 42-118*, pp. 83-114, August 15, 1994.
- (5) J. Lesh, "Tracking Loop and Modulation Format Considerations for High Rate Telemetry," *DSN Progress Report 42-44*, pp. 117-124, April 15, 1978.
- (6) M. K. Simon and W. C. Lindsey, "Optimum Performance of Suppressed-Carrier Receivers with Costas Loop Tracking," *IEEE Transactions on Communications*, Vol. COM-25, No. 2, pp. 215-227, February 1977.
- (7) L. C. Palmer and S. A. Klein, "Phase Slipping in Phase-Locked Loop Configurations That Track Biphase or Quadriphase Modulated Carriers," *IEEE Transactions on Communications*, pp. 984-991, October 1972.
- (8) S. Shambayati, L. Tadjpour, and P. Kinman, "Turbo Code Carrier Synchronization Losses (Radio Losses)," *AIAA 19<sup>th</sup> International Communications Satellite Systems Conference and Exhibit*, Toulouse, France, April 17-20, 2001.
- (9) S. Shambayati, "Radio Losses for Concatenated Codes," *IPN Progress Report 42-151*, November 15, 2002.
- (10) W. J. Hurd and S. Aguirre, "A Method to Dramatically Improve Subcarrier Tracking," *TDA Progress Report 42-86*, pp. 103-110, August 15, 1986.
- (11) M. Aung, "Tracking Performance and Cycle Slipping in the All-Digital Symbol Synchronizer Loop of the Block V Receiver," *TDA Progress Report 42-111*, pp. 179-191, November 15, 1992.
- (12) J. H. Yuen, editor, *Deep Space Telecommunications Systems Engineering*, Plenum Press, New York, 1983.
- (13) S. A. Stephens and J. B. Thomas, "Controlled-Root Formulation for Digital Phase-Locked Loops," *IEEE Transactions on Aerospace and Electronic Systems*, Vol. 31, No. 1, pp. 78-95, January 1995.

- (14) D. Halford, J. H. Shoaf, and A. S. Risley, "Spectral Density Analysis: Frequency Domain Specification and Measurement of Signal Stability," *Proceedings of the 27th Annual Symposium on Frequency Control 1973*, Cherry Hill, New Jersey, 1973, pp. 421-431. (Also published as *NBS Technical Note 632*.)
- (15) R. Woo and J. W. Armstrong, "Spacecraft Radio Scattering Observations of the Power Spectrum of Electron Density Fluctuations in the Solar Wind," *Journal of Geophysical Research*, Vol. 84, No. A12, pp. 7288-7296, December 1, 1979.
- (16) J. W. Armstrong and R. Woo, "Solar Wind Motion Within  $30 R_{\odot}$ : Spacecraft Radio Scintillation Observations," *Astronomy and Astrophysics*, Vol. 103, pp. 415-421, 1981.